THE BENEFITS OF THERMAL MANAGEMENT TO REDUCE FRICTION LOSSES IN ENGINES

James Edward Addison

Thesis submitted to the University of Nottingham

for the degree of Doctor of Philosophy

February 2015

Contents

Key 4
Abstract 9
Acknowledgments 11
Chapter 1. Introduction and Background 12
1.1 Introduction 12
1.2 Background 13
1.3 Modelling and PROMETS 16
1.4 Experimental engine 17
1.5 Project aims and objectives 17
1.6 Thesis layout and content 18
1.6 Project context 19
Chapter 2. Literature review 20
2.1 Introduction 20
2.2 Tribology fundamentals 20
2.3 Friction modelling 22
2.4 Reduction in fuel consumption 24
2.4.1 Current industry trends 24
2.4.2 Thermal management and promoting engine warm up 26
2.4.3 Friction reduction 29
2.5 Discussion 32
Chapter 3. The PROMETS model 33
3.1 Introduction 33
3.2 The current PROMETS and PROGEN models 35
3.3 The single cylinder model 41
3.4 Structure heat transfer 41
3.5 Cylinder and port heat flux 43
3.6 Coolant heat transfer 44
3.7 Oil heat transfer 46

3.8 Exhaust gas temperature 48
3.9 Frictional losses 49
3.10 Fuel flow rate 52
3.11 Discussion 54
Chapter 4. Advancing the PROMETS friction model to account for local thermal conditions 55
4.1 Introduction 55
4.2 Friction correction based on local temperatures 58
4.2.1 Crankshaft friction 60
4.2.2 Reciprocating friction 63
4.2.3 Valvetrain 66
4.2.4 Ancillaries 68
4.5 Empirical C constants 71
4.6 Validation of friction model 75
4.6.1 Constant speed 75
4.6.2 Transient behaviour 77
4.7 Predicted temperature responses 78
4.8 Coolant temperature plunge test 81
4.9 Viscometry 83
4.7 Discussion 88
Chapter 5. Modelling the VIPER oil circuit 91
5.1 Introduction 91
5.2 VIPER oil circuit layout 93
5.3 Oil circuit updates for modelling the VIPER engine 96
5.4 Oil sump temperature 99
5.5 Filter cooler heat transfer 105
5.6 Main bearing model 107
5.7 Bearing model results 112
5.8 Piston cooling jets 115
5.9 Oil circuit predictions 118
5.10 Discussion 121
Chapter 6. Assessing engine performance over the NEDC 124
6.1 Introduction 124
6.2 Pumping losses 125

6.3 Fuel consumption 131
6.3.2 The cold start fuel consumption penalty 134
6.3.3 Fuel energy utilisation 136
6.4 Reducing fuel consumption over the aNEDC 139
6.4.1 Stop-start 139
6.4.2 Heat exchange devices 143
6.4.3 Reduction of parasitic losses 146
6.4.4 Supplementary oil heating 149
6.5 Discussion 151
Chapter 7. Discussion and conclusions 155
7.1 Conclusions 159
7.2 Future work 161
References 163

Key

Nomenclature

A	Area	(m^2)
a	Bearing Groove Length	(m)
B	Bore	(m)
C_{cb}	Constant for crankshaft bearing term	(kPa· min/rev·m)
C_{cs}	Constant for main bearing seal term	(kPa· m^2)
C_{ff}	Constant for flat follower term	(kPa·m)
C_{oh}	Constant for oscillating hydrodynamic term	(kPa·[m· min/rev]$^{0.5}$)
C_{om}	Constant for oscillating mixed term	(kPa)
C_{pr}	Constant for piston rings term	(kPa.m^2· [rev/min])
C_{ps}	Constant for piston skirt term	(kPa.s)
C_p	Specific Heat Capacity	(J/kg· K)
C_{td}	Constant for turbulent dissipation term	(kPa· [min/rev·m]^2)
C_{vb}	Constant for valvetrain bearings term	(kPa.m^3· [min/rev])
c	Bearing radial clearance	(m)
D	Gallery Diameter	(m)
D_b	Bearing Diameter	(m)
D_v	Valve Diameter	(m)
H	Enthalpy	(J)
h	Heat transfer coefficient	(W/m^2K)
k	Thermal conductivity	(W/mK)
L	Gallery length	(m)
L	Bearing length (Petroff's Equation)	(m)
L_v	Valve lift	(m)
$\dot{m}$	Mass flow rate	(kg/s)
N	Engine Speed	(rev/min)
n	Friction index	(-)

n_c	Number of cylinders	(-)
n_v	Number of valves	(-)
P	Power	(W)
P	Pressure	(Pa)
Pr	Prandlt number - $C_p\mu/k$	(-)
$\dot{Q}$	Heat transfer	(W)
$\dot{Q}_h$	Hydrodynamic flow rate	(m^3/S)
$\dot{Q}_p$	Pressure driven flow rate	(m^3/S)
Re	Reynolds number Chapter 3- $4\dot{m}/\pi D\mu\rho$	(-)
	Chapter 6- $\rho_o v_o {}^{d_o}/_{\mu_o}$	
R	Bearing radius	(m)
r_c	Compression ratio	(-)
S	Stroke	(m)
S	Seebeck coefficient (TEG)	(V/K)
S_p	Mean piston speed	(m/s)
T	Temperature	(°C)(K)
U	Surface Speed	(m/s)
V	Volume	(m^3)
W	Load on bearing	(nm)
ΔX	Distance between element centres	(m)

Subscripts

0	At a reference value
a	average
air	Air
amb	Ambient
b	Brake
b	Bearing (viscosity)
c	Combustion (efficiency)
c	Compression

conv	Convective
cool	Coolant
cyl	Cylinder
d	Discharge
e	Effective
eng	Engine
ex	Exhaust
f	Friction
fuel	Fuel
fw	Value for fully warm
g	Gas
g	Gross (MEP)
h	Hydrodynamic
i	Indicated
in	Temperature at inlet
ind	Indicated
LHV	Lower Heating Value
m	Metal
man	Inlet manifold
min	Minimum
mist	Mist
nb	Nucleate boiling
o	Oil
o	Outlet (Piston cooling jets)
p	Piston
p	Pumping (work)
pt	Port
r	Reciprocating
s	Surface
s	Sump (Temperature)
sat	Saturation
th	Thermal

v	Volume
v	Valve
v	Valvetrain (Viscosity)
wu	Value during warm up

Symbols

ϕ	Fuel-air equivalence ratio	(-)
η	Efficiency	(-)
μ	Dynamic Viscosity	(mPa.s)
ρ	Density	(kg/m^3)
λ	Latent heat of vaporisation	(°C)
ε	Effectiveness (Heat Exchangers)	(-)
ε	Eccentricity (Bearings)	(-)
φ	Bearing Attitude Angle	(°)

Abbreviations

ASTM	American Society for Testing and Materials
AFR	Air Fuel Ratio
aNEDC	Approximated New European Driving Cycle
BMEP	Brake Mean Effective Pressure
CAFE	Corporate Average Fuel Economy
CCS	Cold Cranking Simulator
DLC	Diamond-Like Coating
FEAD	Front End Ancillary Drive
FMEP	Friction Mean Effective Pressure
FTP	Federal Test Procedure
HTHS	High Temperature High Shear
IMEP	Indicated Mean Effective Pressure
MBT	Minimum Advance for Best Torque
NEDC	New European Driving Cycle

NTU	Number of Transfer Units
PMEP	Pumping Mean Effective Pressure
PNH	Patton-Nietsche and Heywood
PROMETS	Program for Modelling Engine Thermal Systems
PROGEN	Program for creating Generic engine representations
SAE	Society of Automotive Engineers
SI	Spark Ignition
TEG	Thermo-electric Generator
VIPER	Vehicle Integrated Powertrain Energy Recovery
WHLTP	World Harmonised Light Vehicles Test Procedures

Abstract

The research reported in the thesis addresses questions of how engine fuel consumption and carbon dioxide emissions are can be reduced through improvements in thermal management, lubricant design, and energy recovery. The investigations are based on simulation studies using computational models and sub-models developed or revised during the work, and results provided by complementary experimental studies carried out by collaborating investigators.

The brake thermal efficiency of the internal combustion engines (ICE) used in cars and light duty commercial vehicles is reduced by frictional losses. These losses vary with engine design, lubricant formulation and thermal state. They are most significant when the engine is running cold or partially warm. Over the New European Drive Cycle (NEDC), engine friction losses raise vehicle fuel consumption by several percentage points. A version of the computational model, PROMETS, has been developed and applied in studies of thermal behaviour, friction and engine lubricant to investigate the performance of a 2.0l, I4 GTDI spark ignition engine and in particular, how these influence fuel consumption over the NEDC.

Core parts of PROMETS include a physics-based, empirically calibrated friction model, a cycle averaged description of gas-to-structure heat transfer and a lumped capacity description of thermal behaviour of the engine block and cylinder head. In the thesis, revisions to the description of friction and interactions between friction, local thermal conditions and lubricant are reported. It is shown that the bulk temperature of coolant rather than oil has the stronger influence on friction at the piston-liner interface, whilst bulk oil temperature more strongly influences friction in crankshaft bearings and other lower engine components. However, local oil film temperatures have a direct influence on local friction contribution. To account for this, local values of oil temperature and viscosity are used in describing local friction contributions. Implementation required an oil system model to be developed; an iterative model of the frictional dissipation within the

main bearings, and a prediction of piston cooling jet heat transfer coefficients have been added to the oil circuit.

Simulations of a range of scenarios and design changes are presented and analysed in the thesis. The size of the fuel savings that could potentially be made through improved thermal management has been demonstrated to be 4.5% for the engine being simulated. Model results show that of the friction contributing surfaces, the piston group is responsible for the highest levels of friction, and also exhibits the largest absolute reduction in friction as the temperature of the engine rises. The relatively low warm-up rate of the lower engine structure gives a correspondingly slow reduction in friction in crankshaft bearings from their cold start values. Measures to accelerate this reduction by raising oil temperature have limited effect unless the strong thermal links between the oil and the surrounding metal are broken. When additional heating is applied to the engine oil, only around 30% is retained to raise the oil temperature due to these thermal links.

Acknowledgments

My thanks go to Professor Paul Shayler for giving me this opportunity, as well as for his patience, knowledge and anecdotes throughout this project. I hope that my ducks remain firmly in a row, and that I never nail my sail to the wrong mast.

I am also grateful to the students and staff of the Engines Research Group for their helpful input and constant distractions throughout the past four years. It has been a truly enjoyable experience. Special thanks go to my colleagues on the VIPER research project, Dr. Richard Gardiner and Chen Zhao. My introduction to PROMETS came courtesy of Dr. Jean-Paul Zammit, and his insight is greatly appreciated.

I would like to acknowledge the backing for PhD studies from Innovate and the EPSRC. The help and collaboration from members of the VIPER consortium has been valuable to this research; in particular I would like to thank Ian Pegg of Ford, and Bob Gillchrist of Jaguar Land Rover.

To my parents Robert and Sylvia, I am indebted. Their encouragement and support can never be repaid. I promise to move out soon.

Chapter 1. Introduction and Background

1.1 Introduction

This thesis is concerned with the development of a computational model and its application in the assessment of engine thermal behavior and efficiency improvements. The main area of interest examined here has been engine warm up and the use of thermal management to reduce the fuel consumption penalty incurred during engine operation before the fully warm thermal state is reached.

A major driver of work in this area is the imperative to reduce emissions of greenhouse gases, particularly CO_2, which is produced by the use of hydrocarbon fuels in internal combustions engines in the automotive field. Automotive transport is a significant contributor to global greenhouse gas emissions. In the United Kingdom it accounts for an estimated 20% of the total annual greenhouse gases produced, with motor vehicle traffic accounting for 302 billion miles travelled according to Department of Transport statistics for 2012 [1] [2]. It is estimated that for a typical European car user, 53% of their total fuel consumption will be during journeys of less than 10km in length [3].

Journeys that occur with the engine starting from cold temperatures account for a large proportion of car usage within Europe, with estimates being that between 25% and 30% of journeys begin with the engine at less than 30°C [4]. Starting under cold conditions causes the engine to suffer penalties to both fuel consumption and emissions, which continue until the engine temperatures stabilise at their fully warm values. The cold start fuel consumption penalty is dependent on the engine in question, with values of 15% over the NEDC reported for 4.0l inline 8-cylinder gasoline engine [5], and 6% for a 2.7l V6 diesel [6]. A large part of this increase in fuel consumption is due to elevated engine friction at low temperatures.

This increased friction is mainly observed in the journal bearings found on the crankshaft, and the piston assembly. These components typically account for a large proportion of the total engine friction. Due to the separation of the sliding

surfaces in the largest friction contributors by a fluid film, friction is greatly influenced by the properties of the lubricant. The lubricating oil of the engine is significantly more viscous at cold temperatures than it would be when the engine is fully warm.

The need for efficient thermal management is an important area of research due to the large number of vehicles that start from cold and the political, market and environmental pressures to reduce fuel consumption and CO_2 emissions. By bringing the engine to a steady thermal state more rapidly, the friction and fuel consumption penalty experienced due to cold running can be reduced. Additional pressure on thermal management arises from the increasing efficiency of modern engines. As the fuel used by the engine is decreased due to gains in efficiency, the amount of energy available to warm the engine similarly falls. Fuel saving technologies such as stop start, and hybridisation will further compound this effect making effective use of the available energy more important. By reducing the rate of engine warming, these technologies are reducing their own effectiveness and efficient thermal management is necessary to reach the full potential of these measures.

1.2 Background

Pressure on manufacturers to improve the fuel economy of their vehicles is increasing, due to a combination of factors. Political, environmental, and customer concerns all contribute to the drive towards vehicles that are increasingly fuel efficient. The fossil fuels used as the primary fuels for transportation are petroleum fractions that have finite reserves. The demand for oil is steadily growing, with the global demand of 93 million barrels per day as of 2014 having risen by over 10% in the past decade, and with production growing to match this [7] [8]. In developed countries, such as the USA where personal wealth is high, gasoline and diesel used for transportation often account for large proportions of national petroleum usage. Indeed in the USA over 60% of the petroleum used each year is consumed in the transport sector excluding those from aviation and marine sources [9]. The demand, as a percentage of total oil usage, from the

transportation sector is not as great in developing countries, but will rise as the number of people who can afford personal motor transport increases.

Automotive manufacturers are heavily regulated to limit the emission of pollutants from their vehicles. The limits depend on the location in which the vehicles are sold. Early restrictions were placed on $NO_{x,}$ CO, and hydrocarbons, and these were later extended to restrict particulate matter (PM) emissions because of concerns over their health impacts, and also to CO_2 due to its association with climate change. There is direct correlation between the amount of hydrocarbon fuel used by a vehicle and the CO_2 emissions which it produces. Petrol vehicles will produce 3.1kg of CO_2 for every kg of fuel burnt. Other pollutants such as NOx, CO, and unburnt hydrocarbons are more dependent on engine design, operating conditions and after-treatment systems. European regulations on the emissions of passenger vehicles are becoming increasingly restrictive over time, in order to reduce the impact of vehicle pollution on the environment. This is especially true for diesel vehicles, with the upcoming Euro 6 regulations focusing heavily on NOx emissions. European Environment Agency regulations also govern the permissible fleet average CO_2 emissions based on the average mass of a manufacturer's vehicle models and financial premiums are levied on manufacturers that fail to meet these targets [10]. The Corporate Average Fuel Economy (CAFE) regulations in the USA impose a similar but more lenient restriction and are worded in terms of fuel consumption [11].

The fuel consumption of a vehicle is a published figure of merit and the corresponding level of CO_2 emissions contributes to fleet target values which manufacturers must meet or face financial penalties levied by the EU. Currently new vehicles sold in the EU are required to be assessed for emissions and fuel economy over the New European Drive Cycle (NEDC) as described in Directive 70/220/EEC [12]. This standardised test, which was designed to represent a typical journey in and around a European city, is conducted from a cold start and the results are required to be made available to both consumers and governments in Europe. The speed profile of the NEDC over time is reprinted from [13] and shown in Figure 1.1. The NEDC is a stylised test profile, and consists of four

repeats of a low speed urban cycle, designed to replicate stop-start driving in a city, followed by one cycle of higher speed driving to represent driving on a motorway. As can be seen in Figure 1.1, the NEDC uses fixed accelerations and decelerations as well as periods of constant speed. Other current test procedures include the American FTP-75 and Japanese 10-15 mode cycles. The World Harmonised Light Vehicles Test Procedures (WHLTP) programme, due to be finalized in 2015 is an effort to define a global standard in testing for emissions and fuel economy. The choice of drive cycle and the constrictions on the technology used, play a large role in the direction of research and development in the automotive field. As part of complimentary work undertaken within the VIPER project, an approximated NEDC cycle, the aNEDC, has been defined for use on eddy current dynamometers. This cycle shows good repeatability and has a comparable fuel consumption, engine speed transients and warm up characteristics to those of the NEDC. Experimental data from this cycle is used for comparison with simulated results.

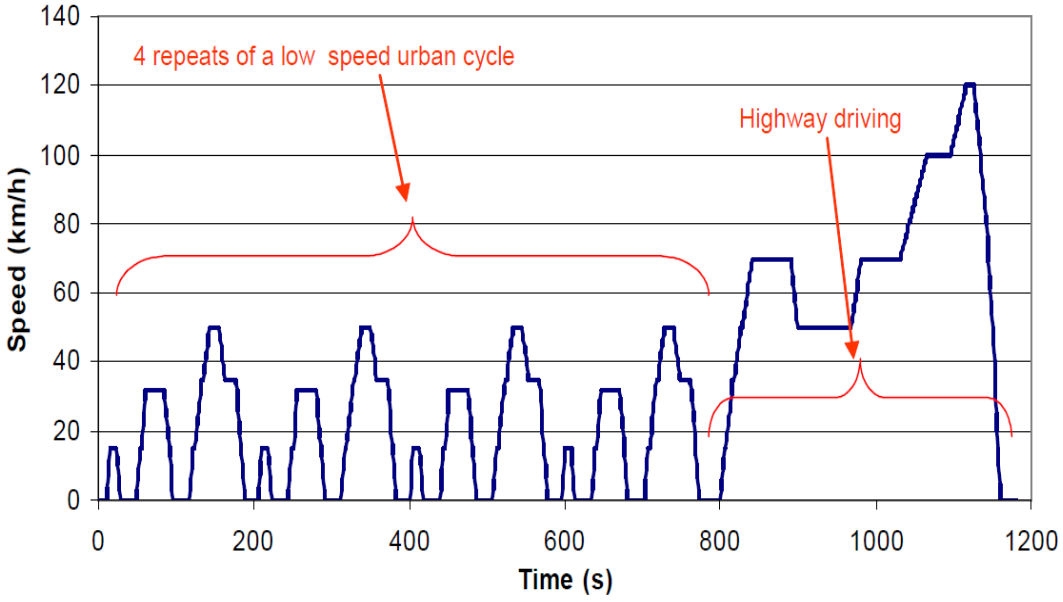

Figure 1.1 The NEDC speed profile. Reprinted from [13]

1.3 Modelling and PROMETS

Computational modelling of engines is an important tool when investigating the effects of engine design changes and assessing performance. Modelling of engines has ranged from one dimensional modelling of flows through oil passages to full three dimensional CFD packages. Modern modelling software packages allow for changes to engine design to be examined with reduced time and cost implications compared to iterating physical prototypes. Computational modelling allows for responses to a wide variety of conditions to be simulated without using valuable time on engine test beds, and depending on the complexity of the model, tests can be run at accelerated time scales. In the scope of this project, in which savings from individual strategies may account for less than 1% savings, modelling is important as it also removes the problem of experimental noise obscuring results.

The software package discussed in this thesis is the PROgram for Modelling Engine Thermal Systems (PROMETS). PROMETS has been developed at the University of Nottingham and is a collection of subsystems that model important thermodynamic processes in an internal combustion engine, namely cylinder and port heat flux, frictional losses, coolant heat transfer, oil heat transfer, exhaust gas temperature, fuelling predictions and heat transfer with the engine structure. The PROMETS model uses a lumped capacity representation of the engine, which is generated using the PROgram for creating GENeric engine representations (PROGEN). This representation relies on the input of a number of fundamental engine dimensions to modify generic engine templates and build the lumped capacity description of the desired engine. The model allows for the simulation of a single representative cylinder, or a full multi-cylinder simulation. Unless data on the thermal interaction between cylinders is required, the single cylinder model is capable of producing results comparable with the multi-cylinder model and scales appropriate predictions such as gas side heat transfer and fuel consumption by the number of cylinders [14]. The PROMETS model is discussed in more detail in Chapter 3.

1.4 Experimental engine

The studies reported in this thesis draw upon experimental work carried out on an engine referred to as the VIPER engine. This is used in light duty vehicles manufactured by both Ford and Jaguar, in models such as the Ford Mondeo, Jaguar XF and Land Rover Evoque. It was supplied for testing by Jaguar Land Rover and is an inline 4 cylinder 2.0 litre 16 valve gasoline turbocharged direct injection unit. The camshafts are in a double overhead configuration, and are chain driven with direct acting roller followers and oil pressure actuated variable valve timing. Both the cylinder head, and the engine block are constructed from cast aluminium. Engine instrumentation and data acquisition are described in more detail in [15]. More specific description of oil circuit instrumentation is included in Section 5.2.

1.5 Project aims and objectives

The aim of this project is to take the existing PROMETS model, and enhance its functionality to give a more complete description of the interactions between thermal systems and friction behaviour in the engine. With this model, methods of altering the thermal balance of the engine will be investigated with the intention of reducing the fuel consumption penalties experienced during cold and sub-warm engine running in the NEDC.

To achieve the aims of the project, the following objectives have been laid out. Firstly, the oil circuit representation included in the standard PROMETS model will be reworked to represent the oil circuit found in the VIPER engine. This will allow better predictions of the response of oil temperature and viscosity to changes made to thermal coupling around the engine. The main differences between the stock and VIPER oil circuit is the addition of piston cooling jets, which will dramatically alter the heat distribution around the engine, and the position of the internal galleries, which are positioned significantly closer to the cylinder in the VIPER engine.

The first objective will be to change the method in which engine friction is calculated to account for changes in oil viscosity with temperature. The current version of the model uses changes to bulk oil temperature to evaluate the friction

response at all of the rubbing surfaces. This will be changed so that the thermal conditions at the key engine locations of the rubbing surfaces are considered when evaluating friction. The model will be calibrated against a modern engine and lubricant to adjust empirical constants formulated against older data.

As an improvement to the oil circuit, a model of the main bearings will be included; this will predict the temperature of the oil film in the bearings. To do this an energy balance for the bearing which considers the heat retained in the film as well as the conduction into the surrounding metal elements will be implemented. Additionally, to increase the fidelity of the heat transfer predictions in this region, the number of elements surrounding the bearing will be increased. The heat transfer of piston cooling jets to the oil will also be modelled.

The improvement of the friction and oil predictions should tie together to improve the description of the thermal-friction interactions in the engine, and provide a more realistic model to investigate friction responses when perturbations to the engine's thermal balance are made.

1.6 Thesis layout and content

This thesis consists of the following chapters:

Chapter 2 covers a review of the literature that is relevant to modelling, thermal management, friction and improving fuel economy.

An introduction to and description of the current state of the PROMETS model and its major sub models will be given in Chapter 3. Specific focus has been centred on the oil and friction sub models, given that they are the most relevant to the work contained in this thesis. Areas have been identified in which progress is required.

The updated local temperature based friction model will be discussed in Chapter 4. Decisions made in the choice of critical temperatures used to calculate friction is explained, and the rationale behind the selection of viscosity response indices is

given. Validation against a range of steady state and transient test conditions is also included.

Chapter 5 contains the work done in updating the representation of the oil circuit in the PROMETS model to bring it in to line with the VIPER engine. Description of a bearing model and piston cooling jet model will be included along with validation of simulated results against experimental data.

In Chapter 6, the VIPER engine fuel consumption is assessed over the aNEDC. The potential benefits of external heating of the oil are predicted. The effect of increasing the coupling between the coolant and oil has been determined by increasing the effectiveness of the oil cooler. Investigations into the effects of insulation on oil pathways are also examined.

Chapter 7 contains the discussion of the work contained in the thesis, and the major conclusions of the work.

1.6 Project context

The research forms part of a larger project concerned with the thermal behavior of engines, and the author's contributions revolve around the development and use of computational modeling of engine thermal behavior and friction, in particular PROMETS, a lumped capacity model. The project is named Vehicle Integrated Powertrain Energy Recovery (VIPER) and is a being undertaken by a consortium which includes the University of Nottingham, Ford, Jaguar Land Rover, BP, IAV, CPT, Dana and Imperial College. The overarching goal of the project is to realise a 4.5% reduction in Carbon Dioxide emissions over the New European Drive Cycle. This is to be done by optimizing the use of energy using both changes to conventional engine design, and through use of new technologies to harness heat.

Chapter 2. Literature review

2.1 Introduction

In this chapter, relevant research concerned with reducing the fuel consumption of automotive engines is examined. The use of computers to model engine systems is important to this work, and covers a wide range of approaches and objectives. Therefore the modelling of thermal systems and friction is focused on.

The fuel consumption penalty incurred by running the engine at sub-optimal temperatures is described before investigations into reducing this are explored. Current trends in the automotive industry are also covered and possible conflicts between technologies identified.

2.2 Tribology fundamentals

Mechanical frictional losses account for the difference between the net work done on the piston from the in cylinder gases, the brake work output to the driveshaft and the electrical output to the battery. Friction acts to raise the fuel consumption of the engine, and increases the wear on the rubbing surfaces.

Friction losses in an engine can be broken down into the power lost at the rubbing surfaces and the ancillary losses on the crankshaft. Pumping work can also be considered as a friction loss, but this is not accounted for when considering net work.

The pumping losses describe the work lost in moving gases into and out of the engine as air is drawn into the cylinder during the intake stroke, and exhaust gases are removed during the exhaust stroke. Ancillary losses arise due to the load placed on the crankshaft as a result of driving the ancillaries required to run the engine.

The rubbing friction is the force that occurs between two surfaces in relative motion, and the contributors in the engine can be divided into the piston assembly,

the crankshaft and the valvetrain. Of these, the piston is the dominant source of friction, making up between 50 and 60% of the total engine friction. The bearings contribute around 20-30% and the valvetrain contributes 10-20% [16] [3]. These proportions vary with engine type and design.

Each rubbing surface can be considered to be operating in one of three main lubrication regimes, which have different characteristics when it comes to frictional response to factors such as relative speed or temperature. The Stribeck curve in Figure 2.1 (reprinted from [17]) shows the regimes of lubrication experienced by the rubbing surfaces. Here, the coefficient of friction is plotted agains a duty parameter which is a function of oil viscosity, relative speed between the surfaces, and load. Hydrodynamic lubrication, experienced in the piston and the bearings occurs when there is an oil film of sufficient pressure to separate the surfaces completely. The friction here is due to shear in the oil film. Mixed friction occurs as the thickness of the film is reduced enough to allow contact between the asperities from each surface. Accordingly, the coefficient of friction begins to increase. Boundary friction occurs during full metal to metal contact, and friction is highest in this regime. Here, the material properties of the metal dominate the friction forces. Elasto-hydrodynamic lubrication is a special form of hydrodynamic lubrication where the surfaces deform due to load, and allow the formation of a fluid film.

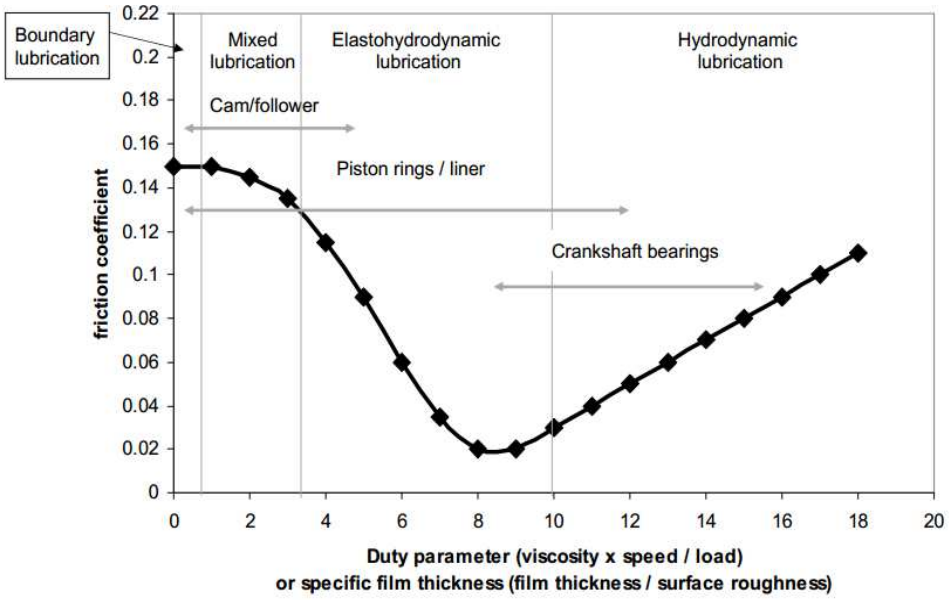

Figure 2.1 The Stribeck Curve. Reprinted from [16]

2.3 Friction modelling

Friction losses will impact the fuel consumption of the engine, as well as heat rejection to the coolant and oil systems, making accurate prediction important to engine simulation. There are several approaches to modelling engine friction. These range from simple models that aim to predict friction from whole engines, to more detailed models that break down friction contributions to their individual contributing parts. Models tend to fall into the category of either crank angle resolved formulations which aim to predict friction levels at any point during the crank rotation, or cycle averaged variants which predict a mean friction level.

An early crank angle resolved model was put forward by Rezeka and Henein [18] for a diesel engine. Here, the variation in flywheel angular velocity were used to characterise the instantaneous friction forces, based on the gas pressure on the piston, the inertial forces of the engine and the load on the crankshaft. This code was subsequently used in work by Kouremenos et al. [19] and further investigated by Rakopoulos et al. [20] [21]. This approach used a physical formulation with empirical correction coefficients. The conclusion of [20] was that maximum combustion pressure in diesel engines has a very weak effect on engine friction, mainly due to the large influence of engine speed.

A more fundamental version of the model presented in [18] was developed by Taraza and Henein [22] which reduced the number of parameters that must be input to the model.

Zweiri et al. [23] developed a crank angle resolved model using a mostly physics-based analysis of lubrication regimes. Friction is calculated as a torque for each assembly. A similar approach was taken by Livanos and Kyratos [24], whose model also included predictions of oil film thickness.

Patton et al. [25] created an example of a cycle averaged model, which will be referred to as the PNH model in this work. The model was based on empirical results from engine teardown tests, along with assumptions of lubrication regimes. This model predicted FMEP values as opposed to the torque predictions of those previously described. Friction predictions were separated to predict for each of the

major rubbing components: the crankshaft, pistons, valvetrain and auxiliary. All components were assumed to be lubricated in one of the hydrodynamic, mixed or boundary lubrication regimes. Equations were developed to reflect the dependence of friction on basic engine design and operating parameters. Constants for each term were used to match predictions to experimental data. Due to its modular and physically based formulation, a version of this model was implemented in PROMETS to calculate engine friction at fully warm running conditions.

The original PNH friction model was improved in subsequent work by Shayler and Leong [26] and Sandoval and Heywood [27] to account for changes in engine friction during warm up by correcting for oil viscosity and give better agreements with experimental results. In [27], assemblies that are lubricated in the hydrodynamic regime are selectively corrected for viscosity based on the temperature of the bulk oil. This differed from the previous viscosity correction implemented in PROMETS in which a global correction was applied, regardless of lubrication regime, and in contradiction with the Stribeck curve. The curve and Stribeck number show hydrodynamic friction increasing with oil viscosity and speed, but no effect in the boundary or mixed lubrication regimes.

Shayler and Leong [26] made a concurrent and similar revision to the model. This differed to the Heywood approach as each individual assembly had separate indices in the viscosity ratio as opposed to a universal value of 0.5 in the Heywood revision, and there were several other modifications to the terms and constants to reflect the engine under consideration as well as improved understanding of friction behaviour. The viscosity indexed used in this work are given in Table 2.1. Friction dependence on oil viscosity was introduced for the mixed and follower contributions in the valvetrain and all piston components. The turbulent dissipation term in the crankshaft group was removed as it was assumed to be taken account of in the work required to pump the oil. The auxiliary friction term was broken down to include separate equations for all three of the main auxiliary components: the coolant pump, oil pump and fuel pump.

Table 2.1 Viscosity Indexes for the Shayler Leong friction model [26]

Component	**Viscosity Index**
Crankshaft	0.4
Piston	0.3
Valvetrain	0.7
Oil Pump	0.3
Water Pump	0.7
Fuel Pump	0.5

2.4 Reduction in fuel consumption

The reduction of engine fuel consumption is a multi-disciplinary field of research and in this section some of the techniques that are either currently used, or are under development are examined. Current trends in the automotive industry towards improved fuel economy are described. Due to the importance of friction and thermal management on this work, particular attention will be paid to these areas.

2.4.1 Current industry trends

One of the most apparent of the current trends in industry is the downsizing of spark ignition engines to provide the power output of a larger engine at a lower fuel and emission cost. This is achievable with the use of forced induction methods such as supercharging or turbocharging to restore power lost through the reduction in engine displacement. The engine used as part of the VIPER project, and described in Chapter 1, is a 2.0l turbocharged direct injection engine, that was used by Jaguar to replace a 3.0l naturally aspirated V6 engine in their XF model. The two engines provide very similar peak power (177kW and 175kW respectively) but the fuel consumption of the smaller engine was 18% better over the NEDC cycle. This is in line with parametric analysis of the effect of engine downsizing performed by Shahed and Bauer [28] who predicted fuel consumption benefits of 20% when downsizing by 40%.

During the low speed and load conditions that are representative of the majority of real world driving, the efficiency of spark ignition engines is low due to the throttling of the intake air. Reducing the engine displacement will allow the engine to run at a higher load for a given engine speed which reduces the pumping losses [29]. The higher specific power of downsized engine will lead to higher oil temperatures which will in turn reduce engine friction, but at the cost of additional oxidative stress on the lubricant [30].

There are drawbacks to the use of small turbocharged engines. Turbocharging gasoline engines can make them more susceptible to knock due to higher in cylinder pressures and temperatures. The use of direct injection can reduce the likelihood of knock by cooling the air charge in the cylinder which also serves to improve the volumetric efficiency of the engine [31].

The use of variable valve train systems can allow the deactivation of the cylinders by eliminating airflow into the cylinder and has been shown to have beneficial effects on fuel economy for spark ignitions automotive engines. In [32], Leone and Pozar reported a reduction in pumping losses of up to 15% at light load, and predicted fuel consumption benefits of up to 11% for large displacement passenger vehicles in the FTP-75 drive cycle. As with engine downsizing, there are drawbacks to cylinder deactivation. Noise Vibration and Harshness (NVH) issues, idle stability and knock were all identified in [33] as limiting factors.

Hyrbidisation, or the use of multiple energy sources in a single vehicle, is another current technology that is becoming more prevalent. Hybrid vehicles offer lower fuel consumption and emissions over regular ICE vehicles, but at higher manufacturing costs [34]. Analysis of lifetime cost of current hybrid vehicles in [35] has shown that the breakeven point for the customer is between 6 and 12 years when compared to the cheaper purchase price but higher running costs of a conventional vehicle.

Electrical hybrid systems are offered by several manufacturers and generally fall into one of two major categories. Parallel hybrid vehicles such as the BMW i8, or Toyota Prius couple both an internal combustion engine and an electrical motor to

the driveshaft and allow power to be supplied by each individually, or by both in tandem. Series hybrid systems as featured in Nissan's Leaf use the ICE to power a generator which produces electricity that can either be used to charge a battery or drive an electric motor that is connected to the driveshaft [36] .

2.4.2 Thermal management and promoting engine warm up

Reducing the time taken for the engine to reach fully warm conditions is one method to reduce fuel consumption over the NEDC cycle, by reducing the penalty to engine friction that comes with colder oil temperatures. There have been several different approaches to this. These generally revolve around manipulation of either the coolant or the lubrication circuits.

Choukroun and Chanfreau [37] introduced electronic control to an engine coolant circuit in order to optimize the warm up rate of the engine. Use of an electric water pump, thermostat valve and a variable speed fan gave them much greater control over the coolant circuit and consequently they were able to delay thermostat opening in the engine until it reached 110°C during part loaded running. The reduction in fuel consumption was reported to be between 2 and 3% over an NEDC cycle.

A similar approach was taken by Cortona et al. [38], who also replaced the mechanical water pump, and wax thermostat valve with electrical models. They showed savings of 3% in terms of fuel consumption over the NEDC. Similar results for this strategy were reported by Edwards et al. and Geels et al. [39] [40]. Increased coolant temperatures caused higher temperatures in the engine oil, which consequently reduced engine friction. Also presented, was the ability to run the electrical coolant pump at much lower speeds and consequently lower flow rates throughout the NEDC. This reduced the energy consumption of the pump, even given the added inefficiency of the alternator supplying the power to the pump as opposed to the efficiency of the mechanically driven pump usually fitted to a vehicle.

Bent [41] used electrical coolant pumps to stall the coolant flow until cooling was required and also pulsed to flow once the engine reached fully warm to minimise ancillary losses whilst still providing adequate cooling. Results showed a 0.5% reduction in fuel used over a 30 minute constant speed warm up.

Brace et al. [42] used a variable flow oil pump as well as a second oil cooled EGR cooler in parallel with a coolant cooled EGR unit to increase oil temperature over the baseline warm up rate. The greatest savings seen in these experiments were given by the variable flow pump, with the EGR cooler giving slightly lower benefits. 22g of fuel was saved over the NEDC which translates to a 2% saving for the engine under consideration.

There have been several investigations into the use of thermal stores as ways to improve the warm up rate of engines. Schatz [43] used a thermal battery that relied on a phase change salt mixture inside an insulated tank. This device allows the salt solution to melt during engine operation, and maintains the temperature of the solution overnight, before cold fluid is flushed through the tank causing the solution to solidify and provide heat to the coolant. Heating of between 50 and 100kW were reported to be available for 10 seconds, before the heat transfer levelled off. Fuel economy improvements of 14% over the first phase of the FTP-75 cycle were recorded. By using only a single phase of a drive cycle, the fuel penalty experience is proportionally larger that it would be if the technology were to be evaluated over a full cycle, inflating the percentage fuel economy gains.

More recently, Kuze et al. [44] have used a tank that does not rely on a phase change solution, and instead captures hot coolant in an insulated tank. This system was able to maintain coolant temperature above 50°C for more than 36 hours from a 90°C starting temperature. More modest improvements in fuel economy of 5-6% over a 10 minute drive from cold start were seen using this tank system.

By encapsulating the engine with insulating material, Bent [41] was able to demonstrate a 5°C increase in engine starting temperature after a 12 hour soak from fully warm operation. This translated to a fuel saving of 1.1% over the NEDC. Due to the presence of a power take off instead of a gearbox on the

engine, it was suggested that the cool down rate was slower than if the technique was applied to a vehicle.

A paper by Kunze et al. [45] simulated the most beneficial use of energy in terms of pre-heating vehicle components. 2 Mega joules of energy was taken; roughly double that available during high heat flow operation from systems described by Schatz, to heat the fluids which accompany each of the engine, gearbox or rear axle drive. The greatest fuel economy improvements over the NEDC were seen when the energy was used to heat the gearbox and rear axle drive oil, using 75% and 25% respectively. The lowest benefit came when all of the energy was used to heat the engine coolant, closely followed by heating the engine oil. These methods reduced fuel consumption by roughly 1% over the NEDC, around half of the benefit seen by heating oil in the gearbox and rear axle drive. This was due to the higher volume of fluid. These results proved hard to replicate experimentally.

Another approach was taken by Law et al. [46], who investigated the effect of changing oil sump design on oil temperature. By altering oil flow paths in the sump, they were able to redirect hot oil that had already been circulated around the engine, more directly to the pump pickup, essentially reducing the amount of oil in circulation during the warm up. This increased the temperature of the oil being circulated by the pump, and supplied to the engine. It was observed that although the temperature of oil entering the pump was increased by over 25°C, that by the time the oil had reached the main gallery, the increase had reduced to around 5°C for a test started at 20°C. Consequently, it was difficult to show improvements in engine friction in these cases. However, in tests conducted from a -10°C start, the delta T recorded in the main gallery against those found when using a standard sump more than doubled at one point during the test, and were maintained over a longer period. This reduced engine friction by 50kPa from the baseline test at 2000RPM.

These results seem as if they would provide good synergy with recent experiments done by Roberts et al. [47]. This study considered a single oil gallery, 380mm in length, which is representative of the VIPER oil gallery. This gallery was insulated using 2mm nylon insulation in an attempt to reduce heat transfer from

the oil to the structure during warm up. Results showed a greater temperature difference between the oil and the metal used to simulate the engine structure when insulation was applied, which implied a reduced heat transfer between the two. Simulations of the test predicted that the amount of energy lost to the oil would be reduced from 7% of the total energy input to the oil, to 2.75%. This equated to a predicted rise in gallery temperature of 0.5°C.

2.4.3 Friction reduction

Another approach to reducing fuel consumption is the reduction of engine friction outside of thermal means. This usually focuses on the use of surface finishes, low viscosity oil and modifiers, and mechanical changes to the design of the rubbing surfaces.

Work by Ryk et al. in [48] [49] assessed the performance of flat faced piston rings subjected to Laser Surface Texturing (LST) over traditional barrel shaped gas control rings in terms of the friction produced. By creating micro-dimples of around 80µm diameter in the face of the piston ring, a large hydrodynamic effect was created, and a reduction in friction of 30% was demonstrated experimentally over the traditional barrel shaped piston rings, albeit at the small range of engine speeds that was available with the experimental set up.

Another method that has been investigated when considering how to reduce friction in the piston assembly concerns the coating of piston rings or the piston skirt in a low friction, low wear substance. One notable example of these are Diamond Like Carbon (DLC) films. The properties of these coatings are highly variable and depend upon factors such as deposition process, substrate material and the presence of other elements in the film [50]. Experiments by Erdemis [51] show that hydrogenated DLC films exhibited coefficients of friction as low as 0.003, a value 200 times lower than an ahydrogenated sample tested. This low coefficient of friction make the application of DLC films to engine components quite appealing, with work carried out into the application of films onto many different engine components. It should be noted though that only areas of the engine in which mixed or boundary lubrication are present will benefit, as the

separation of surfaces by a lubricant film as seen when a component is lubricated hydrodynamically will not allow any of the physical properties of a DLC film to influence friction [52]. This still leaves the piston rings and valvetrain as suitable candidates for friction reduction through DLC film coating. A study into the behavior of different ring coatings when lubricated with an ethanol fuel blend and engine oil showed that although the rings coated with DLC showed the lowest coefficient of friction when lubricated with standard mineral oil, the result was not significantly lower than that obtained when using a standard nitride steel ring with a coefficient of approximately 0.11 compared to that of 0.115. When the oil was replaced by one containing a Molybdenum friction modifier, the results actually favored the nitride steel ring. It is unclear from the paper what kind of DLC film had been used in the experiment. The work on DLC coatings in the valvetrain, presented by Gangopadhyay et al. [53] shows that a small reduction in friction was seen in the valvetrain, but only when the component was unlubricated. Under lubricated conditions, valve buckets coated with DLC exhibited higher levels of friction than those with no coating. It seems from the literature, that although DLC testing in isolation has shown very promising results when it comes to friction reduction, that the practical applications in engines seem limited from a perspective of reducing friction. The benefits of DLC in both cases mentioned seem to be degraded by the introduction of lubricant. The use of DLC films may play a part in protecting the engine in the case of oil starvation. This also highlights the importance of lubricant choice and performance on the levels of friction in an engine.

In a 2009 paper, Fontaras et al. [54] studied the benefits of using low viscosity synthetic 0W-30 oils over higher viscosity 15W-40 mineral oils and 0W-40 synthetic oil. They reported reductions in Carbon Dioxide emissions of around 3% when using the low viscosity oil versus the 0W-40 oil. Surprisingly, this reduction was more pronounced than that observed between the low viscosity and the mineral oils. No consideration of any additives that may have been present in any of the oils was made in this paper, and these can have significant effects on the properties of the lubricant, as will be discussed later. The fuel consumption findings presented by van Dan et al. [55], in which a baseline 15W-30 was shown

to give 0.8% better fuel economy than a 15W-40, and 0.4% poorer fuel economy than a 5W30, are in agreement with the research by Fontaras. Tanaka [56] showed that using a 0W-20 lubricant would have similar effects on engine fuel economy, but also noted that the effects on engine wear were negligible when changing to this grade of lubricant.

Oil additives can be used to enhance the properties of oil in several ways. Common friction modifiers include oleochemical based (i.e. those derived from plants or animals) modifiers and Molybdenum based substances. Friction modifiers work by forming thin films on surfaces that have coefficients of friction lower than those of the surfaces themselves. The addition of a friction modifier to a baseline oil carried out by Sutton et al. [57] gave fuel economy improvements of 1% over the CEC M111 test cycle, which is a test designed to evaluate lubricant performance over conditions similar to the NEDC. No mention is made of what exactly the friction modifier was, other than it was a "new" organic friction modifier by Lubrizol.

Several studies have shown reduced friction when starving journal bearings of lubricating oil. Oil starvation of journal bearings can be accomplished by either reducing the width of the oil supply groove, or by reducing the feed pressure. Early work by Heshmat and Pinkus [58] observed that the reduction in power loss in the bearing was due to two main factors. Firstly, the starved bearing was able to support a film of smaller extent. This would reduce the shearing losses in the film. Secondly, the temperature of the film was increased due to the smaller volume of oil present. This led to lower oil viscosity and lower friction. Tanaka [59] reported the same effect of starving the journal bearings. Starvation also led to increased bearing eccentricity, which negatively impacted the bearing's ability to support load. In addition to the reduced frictional losses in the bearings due to starvation, the opportunity for a reduction in ancillary losses exists, as reduced feed pressure will require less work from the oil pump.

2.5 Discussion

The approaches to thermal management of internal combustion engines adopt the common goal of increasing the rate of warm up of the engine and its fluids in order to reach the fully warm operating temperature earlier. Methods of achieving this have ranged from heat exchange devices, to thermal optimization or energy recovery.

Reductions in fuel consumption of up to 3% have been reported in the literature through better thermal management. The potential for thermal management is an important starting point when assessing the usefulness of an approach. The works mentioned utilizes a variety of different engine capacities in their work, with 1.4 and 1.6l engines used in [37], and 3.0l engines used in [45]. Larger engines will emphasise the effect of thermal management techniques on an engine's fuel economy.

Modelling of the improvements that can be made through thermal management often over-predicts the effects of an approach to the fuel consumption of the engine. This is because the complex thermal interactions around the engine are often not being taken into account [60]. A review of modelling techniques carried out here showed that the benefits of using variable flow oil pump were only half of the simulated benefits, because the reductions in heat transfer resulting from reduced oil flow rates in the engine was not considered. This highlights the need for a computational model that is able to include the thermal interactions between the engine fluids and the structure into account, and make appropriate friction predictions that allow for such.

Chapter 3. The PROMETS model

3.1 Introduction

In this chapter, the history and background of the PROMETS model are described, to give an understanding of the purpose and scope of the model, and contributions from previous authors are identified. The rest of the chapter is concerned with an overview of the state of the model at the start of the project to describe the starting point for the work contained in the rest of the thesis. The engine dimensions and characteristics required for PROGEN to create a lumped capacity representation are listed along with the required test conditions. Finally, descriptions of each of the 7 sub models that make up PROMETS will be given along with their main governing equations.

3.2 PROMETS History and Development

PROMETS was developed at Nottingham University in collaboration with Ford Motor Company in order to simulate thermal behavior and other influences on the fuel economy of a range of engine types. The early work on PROMETS was reported by Christian [61] who developed a single cylinder, 23 element lumped capacity model written in C code. The results from this model compared favorably with those from existing Finite Element engine models, while being significantly more efficient in terms of the time and computing power required. Comparisons made in [61] showed high levels of agreement between the lumped capacity and finite element solutions when predicting cylinder temperatures during warm up, and when modelling valve train temperatures in [62]. The program included sub-routines describing in-cylinder heat transfer, oil heat transfer, coolant heat transfer and frictional dissipation.

PROGEN was developed to support the generation of the lumped capacity elements representing the engine structure and coolant volume. Data from analysis of engine design constraints and physical ratios found in production

engines were used to construct generic engine templates. Given certain fundamental attributes of the engine's design, for example, the bore, stroke, number of bearings and materials, PROGEN can build the templates into a lumped capacity representation of an engine with predicted mass and heat transfer characteristics.

Over the course of several more projects, the PROMETS model was expanded and refined, growing in complexity but still retaining its computationally efficient nature.

Yuen [62] added elements to represent the valves in both the intake and exhaust sides of the cylinder head as well as implementing solutions to calculate heat transfer around the intake and exhaust ports. Additionally, a model for predicting exhaust gas temperature was developed based on an engine energy balance, which also allowed for the effect of spark advances to be taken into consideration. Pinkerton [63] modified both PROMETS and PROGEN to allow for consideration of V-type engine designs, where both had previously only described inline 4 cylinder engines. Improved methods for predicting engine fuel consumption, as well as a friction model were added by Chick [64]. Fuel consumption was calculated using an iterative process that related gross indicated mean effective pressure to rate of fuel release, fuel lower heating value, combustion efficiency and gross indicated thermal efficiency. The friction model added was the PNH model mentioned in Chapter 2. Improvement to the gas side heat transfer correlation was done by Shayler et al [65] to form the QC1C2 correlation that separated the heat transfer rates for the cylinder and the exhaust port, allowing for greater fidelity in the description of heat transfer to the structure and the coolant from the working gas. Further refinement against experimental friction data was carried out by Leong [33], who implemented the improved PNH model that allowed each friction causing member to respond individually to changes in bulk oil temperature. The entire model was moved over to run in the Simulink modelling environment by Morgan [14], and rewritten in M code. Simulink provides a graphical user interface to manage the model and allows for a hierarchical model structure that was well suited to the PROMETS system. Law

[66] conducted work on the diesel version, and added models describing heat transfer around the piston and the interaction with piston cooling jet oil flow. Additionally, the number of elements surrounding the crankshaft main bearings was increased and the oil flow rate and thermal-friction interaction better described.

To summarise, work has been continuing on the PROMETS model for over 20 years, with a constant stream of improvements and updates, as well as a divergence between the spark ignition and diesel versions, as well as the in-line and V versions of the model. Not all changes have been integrated into all versions of the model, and it is often difficult to track the origins of certain pieces of the model.

3.2 The current PROMETS and PROGEN models

Each of the variants of PROMETS mentioned previously (Gasoline, Diesel, Inline, V-type) and be run in either single, or multi-cylinder mode. In single cylinder mode, the state of each cylinder is assumed to be identical and the coolant in the head and in the block is considered a uniform mass. When multi-cylinder mode is run, differences in boundary conditions for each of the individual cylinders and the coolant path through the engine are considered; the inboard cylinders are said to be adiabatically connected on both sides while the outboard cylinders have outer surfaces that are connected to ambient conditions.

The version of PROMETS referred to in the rest of this work will be the single cylinder representation of an inline 4 cylinder spark ignition engine, and the corresponding version of PROGEN. In this section, the model is described in the form before revisions were made as part of the project.

The PROMETS model itself consists of 7 subsections which represent important systems of the engine. There are the Cylinder and Port Heat Flux, Frictional Losses, Coolant Heat Transfer, Oil Heat Transfer, Exhaust Gas Temperature, Fuel Flow Prediction, and Structure Heat Transfer. These subsections are explored in the coming sections.

The 4 cylinder gasoline version of PROGEN generates a representation of the engine consisting of 41 lumped capacity elements of varying physical and thermal properties, depending on the specified materials and design constraints. Element sizes vary throughout the model: areas of greater complexity, or those expected to experience greater thermal gradients, such as the valve and intake/exhaust ports require higher resolution, and therefore smaller element sizes. Areas which are not heavily involved in thermodynamic process or are relatively remote, such as the crankcase walls are represented by fewer, larger elements. The element positions and their numbering are shown in Figures 3.1 to 3.3. Scaling factors are included which can be used to improve the accuracy of predicted element and fluid volumes and masses. They allow adjustment of PROGEN predictions of characteristics such as wall thicknesses in the coolant jacket, cylinders and crankcase, coolant volume in the head, block and auxiliaries and thickness of the piston ring pack. There are 10 scaling factors used in the current version of PROGEN. The scaling factors are not required to be altered before PROGEN runs, and are instead used to refine the results of the lumped capacity generator.

The variables listed in Tables 3.1 and 3.2 are the dimensions and options that need to be specified in order for PROGEN to generate the lumped capacity engine representation. These variables have been physically measured during a tear down of the VIPER engine. In addition to the physical characteristics of the engine, the model must also be supplied with details of the desired operating conditions of the test that is to be simulated. Inputs that are required by the model are engine speed and load. Other conditions such as the fuel flow rate, heater matrix flow rate, AFR, or exhaust temperature can either be predicted within the model, or dictated to the model if specific metrics for these values are required. The workflow for running a simulation is as follows. PROGEN must first be run; this populates a MATLAB workspace with the dimensions and properties of the elements which make up the engine representation. Next, a set of operating conditions must be input to the model to define the desired test. Once this information is received, the PROMETS model can be run.

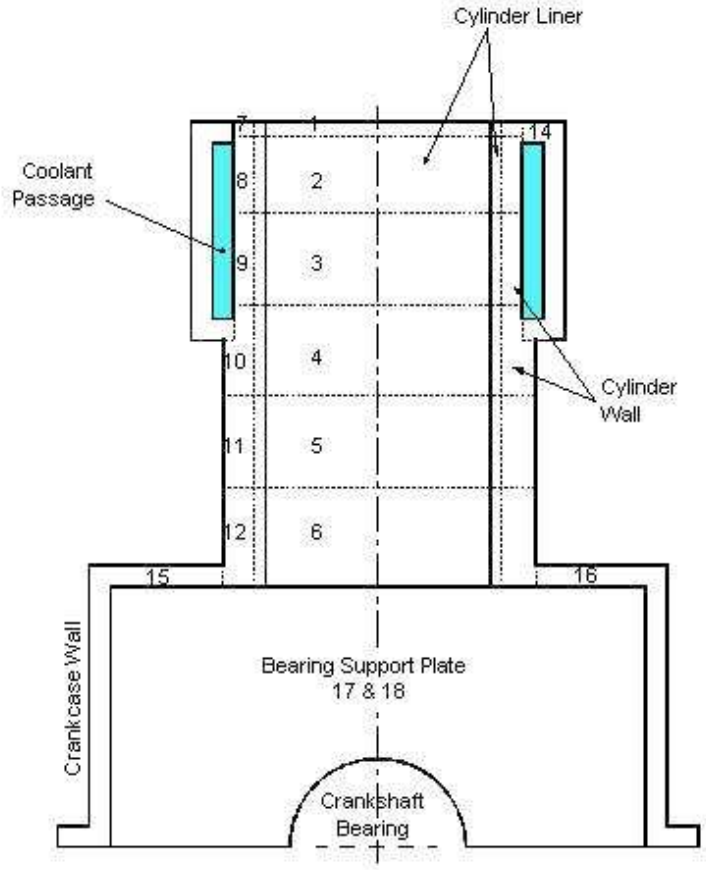

Figure 3.1 PROMETS block element positions

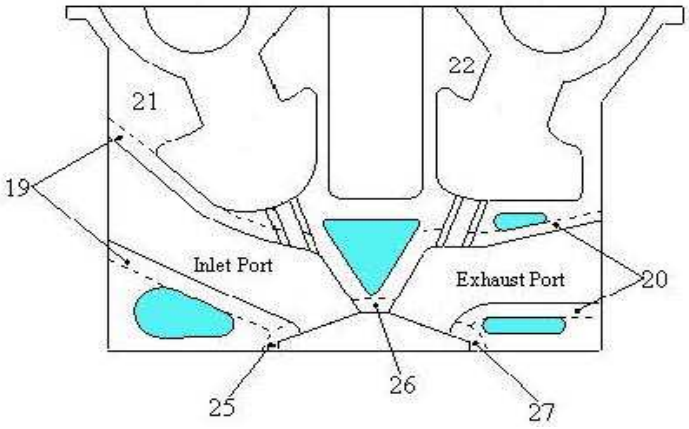

Figure 3.2 PROMETS cylinder head element positions

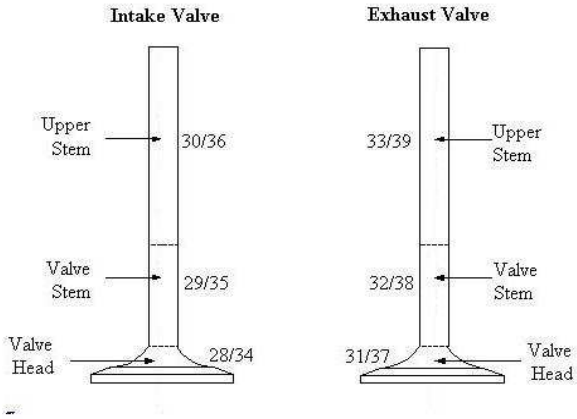

Figure 3.3 PROMETS valve element positions

Table 3.2. Head Variables for PROGEN

PROMETS name	Description	Notes
A2IN	Intake port vertical dimension	
B2IN	Intake port horizontal dimension	
FIN	Distance between head gasket and intake port bottom	
IN_VALVE_DIA	Intake valve diameter	-1=unknown
EX_PORT_LENGTH	Exhaust port length	
A2EX	Exhaust port vertical dimension	
B2EX	Exhaust port horizontal dimension	
FEX	Distance between head gasket and exhaust port exit bottom	
EX_VALVE_DIA	Exhaust valve diameter	-1=unknown
VALVE_ANGLE	Valve included angle	
MAX_VALVE_LIFT	Maximum valve lift	
NUM_IN_VALVE	Number of intake valves per cylinder	
NUM_EX_VALVE	Number of exhaust valves per cylinder	
VT_CONFIG	Valve train configuration	1= Single Overhead Cam with Finger Follower 2= Single Overhead Cam with Rocker Arm 3= Direct Acting Single Overhead Cam 4= Direct Acting Double Overhead Cam 5= Overhead Valve
FOLLOWER_TYPE	Follower type	1= Flat Follower 2= Roller Follower

Table 3.1. Block Variables for PROGEN

PROMETS name	Description	Notes
BORE	Cylinder bore	
STROKE	Engine stroke	
NUM_CYL	Number of cylinders	
WALL_TH1	Total wall thickness surrounding cylinder	
COOL_LEN	Mean Coolant passage height	Of the coolant jacket surrounding the cylinders
COOL_TH	Mean Coolant passage width	See above
BORE_SPACE	Distance between Bore centres	
LINER_TH	Liner thickness	-1 for no liner
HEAD_WIDTH	Head width	-1 for unknown. Mean distance between intake and exhaust manifold decks.
LINER_MAT	Liner material	1=Aluminium alloy, 2= Cast iron
HEAD_MAT	Head material	1=Aluminium alloy, 2= Cast iron
BLK_MAT	Block material	1=Aluminium alloy, 2= Cast iron
PTN_MAT	Piston material	1=Aluminium alloy, 2= Cast iron
PISTON_DEPTH	Piston depth	
CON_ROD	Connecting rod length	Distance between the bearings
RING1TOP	Distance from piston crown to top of 1st ring	
PACK_HGT	Ring Pack height	
DELTAC	Distance between inside and outside edge of ring	Mean of the 3 rings
RING_THK	Piston ring thickness	Mean of the 3 rings
RINGS_K	Piston ring thermal conductivity	
NUM_BEARINGS	Number of bearings	

3.3 The single cylinder model

To improve model running times and load times, a single cylinder representation of the engine can be used. Here, the cylinders are taken to have identical boundary conditions, and no differentiation is made between the inboard and outboard cylinders, or heat shared between cylinders. This approach is suitable when no detailed information about the thermal interactions between the cylinders is required. This approach also assumes the coolant volume to be a single mass with no variation in coolant temperature around the circuit. For the purposes of the VIPER project and the examination of the friction and oil sub models, the single cylinder version of the model has been selected as detailed examination of the coolant system is not part of the scope of the work. Future work on modelling engines that utilise techniques such as stalled coolant flow, or cylinder deactivation however, would require the use of the multi-cylinder model.

3.4 Structure heat transfer

The representation of the engine structure in PROMETS describes the metal that makes up the engine block, cylinder head, piston, valvetrain, crankshaft, camshafts and ancillary components in direct contact with fluids such as the coolant and oil pumps. The boundary of the model does not extend to either the intake or exhaust manifold. Other peripherals such as the alternator or fly wheel are considered to be sufficiently thermally detached to be of little thermal consequence to the engine and are not included in the lumped capacity representation. Each of the model elements is coupled to a number of adjacent elements and in some cases fluids. The coupling with fluids constitutes a boundary condition of the lumped capacity model, and is calculated in dedicated sub-models described later. These are the heat transferred from the in-cylinder gases, the oil circuit and the coolant circuit. Additionally, heat input to the structure from friction between moving surfaces has its own sub model. The final boundary condition of the model is formed by the heat transfer to ambient.

Each of the elements is considered to be isothermal due to the high thermal conductivity of the materials that form the engine structure. The temperature

change in elements is evaluated by calculating the net energy transfer to the element from all adjacent sources or sinks. This can be said to be equal to the total change in the internal energy of the element, and gives rise to the following energy balance:

$$\dot{Q}_i + \dot{Q}_e = \rho c V \left(\frac{T^{p+1} - T^p}{\Delta t} \right) \tag{3.1}$$

Where $\dot{Q}_i$ is the internal heat generated in the element, $\dot{Q}_e$ is the net energy transferred to the element from any combination of other structural elements, fluids, or friction, ρ is the element density, c is the specific heat capacity, V is element volume, T^p is the element temperature at the given time step, T^{p+1} is the temperature at the next time step and Δt is the length of the time step.

In order to calculate the temperature at the next time step, this balance is simply rearranged for T^{p+1} to give:

$$T^{p+1} = \frac{\Delta t}{\rho c V} \left(\dot{Q}_i + \dot{Q}_e \right) + T^p \tag{3.2}$$

In the case of element to element heat transfer, the energy transferred is calculated as follows:

$$\dot{Q} = A \left(\frac{\Delta T}{\frac{\Delta X}{k_1} + \frac{\Delta X}{k_2}} \right) \tag{3.3}$$

Here, A is the area of heat transfer between the two elements, ΔX is the length of the conduction path which is taken as the distance between the centres of the elements, and k_1 and k_2 represent the thermal conductivity of the elements.

3.5 Cylinder and port heat flux

Heat transferred from the in-cylinder gases to the engine structure is one of the major sources of heat in the engine, and accurate modelling of this is important when considering engine thermal behaviour. The correlation used to represent gas side heat transfer to both the cylinder and to the structure surrounding the exhaust ports is called the QC_1C_2 correlation and was developed by Shayler et al. [65] as a modification to the existing Taylor and Toong equation from [67]. The earlier solution did not differentiate between the two sources. The total rate of gas side heat transfer is given as:

$$\dot{Q}_{c1c2} = C_1\left(A_{cyl,eff} + C_2 A_{pt}\right)\frac{k_g}{B}\left(T_{g,a} - T_c\right)Re_g^{0.7} \tag{3.4}$$

This can be rearranged to give expressions for in-cylinder and port heat transfer:

$$\dot{Q}_{cyl} = C_1 A_{cyl,eff}\frac{k_g}{B}\left(T_{g,a} - T_{cool}\right)Re_g^{0.7} \tag{3.5}$$

$$\dot{Q}_{pt} = C_1 C_2 A_{pt}\frac{k_g}{B}(-T_{cool})Re_g^{0.7} \tag{3.6}$$

In these equations, the effective cylinder area $A_{cyl,eff}$ is the weighted area, once the total exposure time of each part of the cylinder throughout a cycle is accounted for. k_g is the value for the thermal conductivity of the gases in the combustion chamber, $T_{g,a}$ is the average temperature of the gas and T_c is the coolant temperature which is the final destination of the rejected heat. The gas temperature is defined using a cubic equation based on the equivalence ratio of the engine.

$$T_{g,a} = \frac{1}{a - b\phi + c\phi^2 - d\phi^3} + 0.35(T_{amb} - 300) \tag{3.7}$$

Equation 3.7 is based on a correlation in [68] that corrects the effective gas temperature from a measured value at ambient inlet temperatures. The cubic term in Equation 3.7 predicts the effective gas temperature when the intake tempereature is 300°K. The data to which these constants are fitted to can be found in [68]. The point at which this correlation was implemented into the PROMETS model is unknown, but comparison with other equations used to predict effective gas temperature in [69] and [70] show predictions that are within 25° of each other. Predictions from Equation 3.7 lie between those from the other correlations which allows for a degree of confidence in the results.

The equations described above are true for gas-side heat transfer when the spark timing is set to allow the generation of the greatest torque. When spark timing is retarded, be it to improve the speed of catalyst light off, or to reduce hydrocarbon emissions, the gas-side heat transfer will be increased [68]. This was tested in experimentally by Chick [64] by gradually retarding the spark from the angle of Minimum advance for Best Torque (MBT- θ) during steady state running and measuring the increase in heat rejection to the coolant. A square dependence on the retardation of the spark relative to MBT was applied to account for this.

$$\dot{Q}_{C1C2} = F_{spark}\dot{Q}_{C1C2} \tag{3.9}$$

$$F_{spark} = 1 + 0.0002\theta^2 \tag{3.10}$$

3.6 Coolant heat transfer

Coolant used to regulate engine temperature is described as a single sink in the PROMETS model, with two additive mechanisms by which heat is transferred from the structure: forced convection, and nucleate boiling. Chen [69] describes the development of heat transfer coefficients for both mechanisms and his relationships are used in the model. Heat transfer in areas of nucleate boiling is significantly higher than in areas where convective heat transfer dominates, as the boundary layer at the heat transfer surface is disrupted. However, beyond certain temperature deltas, a vapour film can begin to form on the surface, which

drastically reduces heat transfer and can lead to engine damage from overheating. The heat transfer coefficient for forced convection is given as:

$$h_{conv} = 0.023 Re^{0.8} Pr^{0.4} \frac{k}{D} \tag{3.11}$$

k is the thermal conductivity of the coolant, Re is the Reynolds number Pr is the Prandtl number and D is the diameter of the coolant passage under consideration.

The term for nucleate boiling is more complex, and is given by Chen [69] as:

$$h_{nb} = 0.0012 \left(\frac{k_c^{0.79} C_{pc}^{0.45} \rho_c^{0.49}}{\sigma^{0.5} \mu_c^{0.29} \lambda^{0.5} \rho_v^{0.24}} \right) (\Delta T_e^{0.24})(\Delta P_e^{0.75}) S \tag{3.12}$$

Here, the subscript c denotes a value for the coolant, v a value for the vapour and e an effective value. g is the gravitational constant, λ is the latent heat of vaporisation and σ is the vapour-liquid surface tension. S is a suppression factor that tends to unity at zero flow conditions, and zero at infinite flow. With the two component heat transfer coefficients found, the total heat transfer coefficient can be found as:

$$h = h_{conv} + h_{nb} \frac{T_s - T_{sat}}{T_s - T_{cool}} \tag{3.13}$$

Here, T_s is the surface temperature of the element with respect to which the heat transfer is being considered, T_{cool} is the coolant temperature and T_{sat} is the saturation temperature of the coolant.

To allow for the difference in structure and coolant temperature around the engine, the heat transfer coefficient is corrected using the ratio between local and average temperature differences as follows:

$$\bar{h} = \frac{1}{A} \int_0^A hF dA \tag{3.14}$$

where

$$F = \frac{(T_s - T_{cool})}{(T_s - T_{cool})_{ave}} \tag{3.15}$$

The final heat transfer to the coolant is then:

$$\dot{Q} = \bar{h}A(T_s - T_{cool}) \tag{3.16}$$

3.7 Oil heat transfer

The oil circuit in PROMETS is representative of the Ford CVH engine which featured in many Ford production vehicles in the 1980's. A summary diagram of the oil circuit is shown in Figure 5.1. Oil temperatures around the circuit are calculated by evaluating the energy flows at key locations using several different models.

Pressurised oil flows through galleries are described using the following correlation [61] where T_1 is the temperature at the desired location, and T_o is the temperature at the previous node:

$$T_1 = \frac{T_m + T_o\left(\frac{\dot{m}C_p}{\pi hDL}\right) - 0.5}{\left(\frac{\dot{m}C_p}{\pi hDL}\right) + 0.5} \tag{3.17}$$

It is assumed in [61] that the metal surrounding the gallery is isothermal along its length, and that the heat transfer to the oil is equal to the rise in enthalpy, as shown in Equation 3.18.

$$h\pi DL\left(T_m - \frac{T_o + T_1}{2}\right) = \dot{m}C_p(T_1 - T_o) \tag{3.18}$$

Additionally, an assumption that the oil flows through the galleries have low Reynolds numbers has been made [14]. The representative length L is based upon

head or block dimensions, depending upon where the gallery is located and its destination.

This correlation is used for the locations TC1, TC2, TU1 and TU4; See Figure 5.2 for location labels.

At locations where oil is used to lubricate moving surfaces, the frictional dissipation is calculated as a function of the friction power of the assembly, predicted using the PNH model. The thermal/friction interaction is solved by having fixed proportion of friction work driven to the oil; this is currently assumed to be 20% of the friction power.

The oil temperature at the valvetrain and bearings is described as:

$$T_1 = T_0 + \frac{P_f}{\dot{m}C_p} \tag{3.19}$$

Here, T_o is the temperature of the oil entering the valvetrain or bearings, and T_1 is the temperature of the oil leaving these locations.

At the piston, an additional term to account for heat transfer from the underside of the piston is used, assuming a heat transfer coefficient of 50W/m^{2}K [61].

As the oil leaves the bearings an oil mist is formed in the crankcase. The nature and behaviour of this mist is poorly understood. A heat transfer coefficient of 50W/m^{2}K is used to connect the elements in the liner and the crankcase wall to the oil, and the temperature is updated as:

$$T_{M1} = T_{TB1} + \frac{\dot{Q}_{mist}}{\dot{m}C_p} \tag{3.20}$$

The oil is directly thermally coupled to the coolant with a model describing an engine oil cooler. The temperature of the oil leaving the oil cooler is evaluated as the last node in the oil circuit. A fixed effectiveness value –0.4, is used to control the amount of heat transfer in the oil cooler. In the equation below, ε is the effectiveness of the oil cooler and C_{min} is the minimum heat capacity rate.

$$T_{out} = T_{in} + \frac{\varepsilon C_{min}(T_c - T_{in})}{\dot{m} C_p} \tag{3.21}$$

3.8 Exhaust gas temperature

Exhaust gas temperature prediction is based on a full engine energy balance to determine the amount of energy that is wasted in the exhaust flow. The inputs to the engine system are the air and fuel enthalpies at the engine inlet, and the heat released from the fuel through combustion. The energy is utilized or dissipated as brake power, friction power, heating of the cylinder and exhaust ports or is lost to ambient. The rearranged balance for exhaust enthalpy is therefore:

$$\dot{H}_{ex} = \left(\dot{H}_{air} + \dot{H}_{fuel} + \dot{H}_r\right) - \left(\dot{P}_b + \dot{P}_f + \dot{Q}_{cyl} + \dot{Q}_{pt} + \dot{Q}_{amb}\right) \tag{3.22}$$

Brake power is calculated as a function of the speed and load profiles specified in the initialization of the PROMETS model:

$$P = 2\pi NT \tag{3.23}$$

Friction power is calculated using the equations described in the next section, and in-cylinder heat transfer was covered in the previous section. Heat transfer to ambient is handled using a heat transfer coefficient of 10W/m^{2}K from the elements that make up the exterior of the engine. This was shown to be suitable for comparison to engines installed on test beds with no blowers to increase the air flow over the engine [70]. Fuel and air enthalpies are both calculated using the following equation with the appropriate values for each fluid:

$$\dot{H} = \dot{m} c_p (T - T_{amb}) \tag{3.24}$$

The heat released from the combustion of fuel is a product of the fuel flow rate, the lower heating value of the fuel, and the combustion efficiency of the engine. Combustion efficiency and fuel flow rate are calculated as described in a Section 3.10.

$$\dot{H}_r = \dot{m}_f Q_{LHV} \eta_c \tag{3.25}$$

After resolving the energy balance, the exhaust enthalpy is used to calculate temperature:

$$T_{ex} = \frac{\dot{H}_{ex}}{\dot{m}_{ex} c_{p\,ex}} + T_{amb} \tag{3.26}$$

3.9 Frictional losses

The friction model present in PROMETS is an adaptation of the work done by Patton et al. in [25]. The Patton model is not capable of predicting friction levels from a cold start, and can only be used for values when the oil has reached its normal operating temperature. To overcome this, the model was scaled by a ratio of oil viscosity over the oil viscosity at 90°C. Due to divergence of work and focus between versions of the PROMETS model, this is not the most recent version of the friction model considered within the Engines Research Group and although it still produces adequate results, it lacks the ability to examine individual component's sensitivity to changes in oil temperature.

The equations given in [25], and used to calculate engine friction in PROMETS are listed below.

$$FMEP_{crankshaft} = C_{cs}\left(\frac{D_b}{B^2 S n_c}\right) + C_{cb}\left(\frac{N D_b^3 L_b n_b}{B^2 S n_c}\right) + C_{td}\left(\frac{D_b^2 N^2 n_b}{n_c}\right) \tag{3.27}$$

The three terms in Equation 3.27 describe the friction contribution from the crankshaft, specifically from the crankshaft oil seals (C_{cs}), the shearing of the oil film within the bearing(C_{cb}), and the turbulent dissipation arising as the oil is pumped through the bearing (C_{td}) respectively.

$$FMEP_{reciprocating} = C_{ps}\left(\frac{S_p}{B}\right) + C_{pr}\left(\frac{1+1000}{N}\right)\frac{1}{B^2} + C_{gl}\left(\frac{p_i}{p_a}\right)(0.088r_c + 0.182r_c^{1.33-0.0283S_p}) + C_{be}\left(\frac{ND_b^3L_bn_b}{B^2Sn_c}\right) \quad (3.28)$$

The reciprocating friction equation shown in Equation 3.28 represents the piston assembly and big end bearings. The first term describes the friction of the piston skirt, the second the piston rings, the third the increase in piston ring friction due to gas pressure loading, and the fourth the contribution from the big end bearings.

$$FMEP_{valvetrain} = C_{vs} + C_{vb}\left(\frac{Nn_b}{B^2Sn_c}\right) + C_{rf}\left(\frac{Nn_v}{Sn_c}\right) + C_{ff}\left(1+\frac{1000}{N}\right)\frac{n_v}{Sn_c} + C_{oh}\left(\frac{L_v^{1.5}N^{0.5}n_v}{BSn_c}\right) + C_{om}\left(1+\frac{1000}{N}\right)\frac{L_vn_v}{Sn_c} \quad (3.29)$$

Equation 3.29 shows the friction generated in the valvetrain. The first term represents the contribution from the camshaft bearing seals. The second term represents the camshaft bearings. The third and fourth terms represent roller followers and flat followers respectively. Only one of these is used in the final equation depending on the engine configuration. The fifth term represents friction from valvetrain components lubricated in the hydrodynamic regime, and the sixth term represents those components lubricated in the mixed regime.

Finally, the auxiliary friction is calculated as a function of engine speed. The auxiliary FMEP gives a predicted value for the parasitic losses imposed on the crankshaft as a result of turning the fuel, coolant and oil pumps.

$$FMEP_{auxiliary} = 6.23 + 5.22 \times 10^{-5}N - 1.79 \times 10^{-7}N^2 \quad (3.30)$$

Overall engine friction is therefore:

$$FMEP = FMEP_{crankshaft} + FMEP_{reciprocating} + FMEP_{valvetrain} + FMEP_{auxiliary} \quad (3.31)$$

As the engine, and therefore the lubricating oil warms, its viscosity will fall. The reduction in friction due to this fall in viscosity is described in equation (3.32). Total engine friction is scaled by a ratio of oil viscosity to fully warm oil viscosity. At low temperatures this ratio will be >1, resulting in higher levels of friction. As the oil temperature increases towards its fully warm value, usually set at 90°C, the friction will fall.

$$FMEP_{wu} = FMEP_{fw}\left(\frac{\mu}{\mu_o}\right)^{0.24} \quad (3.32)$$

The friction index is lower than the value of 0.5 used in the improved PNH model [27]. This is due to the fact that the correction is applied to the entire term in this case, whereas the PNH model used a correction only to terms assumed to be operating in hydrodynamic lubrication regimes.

The friction work is dissipated to either the oil or to the engine structure. This is currently achieved by assuming that 20% of the friction power will be dissipated into the oil, and the remaining 80% will heat the engine structure. Oil viscosity is calculated using the Walther equations (see Equation 4.11, Section 4.9), which outputs values for kinematic viscosity.

3.10 Fuel flow rate

The predictions of fuel flow rate are iteratively calculated to satisfy the gross indicated power requirements of the engine model. Fuel flow rate can be expressed as a product of the indicated gross specific fuel consumption and the gross indicated power.

$$\dot{m}_f = ISFC_{gr}\dot{W}_{g,ind} \tag{3.33}$$

The gross indicated power is a function of gross indicated mean effective pressure, which is itself a sum of the brake, friction, auxiliary and pumping mean effective pressures.

$$\dot{W}_{g,ind} = \frac{IMEP_g V_s N}{120} \tag{3.34}$$

$$IMEP_g = BMEP + FMEP + AMEP + PMEP \tag{3.35}$$

FMEP and AMEP are calculated as described later in this chapter. The BMEP is defined by the operating speed and load profile of the engines running conditions. The PMEP is taken as the difference between the pressures in the intake and exhaust manifolds. The gross indicated specific fuel consumption can be found using an expression including the lower heating value of the fuel, the combustion efficiency and the gross indicated thermal efficiency.

$$ISFC_g = \frac{1}{Q_{LHV}\eta_c\eta_{g,ind}} \tag{3.36}$$

Combining Equations 3.34 and 3.36 gives Equation 3.37, a relationship for the fuel flow rate demand of the engine.

$$\dot{m}_f = \frac{I\dot{M}EP_g V_s N}{Q_{LHV}\eta_c\eta_{g,ind}120} \tag{3.37}$$

The lower heating value for gasoline is approximated as 44 MJ/kg. Combustion efficiency is taken to be 98% when the engine is running lean with high AFR. When the AFR is lower than the stoichiometric value of 14.7:1, a quadratic based on the equivalence ratio is used to calculate combustion efficiency.

$$\eta_c = 2.662 - 2.26\phi + 0.577\phi^2 \tag{3.38}$$

Where ϕ is the fuel-air equivalence ratio.

3.11 Discussion

PROMETS is a collection of models and sub-models that has been under development within the Engines Research group since the 1990's and has diverged into several versions representing different engine types. Functionality has been added and removed from these versions to varying degrees, and this chapter has summarised this development, as well as given an overview of the current state of the 4 cylinder spark ignition version of PROMETS. The main equations used in each of the major sub-models have been given and the reader is directed to the references given for a fuller description of these by their authors.

The PROMETS model is strong in its generic representation of engines and the thermal interactions that take place during running. The model has been well correlated with experimental data over the course of several projects, and on the whole, makes accurate predictions of engine performance. This ability is maintained in the model whilst remaining computationally efficient.

The main weakness of the model from a thermal perspective is the lack of sensitivity to temperature differences around the engine. The current friction model uses the bulk oil temperature to correct for viscosity, and this is adequate for describing the way in which friction decreases as the engine warms under standard conditions. However, a bulk oil formulation will not capture the effects of changes that might be made to the thermal gradients around the engine, which are a focus of this project. The friction model will therefore be changed to evaluate the viscosity of the oil separately for each rubbing surface.

To synergise with the improved friction model, the oil circuit will be updated and additional functionality will be included in the form of piston cooling jet, and main bearing energy flow models. The sequence in which the oil circuit temperature are calculated will also be changed to reflect the oil flow paths in the VIPER engine. This will make the PROMETS oil circuit more representative of the VIPER engine, as well as increasing the robustness of predictions on the effects of changes to the thermal balance of the engine.

Chapter 4. Advancing the PROMETS friction model to account for local thermal conditions

4.1 Introduction

The formulation of the friction model used in PROMETS has been revised in the current studies to address the limitations of using "bulk" oil temperature and viscosity to characterise changes in friction during engine warm up. Although computationally efficient, and generally accurate when used to predict changes to total engine friction, this approach does not allow for differing effects on local conditions at rubbing surfaces. Additionally, results of design changes were unable to be properly explored. The aim here has been to revise the treatment of friction predictions in the model to allow for the effects of "local" oil states to be captured. The underlying physics-based formulation laid out in [71] remains unchanged, but where viscosity affects a component's friction, the correction has been based on a particular temperature local to the rubbing surface. In this chapter the reasoning behind and the process of improving the current friction model are explained.

The friction model in PROMETS draws on the formulation given in [25] which gives predictions for fully warm conditions and has no mechanisms of accounting for increased friction during the engine warm up; The friction equations in the original version of the model contained no dependence on oil temperature. This functionality was added in [27] and [26], using a bulk oil temperature correction.

A version of the original formulation in [25] was modified for use in PROMETS by applying a bulk viscosity based correction to FMEP predictions to reflect the increase in friction due to high oil viscosity during warm up. Petroff's equation (Equation 4.6) shows a dependence of friction on viscosity. All friction contributions are scaled according to a ratio of bulk oil viscosity to the viscosity of oil at a fully warm reference temperature so that:

$$FMEP_{warm\ up} = FMEP\left(\frac{\mu}{\mu_o}\right)^n \tag{4.1}$$

Based on comparisons with experimental results for engine friction changes during engine warm-up, the index n was set at 0.24. This caused total engine friction to decrease as the engine, and more importantly the oil, warms up. The index is low, as the original correction is applied to the entire friction prediction and not all components of engine friction depend on oil viscosity in the same way. Indeed, some elements which operate in the boundary or mixed lubrication regimes are almost totally independent of viscosity. The Stribeck curve in figure 2.1 shows the relationship between the coefficient of friction, and a duty parameter which is a function of relative speed between rubbing surfaces, lubricant viscosity and load.

It is important to note the difference between the friction calculation in the model, and the equations given in [27] and [26]. The first scales the friction for the complete engine by a viscosity ratio as shown in Equation 4.1, while the latter two scale selected friction contributions that are lubricated in the hydrodynamic regime as shown in Equation 4.2.

$$FMEP_{warm\ up} = FMEP_{B,M} + FMEP_H\left(\frac{\mu}{\mu_o}\right)^n \tag{4.2}$$

This dependence on bulk oil temperature did not fully describe observed initial friction, or the reduction in friction throughout the early stages of warm up. At engine start, engine friction is significantly higher than that predicted using a viscosity correction based on bulk oil temperature alone. The fast rate of friction reduction due to localised warming of oil at the rubbing surfaces was also not captured in equation 4.1. An additional correction was formulated by Burrows [72] to take into account increased friction at engine start-up and the first seconds of running during which the early temperature variations around the engine develop. This took the form:

$$C_f = \left(C_{f0} - 1\right)e^{(-1/\tau)} + 1 \tag{4.3}$$

Where

$$C_{f0} = 1 + 0.55e^{-T_{oil}/35} \tag{4.4}$$

The value for τ which defines the rate of decay of this effect was found to accurately model warm up friction when a value of 50 seconds is used. The factor C_f was then further applied to Equation (4.1) to give a final prediction of friction from engine start. This was an empirical approach that does not lend insight into the underlying friction behaviour during these initial seconds.

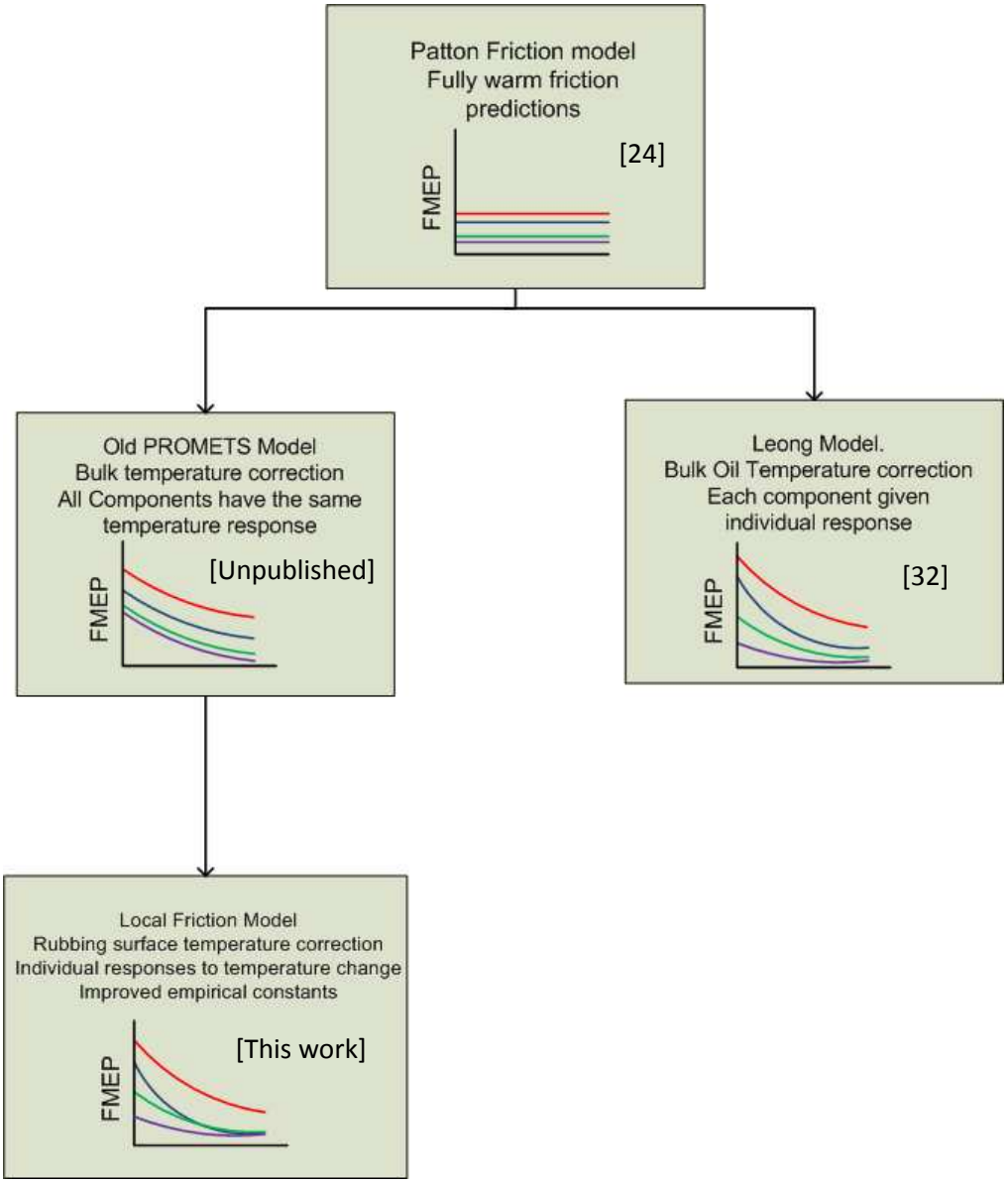

Figure 4.1 Summary of changes made to the original friction model developed by Patton et al. [24]

4.2 Friction correction based on local temperatures

In previous sections, the way in which the prediction of engine friction has been treated in earlier versions of the PROMET model has been examined. The correction to friction contributions based on bulk oil temperature used in the previous versions of the friction model gives good predicted results for steady state running conditions. The success of this approach depends on the temperature variations throughout the engine relative to the bulk oil remaining stable during warm up and over the operating range of speeds and loads of interest. The weaknesses of this include not capturing the effects of the development of temperature variations during early seconds of engine running, and an insensitivity to design changes intended to promote or exploit novel engine features. By having a model sensitive to local changes in temperature due to transient conditions, more accurate friction and fuelling predictions of situations where the engine's thermal distribution has been altered may be made. This is of especial importance if future work on disruption to an engine's natural temperature distribution is required. In order to achieve this, the way in which the friction prediction in the PROMETS model has been examined and altered to give each component a discrete sensitivity to changes in oil temperature. Rubbing surface temperature should rise much more rapidly than the bulk oil temperature, and by using these to evaluate friction, the need for a cold start correction should be removed. The following sections will describe the work done by the author to implement a friction model that uses local temperature to evaluate oil viscosity in the calculation of component friction.

4.2.1 Crankshaft friction

Crankshaft friction is a sum of the resistance to shear in the bearing oil film, the work required to pump the oil and the contributions from the front and rear oil seals. The main bearings operate mainly in the hydrodynamic regime, although it is stated in [23] that due to the sharp increase in torque after the piston reaches top dead centre, the bearing briefly moves into a mixed lubrication regime. For this application, it will be assumed that the bearing always operates hydrodynamically. As the rotating surfaces will almost always be separated by the oil film, it is the properties of the oil that will define the friction. The material properties, minus the thermal expansion coefficients, may be neglected. The bearing seals are said to operate with boundary lubrication exhibiting a reduction in friction with temperature that is reported by Leong [71] to be small enough to neglect, and is dependent on material as opposed to lubricant properties. By far the largest friction contributors of the three components are the main bearings. The factor which most influences the friction of the main bearings is the rotating contact surface area. Given that the length of a bearing is limited by the minimum length required to generate a load supporting film, reducing the diameter is the best candidate for reducing crankshaft friction through design changes [73]. Any reduction in bearing diameter however must be balanced against the accompanying loss in crankshaft stiffness caused by decreased overlap. Partial starvation of journal bearings is another approach to reducing crankshaft friction. This may be achieved by reducing the pressure of the oil supply. This leads to a reduction in the extent of the oil film in the bearing which reduced the losses due to film shearing. Parasitic losses from the oil pump are also reduced.

The starting point for the crankshaft friction formulation was the bulk oil temperature corrected version of the model presented in [25]. Equation 4.5 gives the formulation for the local temperature correction.

$$FMEP_{crankshaft} \tag{4.5}$$
$$= C_{cs}\left(\frac{D_b}{B^2 S n_c}\right) + C_{cb}\left(\frac{N D_b^3 L_b n_b}{B^2 S n_c}\right)\left(\frac{\boldsymbol{\mu_b}}{\boldsymbol{\mu_o}}\right)^1$$
$$+ C_{td}\left(\frac{D_b^2 N^2 n_b}{n_c}\right)$$

Here, the term that describes the contribution from the shearing of the oil film within the main bearings, C_{cb}, has been scaled with the viscosity of oil in the main bearings over the viscosity of oil at its fully warm operating temperature. In the previous PROMETS version of the model, the bulk oil viscosity ratio was raised to the power of 0.24. In the local oil temperature model, each of the terms relating to hydrodynamic lubrication have been given a separate index to reflect the nature of the rubbing surface and their expected response to changes in operating temperature. Friction in the journal bearings in the valvetrain and crankshaft are assumed to follow Petroff's Law [74] which gives the coefficient of friction as:

$$f = \frac{2\pi\mu URL}{c} \tag{4.6}$$

As such, the index value for the crankshaft and valvetrain bearings has been set to 1. As the main bearing term accounts for the bulk of the crankshaft friction contribution, this gives the equation a strong response to changes in viscosity and therefore temperature. The additional friction caused by the oil being below the normal operation temperature is illustrated in Figure 4.2. The friction penalty is around 20kPa at its highest, when the engine starts, and the oil is at is coldest.

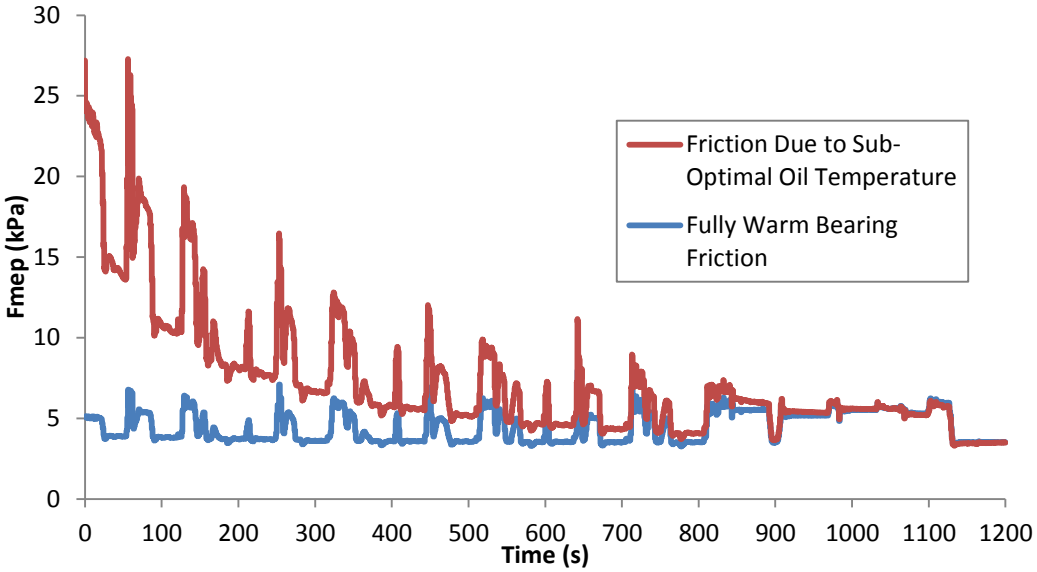

Figure 4.2 Crankshaft friction during the aNEDC. The blue line shows bearing friction if the engine oil were fully warm at the start of the test.

The temperature used to evaluate the oil viscosity for the crankshaft term is taken as T_{b1} in PROMETS: the temperature of the main bearing film. This temperature prediction is described in the next chapter as an iterative process solving for heat transfer to the structure and heat retained in the oil film. This allows for an improved prediction of the final destinations of the heat released though frictional dissipation. The friction calculated in Equation 4.5 is used as an input to this process. The prior solution to the frictional dissipation problem in the PROMETS model was to assume that a fixed proportion of it will be rejected to the structure and the rest retained in the oil.

4.2.2 Reciprocating friction

The reciprocating group describes the friction contributions from both the piston interfaces with the cylinder wall and the big end bearings. The full equation for the reciprocating group is given below. As proposed in [26], the contribution to piston friction from gas pressure has been removed from Equation 3.28. This term represents friction that was previously attributed to the increased tension of the piston rings due to gas pressure. In [26], Shayler and Leong explain that following examination of data from motored engines, the increase in friction could be accounted for by changes in the pumping work as opposed to the ring tension.

$$FMEP_{reciprocating} = C_{ps}\left(\frac{S_p}{B}\right)\left(\frac{\mu_r}{\mu_o}\right)^{0.5} + C_{pr}\left(1+\frac{500}{N}\right)\frac{1}{B^2}\left(\frac{\mu_r}{\mu_o}\right)^{0.5} + C_{be}\left(\frac{ND_b^3L_bn_b}{B^2Sn_c}\right)\left(\frac{\mu_c}{\mu_o}\right) \quad (4.7)$$

These make up the most significant source of frictional losses throughout the operating range of engine speeds and oil temperatures [75].

Literature is divided as to the relative importance of the contributions of the piston rings and the piston skirt. A combination of predicted and measured results in [76] and [77] suggest that the rings are the significant contributor to piston friction, whereas investigation of the effects of piston skirt and ring friction on engine efficiency in [78] suggest the opposite. The model on which this work is based on falls into the former camp.

The rings are estimated to contribute around 70% of the piston assembly friction [79], and so are of significant interest. The piston ring pack comprises of three metal rings that serve to seal the combustion chamber from the crankcase whilst allowing the piston to travel up and down the cylinder. The uppermost two rings are known as the compression rings. The top ring's main function is to prevent gases from the combustion chamber from entering the crankcase past the piston, and will therefore be subject to the highest pressures and temperatures of the

rings. The second compression ring is required to prevent upward migration of oil into the combustion chamber as well as providing a gas seal. The final and lowermost ring is called the oil control ring, which can also feature a spring to improve contact with the cylinder and is used to scrape oil back down to the crankcase after it has been used to lubricate and cool the piston [16]. Results from [80] showed that the largest contributor to the piston ring pack friction was the oil control ring, followed by the first, and then the second compression rings. Viscosity scaling of the terms describing the piston rings and piston skirt has been added with the assumption that these behave as a thrust or slider bearing. The friction coefficient of these bearings is given in [81] and [82] as equation 4.8.

$$f = \sqrt{\frac{\pi U}{W/L}}\mathrm{F} \tag{4.8}$$

Where F is a non-dimensional number dependant on the pad inclination. The root dependence of the friction coefficient to viscosity in this equation led to the adoption of a value of 0.5 for n for both the piston rings (C_{pr}) and piston skirt (C_{ps}). This is in line with modelling described in [18] [20] [23].

This assumption does not account for the changes in lubrication regime experienced by the piston ring pack at TDC and BDC. Bolander et al. [83] showed experimentally that as the piston decelerates as it approaches TDC and BDC the hydrodynamic action of the rings decreases until it is no longer sufficient to form a film that is thick enough to prevent asperity contact. This causes a move towards mixed and eventually boundary lubrication at these crank angles. In the context of PROMETS, which provides crank averaged predictions across the engine it has been assumed that the lubrication regime will be hydrodynamic as this accounts for the majority of the stroke. The big end bearings index is set at 1, in line with that used for the main bearings.

The temperature of the cylinder liner was shown experimentally by Leong et al. [71] as being strongly linked to the friction behaviour of the piston group, with much weaker correlation being shown with top dead centre, bottom dead centre

and oil sump temperatures. The PROMETS element that corresponds to the mid stroke liner is element 3, and this has been used to evaluate the viscosity of oil at this location. Measurements of oil film thickness in [84] and [85] show oil film thickness ranging from 2 to 8.4 microns, which would imply a relatively small thermal capacity. Film temperature at the mid-stroke is therefore assumed to be controlled by the metal temperature at this location and this is used to evaluate the oil viscosity for the piston group. To describe the thermal-friction interaction between the piston rings, skirt and the liner the approach of Zoz [86] has been followed. It is stated here that the energy dissipated as friction is forced directly to the cylinder liner. Figure 4.3 gives the distribution of heat sources for the cylinder liner elements in PROMETS. The majority of the piston friction is assumed to be dissipated at the mid-stroke liner position. The oil in the big end bearings is assumed to be at the same temperature as that of the main bearings and so the temperature T_{b1} is used.

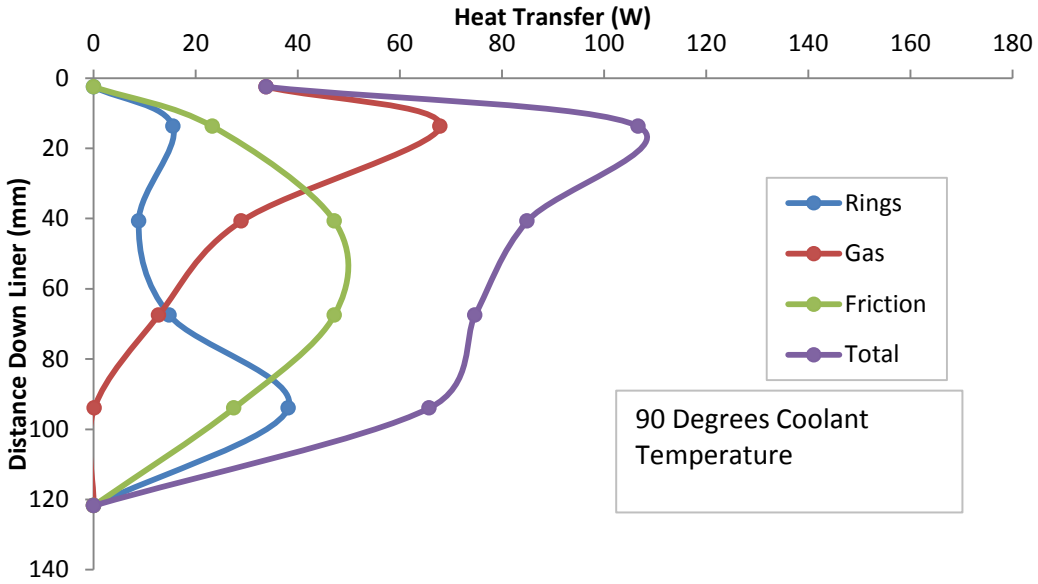

Figure 4.3 Distribution of heat input down the cylinder liner at 2000RPM 120Nm

4.2.3 Valvetrain

The valvetrain prediction accounts for friction that arises from the camshaft bearings, the cam followers, and the valves themselves. The VIPER engine utilises double overhead camshafts with direct acting bucket followers. Valvetrain friction can vary significantly with configuration type, with the type of cam follower and valve lifter used being the largest source of variation. Because of the increased contact area between cam and tappet, bucket followers typically generate higher frictional forces than roller followers [87].

It is well established that, in the valvetrain, boundary lubrication is the dominant regime [16]. Boundary friction occurs at low duty parameters on the Stribeck curve (Figure 2.1), where there is insufficient pressure in the oil film to allow the film to support the load being applied. From this it can be inferred that the oil film is particularly thin in this location, allowing for the film to regularly break down. The assumption therefore has been made that, as with the liner oil film, the surrounding metal temperature will dictate the film temperature at these locations. An average of the metal temperatures of the intake and exhaust sides of the cylinder head has therefore been used as the representative temperature for the valvetrain friction.

Within the valvetrain prediction, viscosity scaling is applied to the terms for the camshaft bearings (C_{vb}), and for the oscillating hydrodynamic term (C_{oh}), which describes the portion of the friction around the valves which are lubricated in the hydrodynamic regime. The constant 4.12 is used to represent the contribution from the camshaft seals. The follower friction (C_{ff}) and the friction from the valves in the mixed regime (C_{om}) receive no viscosity scaling.

$$FMEP_{valvetrain} = 4.12 + C_{vb}\left(\frac{Nn_b}{B^2Sn_c}\right)\left(\frac{\mu_v}{\mu_o}\right) + C_{ff}\left(1+\frac{500}{N}\right)\frac{n_v}{Sn_c} + C_{oh}\left(\frac{L_v^{1.5}N^{0.5}n_v}{BSn_c}\right)\left(\frac{\mu_v}{\mu_o}\right) + C_{om}\left(1+\frac{500}{N}\right)\frac{L_v n_v}{Sn_c} \quad (4.9)$$

Other models, such as that by Rezeka and Henein [18] also use terms that describe the force of the valve springs and stiffness. These are not used in this model and are accounted for in the engine speed terms and the C constant.

The friction thermal interaction in the valvetrain is poorly understood. In the absence of further knowledge of the way that the friction is dissipated into the oil in the valvetrain, the approach from previous versions of the PROMETS model has been retained. A fixed 20% of friction power is assumed to be dissipated in the oil throughout the warm-up. This assumption was based on bulk oil warm-up and friction data. Results were not highly sensitive to changes in this value, because heat transfer to the oil from the structure tends to dominate the thermal characteristics at this location. Predictions of heat transfer to the oil show that 3-4 times more energy is input to the oil from the structure versus frictional dissipation when using this 20% assumption during an aNEDC simulation. While the camshafts could be assumed to operate in the same manner as the main bearings when considering frictional dissipation, their contribution to friction is sufficiently small as to not impact the confidence in simulated predictions for oil temperature.

4.2.4 Ancillaries

The ancillary load on an engine will vary depending on the installation type. On the experimental rig, the VIPER engine is fitted with the fuel, oil and coolant pumps, whereas in a vehicle the front end ancillary drive would also include the alternator and air-conditioning pump. The model has been set up to mimic the engine as installed on the test bed.

The form of the relationship from [26] has been retained to describe the friction of the ancillary pumps.

$$FMEP_{aux} = \alpha + (\beta N + \gamma N^2)\left(\frac{\mu}{\mu_o}\right)^n \tag{4.10}$$

This equation gives a prediction of the parasitic loss incurred on the crankshaft with driving each pump, as opposed to the friction within the pump. Work done experimentally on the VIPER engine to measure coolant pump power consumption demonstrated no significant reduction in the amount of power required to operate an externally driven coolant pump as the temperature of the oil or coolant increased. The term $(\mu/\mu_o)^n$ should therefore be removed from Equation 4.10 when calculating coolant pump FMEP. Coolant and oil pump coefficients have been altered from values in [26] to give better agreement with experimental data, and an updated list of coefficients is given in Table 4.1. The oil and fuel pump both use the bulk oil temperature for viscosity correction. Figure 4.4 shows a comparison between the FMEP contributions from each pump. Figures 4.5-4.7 show experimental pump power derived from measured pump speed and torque for the coolant and oil pump as well as predicted values for fully warm and warm up conditions

Table 4.1 Coefficient Values for Ancillary FMEP Calculation

Pump	**α**	**β**	**γ**	**n**
Coolant Pump	1.3	0.003	$7\text{x}10^{-8}$	0
Oil Pump	8	0.004	$-1\text{x}10^{-6}$	0.6
Fuel Pump	1.72	0.00069	$1.2\text{x}10^{-7}$	0.5

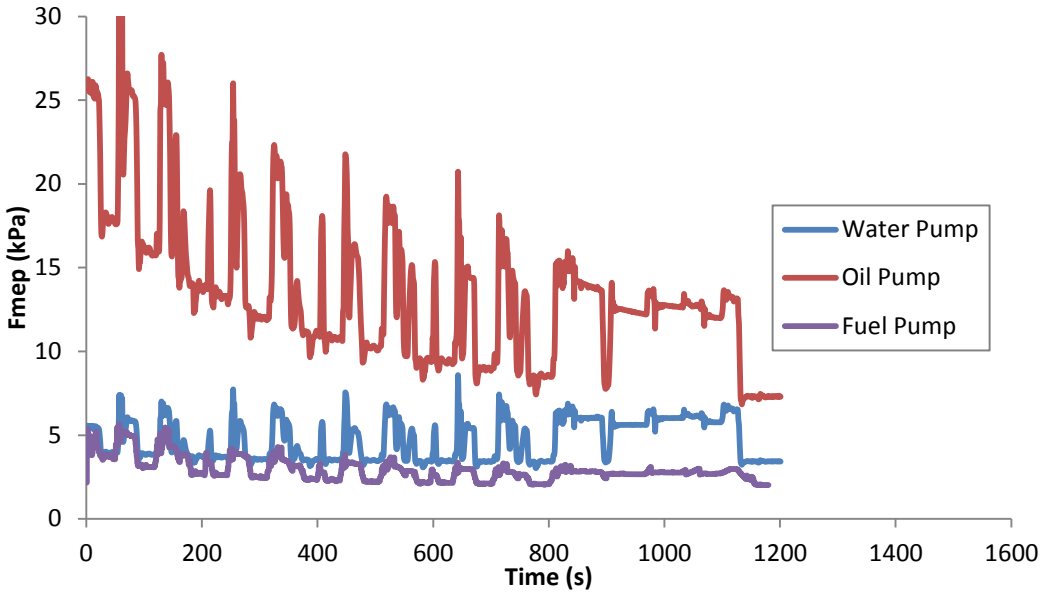

Figure 4.4 Ancillary pump FMEP contributions over the aNEDC. The Oil pump is the most significant source of ancillary friction

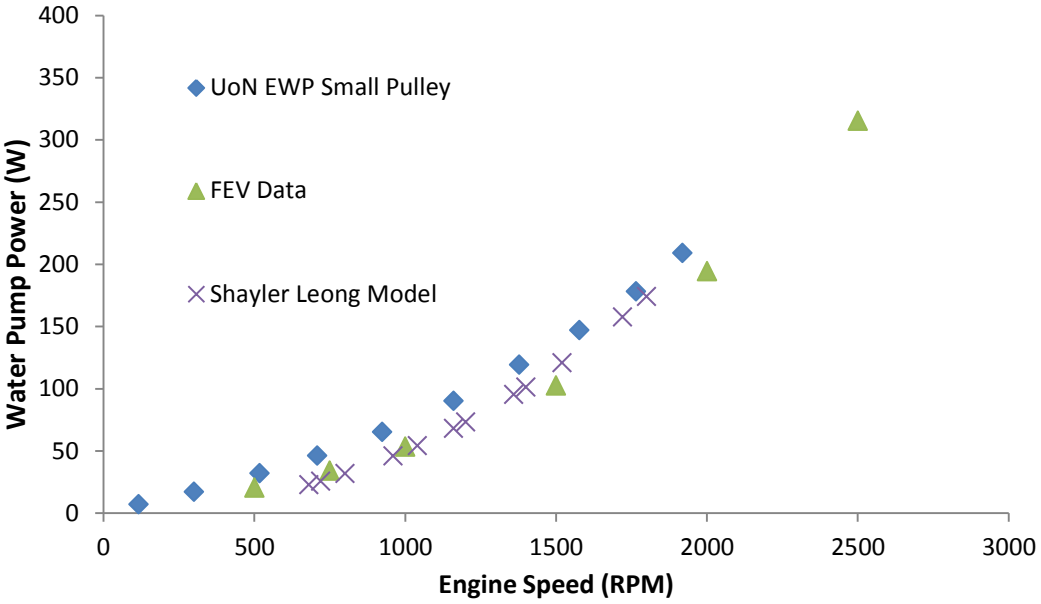

Figure 4.5 Predicted water pump power consumption with experimental measurements

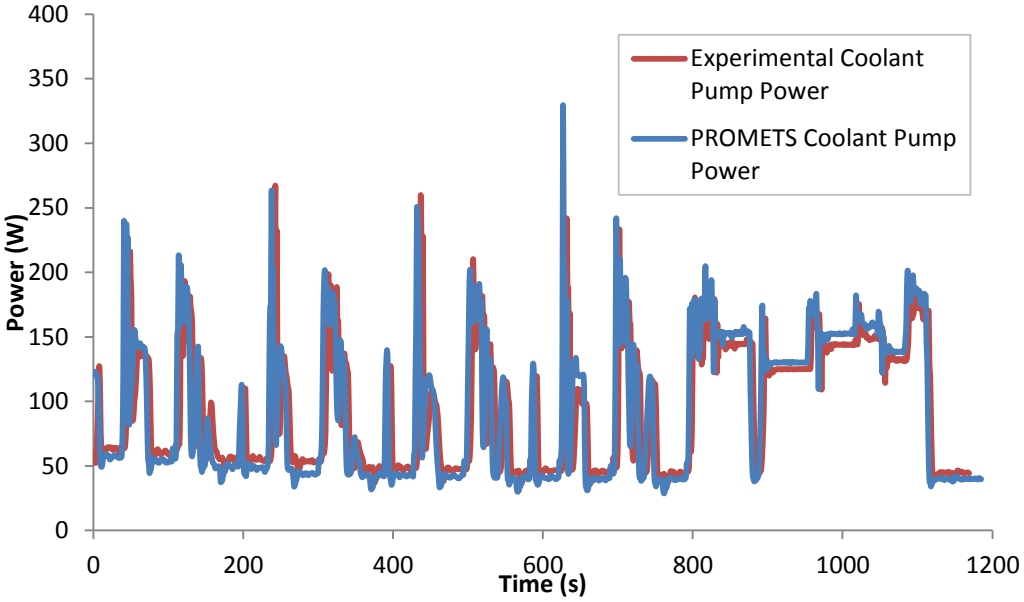

Figure 4.6 Instantaneous measured and predicted coolant pump power consumption over the aNEDC

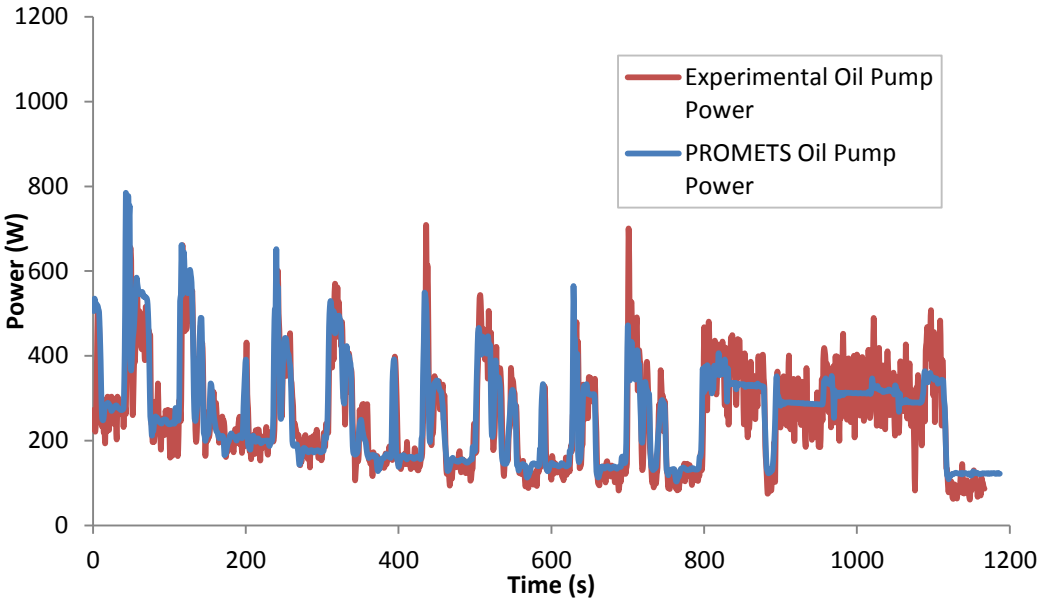

Figure 4.7 Instantaneous measured and predicted oil pump power consumption over the aNEDC

4.5 Empirical C constants

The empirical C constants in Equations 4.5, 4.7 and 4.9 are used in the model to account for factors not explicitly described in the model such as absolute oil viscosity, and to correct predicted friction results to obtained experimental results. When initially set up, the model agreed very well with fully warm friction data provided by Jaguar Land Rover (JLR). However friction data collected at the University of Nottingham using the same version of engine shows fully warm to be consistently around 30% lower than that measured on another example of the 2.0 GTDI engine installed at JLR (see Figure 4.11). Additionally, while the total friction prediction matched well to JLR data, the limited amount of teardown data available suggested that valvetrain friction was over-predicted in relation to the other components.

As the initial fully warm friction predictions correlated well to the data provided by JLR, the distribution of friction, by component, was scaled to match that seen in the teardown data at 2000 and 5000rpm. Total friction was then scaled to match results obtained at the University of Nottingham to obtain a final correction for each component. The required alterations are shown in Table 4.1 below:

Table 4.1 Correction factors for experimental rigs at University of Nottingham and Jaguar Land Rover

Coefficient	Equation number	Original	Revised
C_{bs}	4.5	0.110	0.156
C_{cb}	4.5	0.273	0.388
C_{td}	4.5	0.000122	0.000172
C_{vb}	4.9	1.025E-07	5.12E-08
C_{ff}	4.9	0.0559	0.0279
C_{oh}	4.9	0.210	0.105
C_{om}	4.9	4.49	2.25
C_{ps}	4.8	0.0406	0.0438
C_{pr}	4.8	0.294	0.318
C_{be}	4.8	0.303	0.327

This approach is limited by the fact that friction teardown data must be used to empirically correlate the predicted friction. Additionally, only 2 speed points have been used to correlate the friction, both of which are relatively high compared to speeds experienced during the NEDC for the VIPER engine, which never reaches 2000rpm through the cycle.

Changing these correction factors will alter the relative importance of each component to total engine friction, but will not alter the friction characteristics in terms of response to oil viscosity. The values chosen for the scaling factors can have a very large effect on the interpretation of the model results. The values selected will be specific to the 2.0l GTDI engine under consideration.

While the distributions are correct for fully warm engine operation, the differing responses of the components to oil temperature would require further work to verify. A more complete set of teardown data across a range of temperatures would allow for the friction response to changes in temperature to be modelled more accurately.

Of all the friction contributors, the valvetrain required the largest modification from the original model predictions. The piston group required minimal scaling, and the crankshaft required almost none.

The predicted distribution of friction by component, at fully warm temperature is shown in Figure 4.8. The comparable tear down data from JLR for the 2.0 GTDI are given in Figure 4.9. Only the ancillaries modelled in PROMETS, namely the oil, coolant and fuel pumps are included in the tear down data. After adjustment of the empirical constants, good agreement can be seen between the two cases. Figure 4.10 shows the changing importance of each component group with engine speed. The valvetrain makes up a large proportion of the friction at low engine speeds, due to the inverse dependence of the follower term on speed. This falls away as speed increases. The reciprocating group accounts for the largest proportion of engine friction throughout the range of engine speeds.

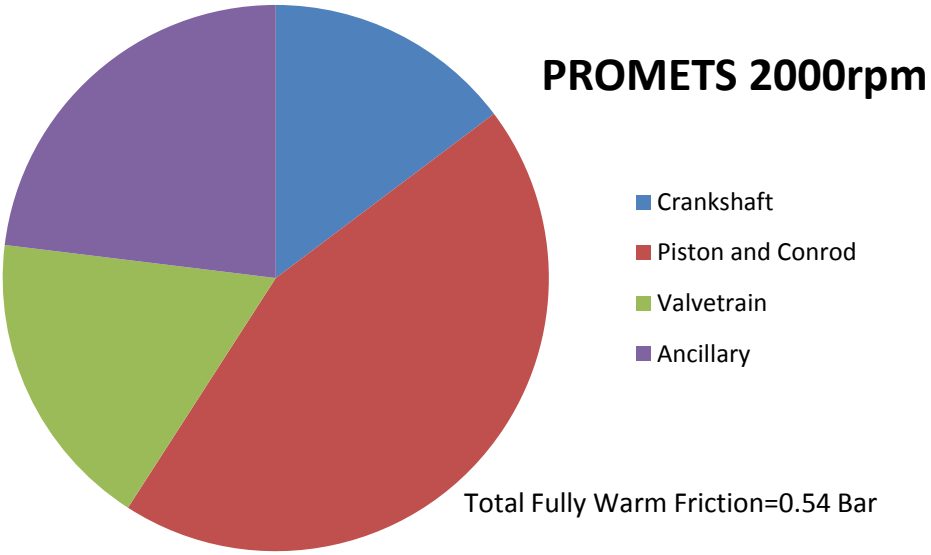

Figures 4.8 2000RPM Friction distribution from PROMETS contributions at fully warm temperatures

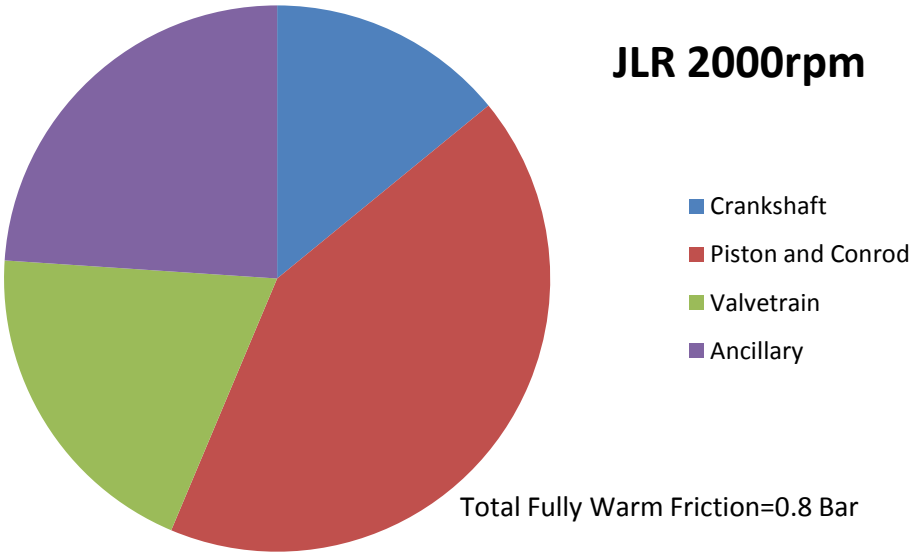

Figures 4.9 2000RPM Friction distribution from teardown data at fully warm temperatures

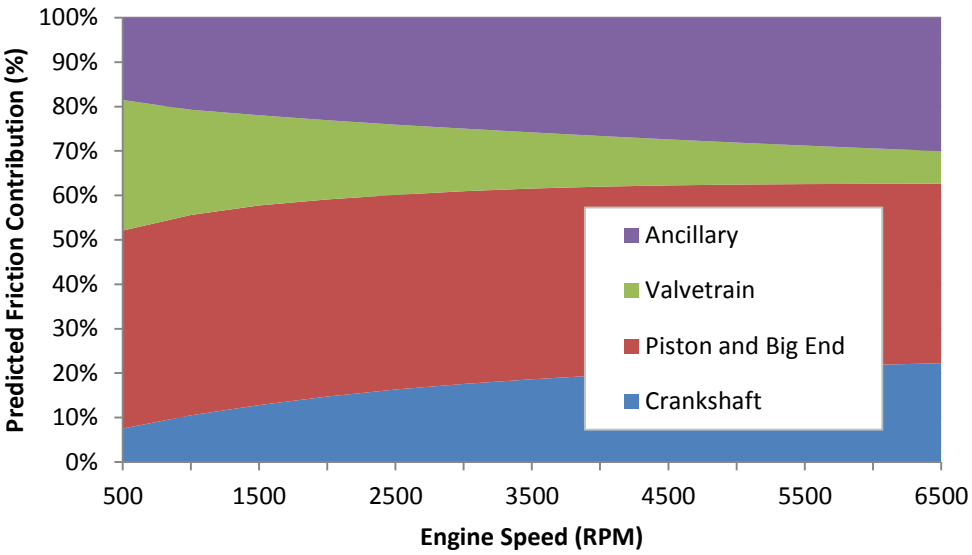

Figures 4.10 Predicted friction contribution variation at fully warm temperature with engine speed

4.6 Validation of friction model

4.6.1 Constant speed

Comparisons between the predicted and measured total engine friction values were done at a range of constant speed conditions for both warm up and fully warm running. Figure 4.11 shows a sweep of fully warm friction. Good agreement is seen with data measured on the test bench at the University of Nottingham and some limited data from Ford test beds after the modification of the C constants discussed previously. Without the changes, agreement is better with the data shared from the consortium. The discrepancy between measured friction levels between the Nottingham, Ford and JLR could be a result of differences in measurement technique. Where the Nottingham data were collected from an engine test bed, with friction calculated as the difference between IMEP and BMEP, the JLR data is from a motored engine. While a motored engine can be brought up to temperature artificially, it is difficult to properly replicate the thermal gradients present in a fired engine; especially at the piston liner interface where the viscosity of the oil is higher than in a fired engine, and the clearances will be greater.

Warm up tests also show good agreement. Figures 4.12-4.13 show constant speed warm ups against experimental data measured at speeds and loads consistent with NEDC conditions. The friction response to increasing temperature is good, with the correct gradient in friction reduction during early running.

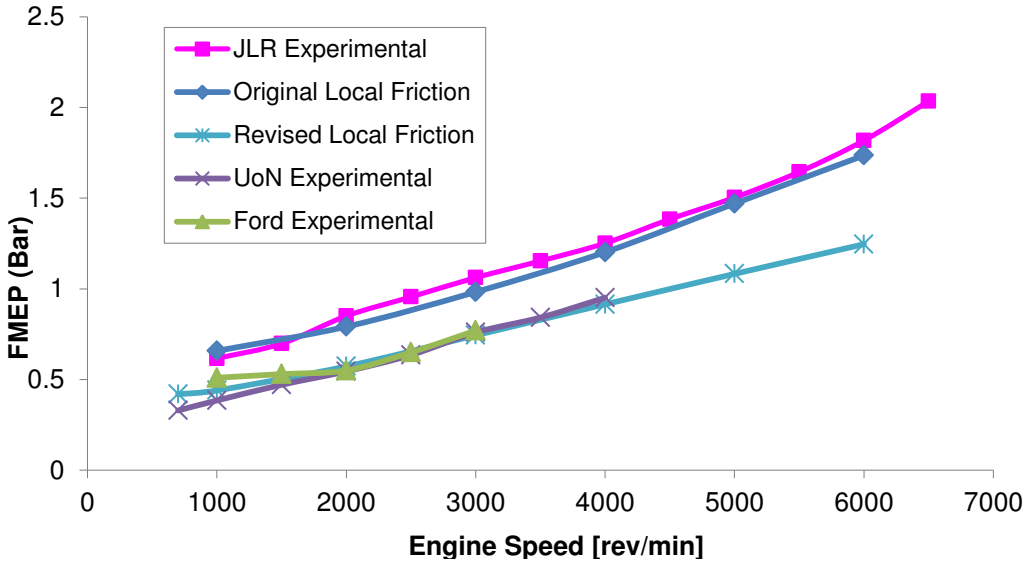

Figures 4.11 Total fully warm friction variations with speed. Three sets of experimental data are shown, along with the predictions using the original and revised constants

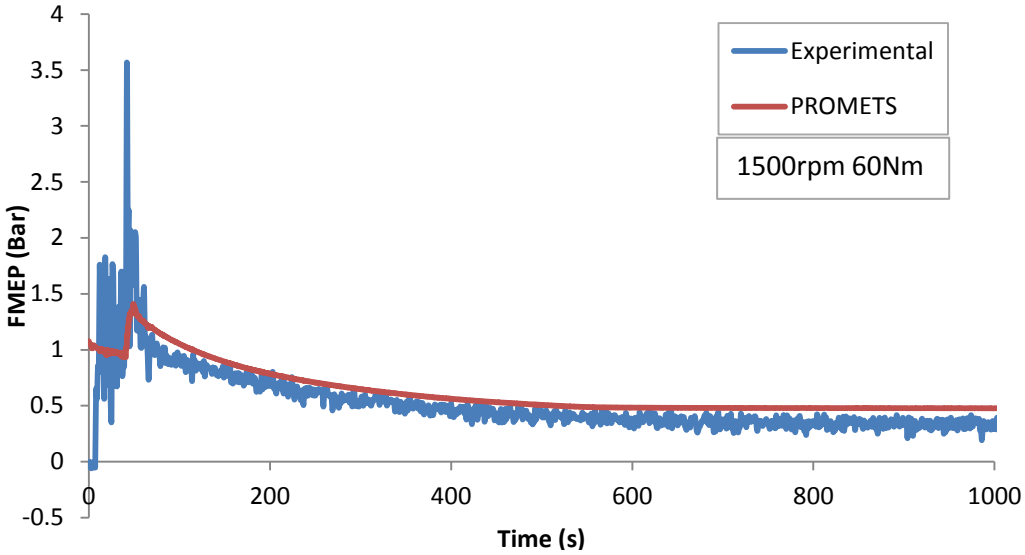

Figure 4.12 Friction warm up comparisons between predicted and experimental friction at 1500RPM 60Nm

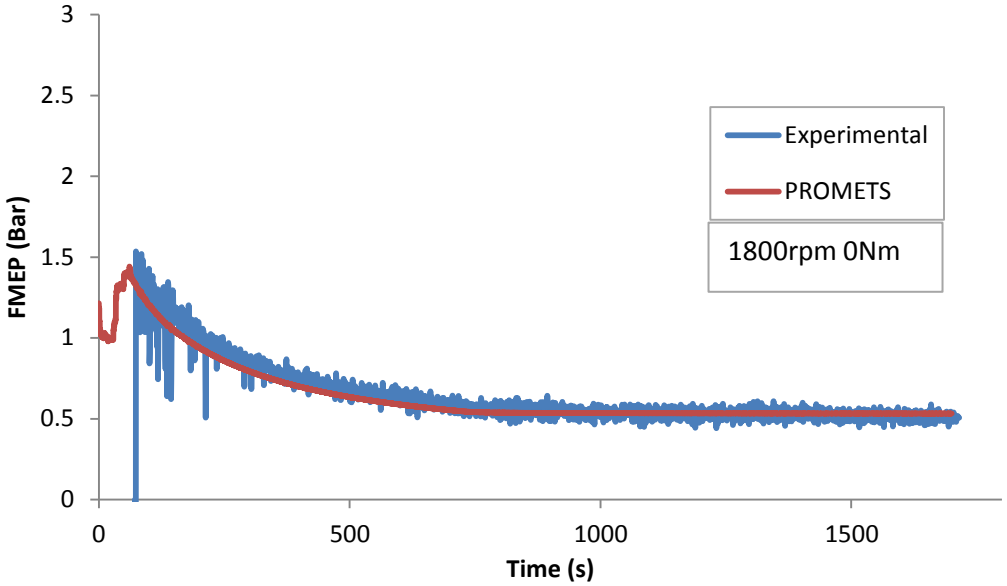

Figure 4.13 Friction warm up comparisons between predicted and experimental friction at 1800RPM 0Nm

4.6.2 Transient behaviour

The transient behaviour of the model has also been compared to experimental results over the aNEDC and is shown in Figure 4.14. The large variations in the experimental friction measurements in this figure are due to the nature of friction measurements on the engine. Experimental friction is calculated using the indicator method. BMEP, measured from the dynamometer, is subtracted from net IMEP inferred from in cylinder pressure measurements. Both of these are large in relation to FMEP values meaning that friction data obtained in this manner will often be noisy. The operating conditions for the aNEDC are shown in Figure 4.15

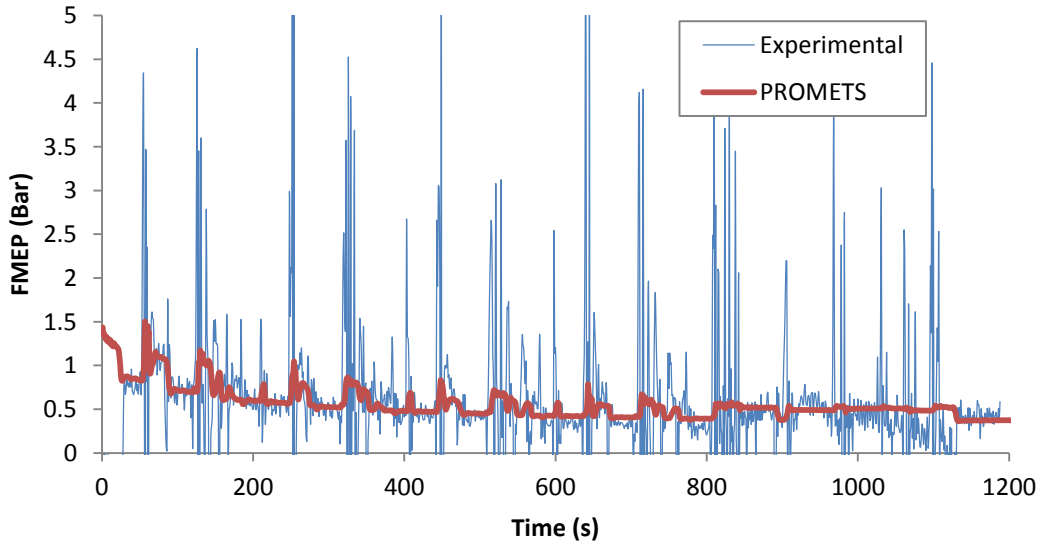

Figure 4.14. aNEDC comparison between predicted and experimental friction values

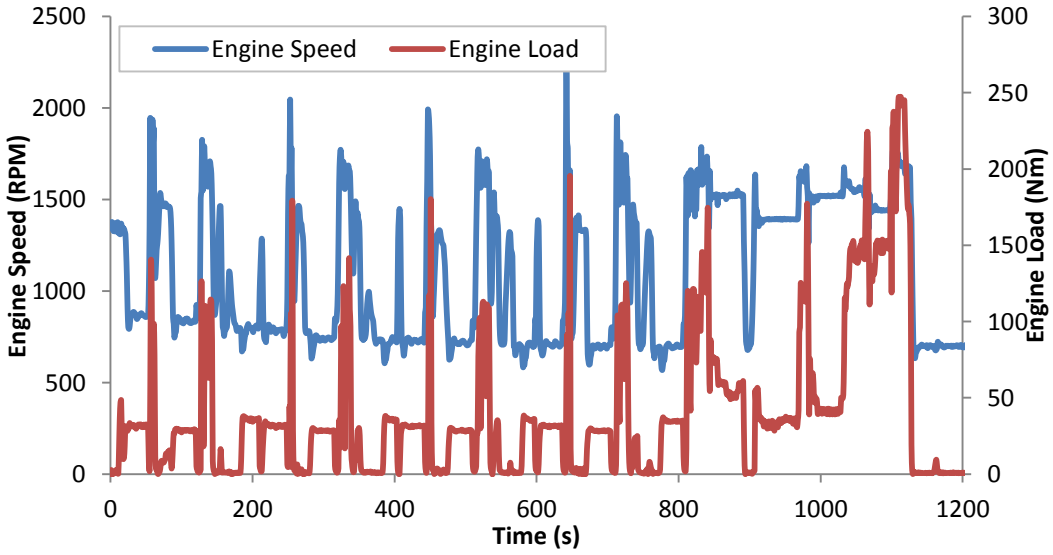

Figure 4.15. aNEDC operating conditions

4.7 Predicted temperature responses

The way in which each component group responds to increasing temperature is shown in Figure 4.16 and 4.17. Figure 4.16 shows a 2000RPM warm up test. The crankshaft group shows the largest relative change in friction as temperature increases with a six fold reduction in friction. The piston exhibits the next greatest relative change, although in absolute terms, the reduction seen here is larger than in the crankshaft. Valvetrain friction is largely insensitive to temperature after a small reduction from cold that is attributed to the bearings in the camshafts. One of the benefits of the local model can be seen in the amount of time it takes for component friction to reach their fully warm states. The friction in the reciprocating group falls relatively quickly due to the fast rise in temperature experienced in the liner, whereas in the bearings, where the large metal mass in the crankcase holds oil temperatures down, the rate of friction reduction is much slower. These results are replicated in Figure 4.17 which shows results from an aNEDC test.

These results show that the greatest gains to be made are in the reciprocating group. Raising the temperature of the mid-stroke liner region would be more beneficial than raising the temperature of the oil feed to the bearings, despite the stronger friction dependence on temperature in the bearing friction formulation. Results from a simulation of this are shown in Figure 4.18, in which either the bearing feed flow, or mid stroke liner temperature was raised by 10°C over the value recorded during normal running. Raising the mid-stroke liner temperature would only be possible if the coolant was warmed significantly given the strong thermal coupling between the cylinder liner and the coolant. Efforts to improve valvetrain friction from a thermal standpoint would not yield good results; friction here would be more effectively reduced through the use of an alternative valvetrain configuration such as roller followers.

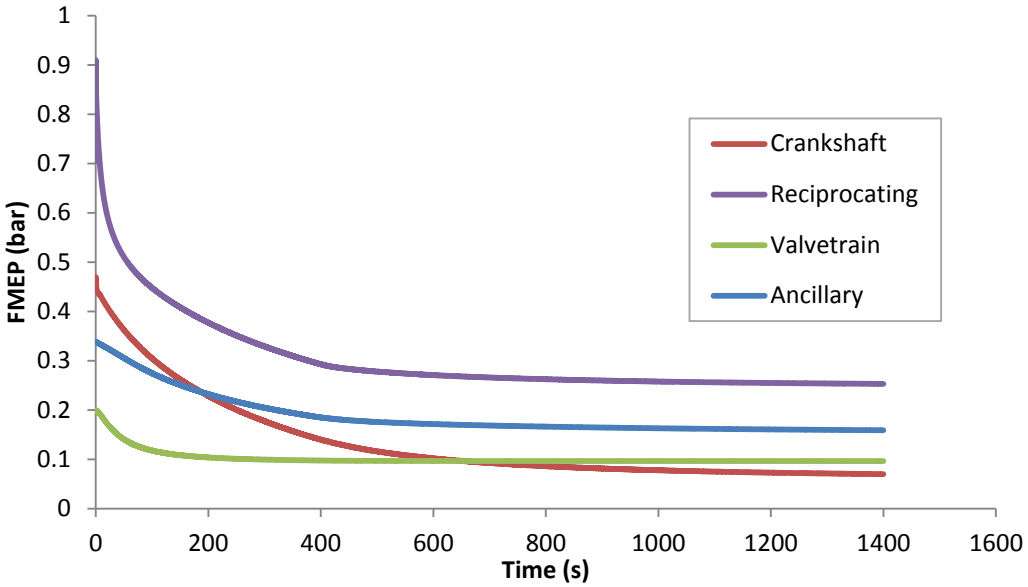

Figure 4.16 Friction components temperature response a warmup at 2000RPM

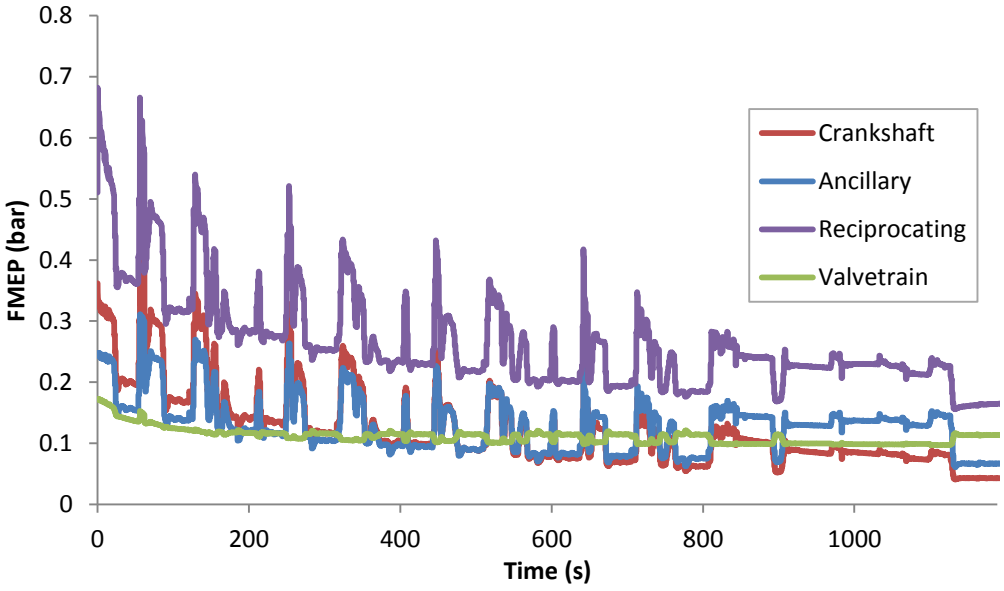

Figure 4.17 Friction components temperature response for the aNEDC

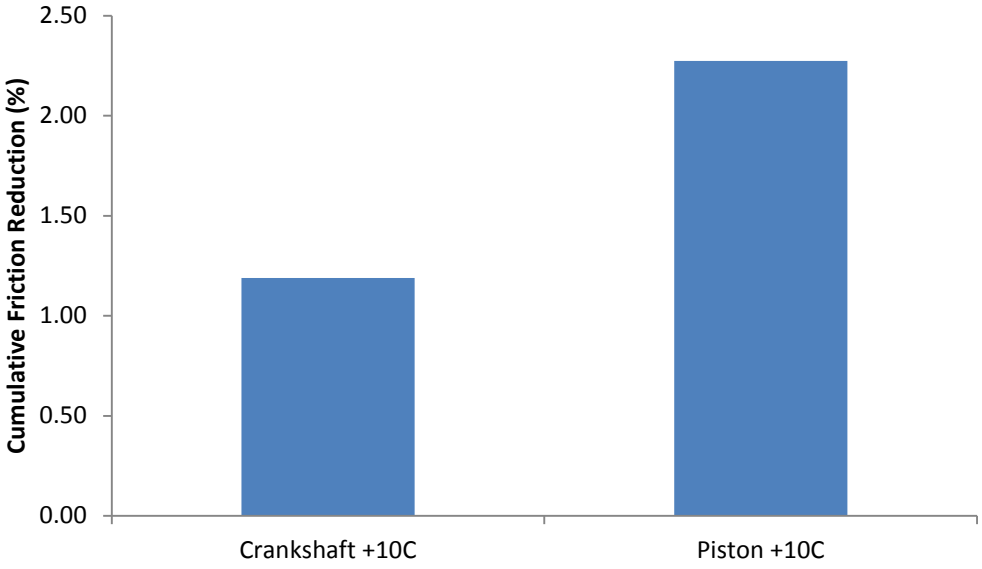

Figure 4.18 Predicted reductions in friction given a 10 degree rise in operating temperature

4.8 Coolant temperature plunge test

Tests involving the rapid drop in coolant temperature were carried out on the VIPER engine in order to test the assumption that the friction of the piston is dictated by the mid-stroke liner temperature, and therefore heavily influenced by the coolant temperature. The experiment was conducted by introducing cold water to the engine once it had reached fully warm conditions. This plunged the temperature of coolant in the engine by 60°C. Experimental values for the bulk coolant temperature were used to fix the response of the coolant in the model, and the changes in engine friction and oil temperature predictions were examined. Figure 4.19 shows the experimental and predicted oil temperature and friction responses to the reduction in coolant temperature. Oil and friction responses are both reasonably accurately predicted. The important observation here is the rate of response of both the experimental and prediction values. The friction responds almost immediately to the change in coolant temperature experimentally showing a strong link between the two. When liner temperature is used to dictate the viscosity of the oil in the model, this quick response time is captured in the model, however when the bulk oil temperature model was used, this response was delayed and of a smaller magnitude. The predicted change in contributions from the rubbing components are given in Figure 4.20, which shows that the majority of the friction increase comes from the piston group. Also shown in Figure 4.20 is the response of piston friction when the bulk oil temperature is used to evaluate the viscosity. This result increases confidence in the assumption that the mid-stroke liner temperature should be used to predict piston friction and also in the choice of index for the viscosity scaling of the piston group. This test also highlights the strength of the model's heat transfer formulations.

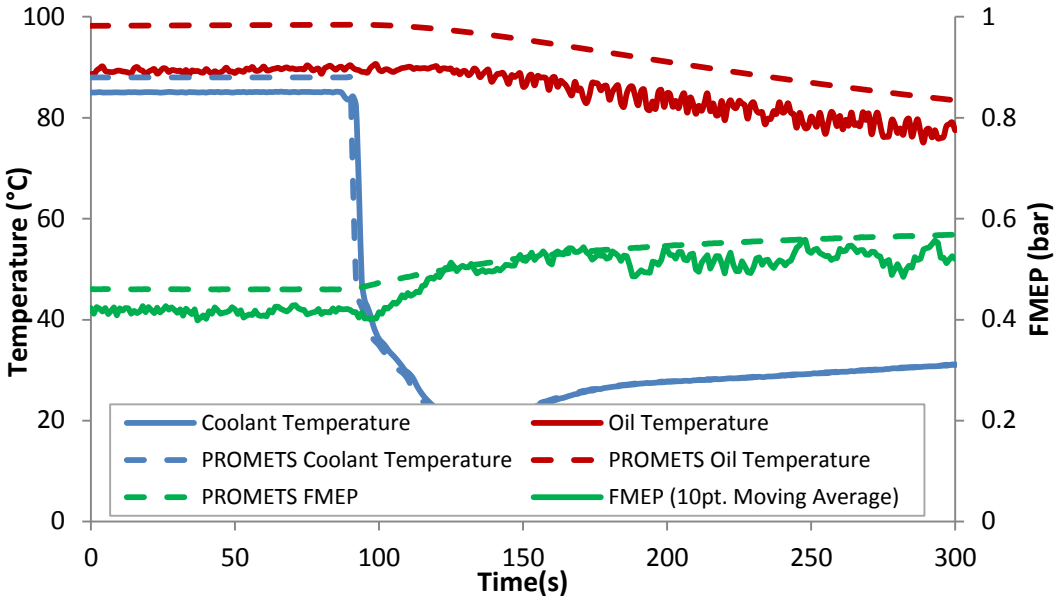

Figure 4.19 Model responses to perturbations in coolant temperature with experimental values

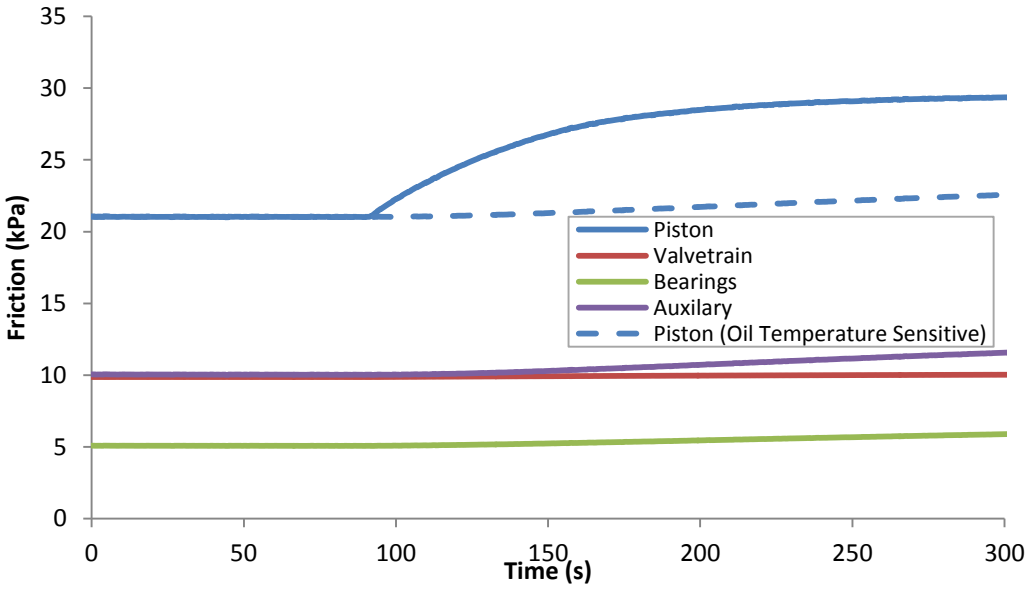

Figure 4.20 Predicted friction component response to coolant temperature perturbations showing the dominant effect of coolant temperature on piston friction. Also shown is the piston friction temperature response if the bulk oil temperature is used to evaluate the viscosity of the oil at the piston-liner interface

4.9 Viscometry

Limiting the levels of friction is one of the primary functions of a lubricant in the engine, and the property which most influences a lubricants ability to do this is its viscosity. Viscosity describes the ability of an oil to resist shearing forces and is highly dependent on temperature. Friction in the hydrodynamic regime is especially sensitive to viscosity, as the friction generated is associated with viscous shearing within the fluid film. In the engine, when the oil is subject to high shear rates and temperatures, the effective viscosity is lower than that found during measurement in laboratory conditions [88].

Oil viscosity if commonly represented as either dynamic or kinematic viscosity, with dynamic being the absolute value, and kinematic being the ratio of dynamic viscosity to the oil's density. The SAE J300 standard defines automotive lubricants in grades based on their temperature viscosity characteristics. A lubricant must be tested using several accepted test procedures such as the ASTM D5293 for the measurement of viscosity in a Cold Cranking Simulator (CCS) between -35°C and -5°C and the ASTM D4683 which measures viscosity at High Temperature and High Shear (HTHS) rates. To be classified in an SAE grade, a lubricant must fulfil but not exceed the viscosity limits specified in the J300 standard for both high and low temperature operation.

Automotive lubricants were of a single viscosity grade before the introduction of multi-grade lubricants in the 1950's. The early lubricants tended to have a steep temperature-viscosity profile, and as such would be unsuitable for use if ambient temperatures were extreme at either end of the scale. Multi-grade lubricants were created through the addition of Viscosity Index Improver polymers, whose chain geometry change depending on the temperature of the lubricant. The result of this was to create lubricants which act as a higher grade at low temperature, and as a lower grade at high temperature allowing for a smaller total viscosity range than that seen in single grade lubricants. The result was a range of lubricants which would remain in the safe operating zone for viscosity over a wider range of lubricant temperatures.

In a recent update to the J300 standard [89], concessions have been made to lubricants with high temperature viscosity that falls below the SAE 20 grade. The new SAE 16 grade maintains the low temperature viscosity profiles, but allows for a reduction in high temperature low shear viscosity and high temperature high shear viscosity of 11%. This will allow for lower levels of friction during fully warm engine operation compared to the older grades.

There are several methods of varying degrees of accuracy used to predict the temperature dependence of a lubricant's viscosity.

The Walther-Mccoull equation is used to evaluate the kinematic viscosity of oil at any given temperature and is the basis for ASTM D341 charts for the viscosity of liquid petroleum products [90]. It is also the equation currently used in the PROMETS SI model. Kinematic viscosity in m^2/s is given in equation 4.11 as:

$$v = \frac{\{exp[exp(Walther1 + Walther2.log(T_{oil}))] - 0.6\}}{100000} \tag{4.11}$$

The constants, Walther 1 and Walther 2 vary by oil, and the constants for 2 common oil grades are given in Table 4.3 below:

Table 4.3 Walther Constants for Viscosity Calculation

Oil	**Walther 1**	**Walther 2**
SAE5W-30	17.9821	-2.8894
SAE10W30	19.0638	-3. 0724

The Walther equation forms the basis of the ASTM viscosity-temperature charts where the loglog of viscosity is plotted against the log of the oil temperature.

The Vogel equation is more accurate than the Walther equation when predicting lubricant viscosity [74], and is present in the Diesel version of PROMETS but has not previously been introduced to the SI version.

The Vogel equation takes the form:

$$\mu_{vogel} = ae^{b/(T-c)} \tag{4.12}$$

Where μ is the dynamic viscosity in Pa.s, a b and c are constants which relate to the oil in question, and T is the temperature.

The Vogel equation predicts the dynamic viscosity of a lubricant at low shear conditions, whereas in an operating engine, the encountered shear will be relatively high. Shayler et al [88] made a modification to the Vogel equation which preserved the temperature-viscosity characteristic predicted by the Vogel equation but shifted the prediction to account for viscosity measured using CCS and HTHS values. This modified prediction better represented the effective viscosity experienced at the rubbing surfaces in the engine.

The modified equation is given as

$$\mu = ae^{b/(T-c)}\left(de^{(fT)}\right) \tag{4.13}$$

Where

$$f = \frac{ln\left[\left(\frac{\mu_{CCS}}{\mu_{HTHS}}\right)\left(\frac{\mu_{vogelt1}}{\mu_{vogelt2}}\right)\right]}{T_1 - T_2} \tag{4.14}$$

And

$$d = \left(\frac{\mu_{CCS}}{\mu_{vogelt1}}\right)exp(-fT_1) \tag{4.15}$$

The measured viscosity for CCS and HTHS are compared to the Vogel predictions at these temperatures, which in this case have been set at -30 and 150°C respectively.

In the absence of a full set of viscosity data, the coefficients may be determined using a script found in [74]. This has been expanded to also produce the coefficients found in the modified Vogel equation. Dynamic viscosity data for three temperatures, as well as for the CCS and HTHS values are required to be input. A table of Vogel coefficients for oil historically used in the Engines Research Group, and for currently used oil is given below. The Ford 913C is the standard factory fill oil used for the VIPER engine and is classified as a 5W30. The values for the Bayliss 5w30 and 10w30 are for older oils found in [91] and no CCS or HTHS data was available for these. The Model and Special oils are new, low viscosity oils developed by BP for use in the VIPER project. Figure 4.21 shows the Vogel equation viscosity predictions for all of the listed oils:

Table 4.4 Vogel and Modified Vogel Coefficients for a range of lubricants

Model Coefficients	Vogel			Modified Vogel	
	A	B	C	D	F
Ford 913c	7.85E-05	979	-115	-0.00093	1.01
Model Oil	4.85E-05	998	-125	-0.00144	1.22
Special Oil	3.76E-05	1098	-134	-0.00260	1.49
Bayliss 5W30	7.80E-05	1180	-133	-	-
Bayliss 10w30	5.90E-05	1160	-125	-	-

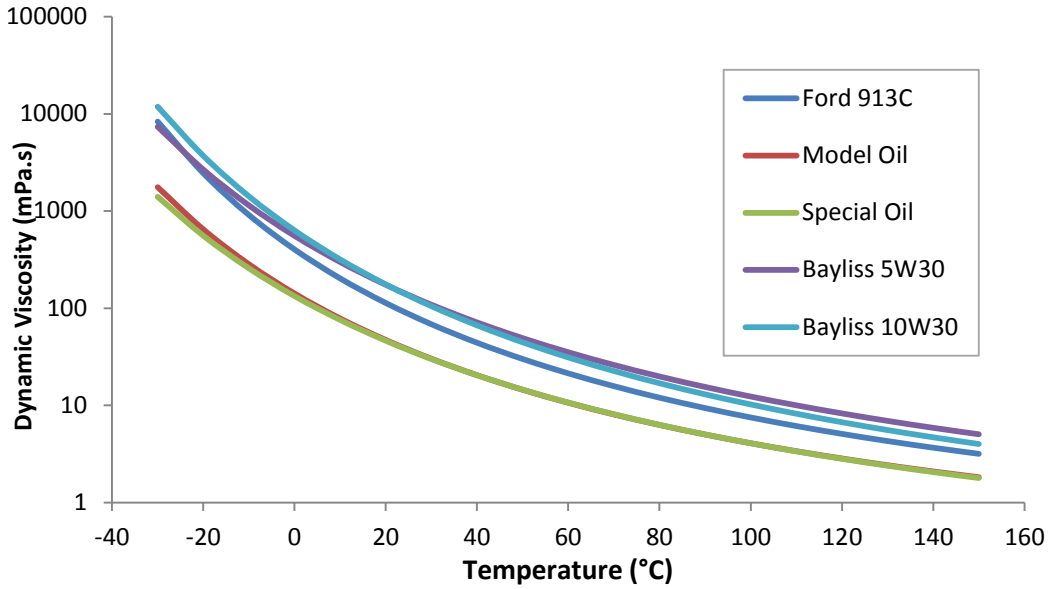

Figure 4.21 Friction components temperature response for the aNEDC

Using lower viscosity lubricants will have positive effects on fuel consumption, not only through the immediately obvious reduction in engine friction at the main rubbing surfaces. The power required to drive the oil pump will be reduced because of the lower viscosity of the fluid for a given flow rate. This reduction in power requirement can enable use of less tension on the auxiliary belt which drives the pump from the crankshaft.

The gains seen from reducing oil viscosity do not synergise well with advanced thermal management techniques. As oil viscosity falls, the potential fuel savings that can be targeted through reducing the cold start friction penalty also drops, making the decision as to which strategy is optimal an important one. The use of new low viscosity oils is likely to be expensive, and the cost will be borne by the customer. Additionally, there is a physical limit to the grade of oil that can be used in engines, as the loads experienced by engine bearings must be supported by the fluid film. The Stribeck curve (Figure 2.1) clearly shows that at a constant load, as viscosity falls, the lubrication regime will change from hydrodynamic to mixed and eventually boundary lubrication which will cause increased friction and potentially damage to the rubbing surfaces. Advanced thermal management

techniques however will be completed by the manufacturer in the design phase, and will essentially be free to the customer over the vehicle's lifetime, minus the initial costs passed on from development.

4.7 Discussion

The model presented in this chapter presents a new approach to evaluating engine friction based on local temperature variations between the rubbing surfaces instead of using bulk oil temperature predictions. This is linked to the main PROMETS model with friction predictions used as heat sources to the lumped capacity elements. The result is a better integrated model, with well-defined links between the friction, oil and structure sub-models.

The fully warm predictions of the model developed in [25] was an attractive starting point for the local temperature friction model. Previous work had been done to adapt the prediction of friction values at a reference value of viscosity to values which apply during warm up to good effect, but this failed to capture the thermal characteristics local to the rubbing surfaces. Improvements to the model have been made to describe these effects for all of the rubbing surfaces. The model shows good agreement with limited teardown data after modification of several coefficients, as well as with full engine friction data throughout a wide range of constant and transient speed operating conditions.

The equations in the model are based on work done in [25], [27] and [26], with updated viscosity indices that agree with lubrication and bearing theory and which no longer require a factor to account for increased friction when the engine starts. The increase in friction at cold start was previously accounted for by the viscosity ratio and cold start correction factor being applied to the entire fully warm friction value. In the local model, only hydrodynamically lubricated friction contributions have been viscosity scaled, and the cold start correction has been removed. This has required a significant increase in the indices used in the viscosity ratios to produce the required increase in friction at low temperatures. The choice of viscosity index agrees with modelling done in [18], [20] and [22].

Assumptions have been made as to the condition of the oil at several key locations, notably the oil film on the liner surface, and the oil in the valvetrain. The nature of the oil in the valvetrain in particular is poorly understood, and the assumption that the oil will be at the temperature of the cylinder head is not fully informed. Observation through a window into the cylinder head of the VIPER engine suggested that the area is partially flooded, which would suggest that the oil temperature here would be lower than the metal temperature. However, with the valvetrain expression as a whole being so insensitive to temperature, the resulting difference in model predictions here would be minor if a change to a cooler reference location temperature was made.

The empirical C constants have been recalculated for the VIPER engine. The most significant changes were seen in the constants for the valvetrain, with those of the crankshaft and piston group remaining largely similar to the values calculated by Leong [33]. Teardown data suggests that the VIPER valvetrain friction is around half of that predicted using coefficient values determined in previous work. The reason for the need to reduce the C values for the valvetrain is not known. Many factors influence this, including better surface finishing techniques [92], reduction in spring loads [93] or reduction in contact area between the cams and valve buckets.

Coolant plunge tests have been used to validate the assumption of dependence of the piston friction on metal temperature as opposed to oil temperature. The immediate response of engine friction to an introduction of a slug of cold coolant to the engine shows the independence of a portion of engine friction on the oil. Model predictions to the change when set up for dependence on metal temperature were of the correct magnitude, increasing confidence in this assumption.

Experiments on coolant flow rate on liner temperature by Gardiner et al. [15] , a paper to which the author contributed, showed increases of 10°C in the mid-stroke liner by reducing the speed of the coolant pump, but were unable to measure any change in friction due to noise in the friction measurements. This highlights the importance of modelling, and especially a model sensitive to local temperature when investigating the effects of thermal manipulation on engine friction.

The magnitude of friction responses to changes in operating temperature has been examined in Figure 4.10 which shows the percentage change in total engine friction for a 10 degree rise in operating temperature over the temperature usually recorded at a particular part of the NEDC cycle. The results show that despite the viscosity dependence of the crankshaft being higher than that of the piston group in the model, the fact that the piston contributes a much larger proportion of total engine friction means that more benefit would be realised by targeting the piston over the crankshaft for friction reduction through improved warm-up. This could be examined through altering the heat transfer coefficients between the coolant and the cylinder in the coolant jacket to increase the temperature of the mid stroke liner to simulate the insulation of the cylinder from the coolant jacket. Insulation of the back of the liner could be used to achieve this. Care would have to be taken to retain sufficient cooling to prevent damage during prolonged running at high speed and load.

There remain areas in which the model can be improved. It is known that as an engine warms up, the differences in thermal expansion between materials will cause changes in clearances between the rubbing surfaces. In the journal bearings found in the crankshaft for example, the thermal expansion of the aluminum block will be greater than that of the steel crankshaft, leading to bearing clearances that will increase during an engine warm up. Larger clearances will reduce the friction in the bearing, but will also lead to a reduced load carrying capacity, as described in Sommerfeld's number. The effect of bearing clearance on friction has not been implicitly taken into account in the model, and this is an area in which the model could be improved upon.

While the model predicts the temperature-friction relationship well, the absolute viscosity of the lubricant is not taken into account in the model, outside of the empirical constants. For predictions to be made about the effect of a lower viscosity lubricant, experiments would have to be carried out to recalibrate the constants for the new lubricant. It would be advantageous for this functionality to be added to the model to eliminate this requirement.

Chapter 5. Modelling the VIPER oil circuit

5.1 Introduction

The primary functions of the lubrication system are to reduce friction at the rubbing surfaces, increase engine life by reducing wear, act as a transport medium for friction work to cool rubbing surfaces, and to remove debris from rubbing surfaces. While there are variations in design, the oil circuit of an internal combustion engine typically consists of a series of pumps, filters, pressurised galleries, unpressurised returns and a sump. The engine's lubrication circuits must be carefully designed to control the flow rate, temperature and pressure of the oil reaching each rubbing component through a wide range of operating conditions. Engines in production feature a crankshaft driven fixed or variable displacement oil pumps, and use a wet sump, oil reservoir design, although variable flow pumps are becoming more common. A wet sump system utilizes a sump directly connected to the bottom of the crankcase which collects oil as it returns under gravity from the rubbing surfaces. An alternative sump configuration, a dry sump system employs scavenge pumps to collect oil from the bottom of the crankcase before returning it in a pressurised state to an external reservoir. Due to the greater number of pumps, filters and external oil routing, dry sump systems are more expensive, and are most often seen in high performance vehicles due to their ability to provide a consistent supply of oil regardless of high lateral loading on the vehicle which can interrupt oil flow from a wet sump if the oil pickup is left exposed. Storing the oil externally to the engine also allows for greater oil volumes to be carried, reducing the risk of the oil overheating during sustained periods of high power operations. A negative effect of this increased volume however, is that the oil will take longer to reach a steady state temperature unless the tanks are fitted with auxiliary oil heaters which further add to the cost of the dry sump system.

There are growing number of new vehicles that replace conventional fixed displacement oil pumps with either electrically driven pumps, or crankshaft driven variable flow rate pumps. An oil pump on an automotive engine is sized to

provide an adequate oil supply in terms of both pressure and flow rate to the engine in the most demanding of conditions; this occurs when the engine is hot, and running at idle speeds. Consequently, the pump tends to exceed the demand of the engine for oil throughout the majority of other running conditions leading to unnecessary power consumption from the pump. The use of a variable flow rate pump allows for more precise matching of the engine's oil supply requirements and the output of the pump, minimising wasted pump power. These pumps can also adapt to changes in conditions, such as the use of different oil grades, high wear on older engines, or filter blockages.

As described in Chapter 3, at the outset of this project the oil circuit in PROMETS was representative of that found in the Ford CVH engine manufactured in the 1980s. Whilst the design of the VIPER oil circuit is not radically different, it does feature a revised flow path, as well as several components not found in the original circuit. Figure 5.1 shows the representation of the CVH engine in PROMETS. The oil circuit representation has been modified to better represent the VIPER engine and to include components not previously included in the PROMETS SI model.

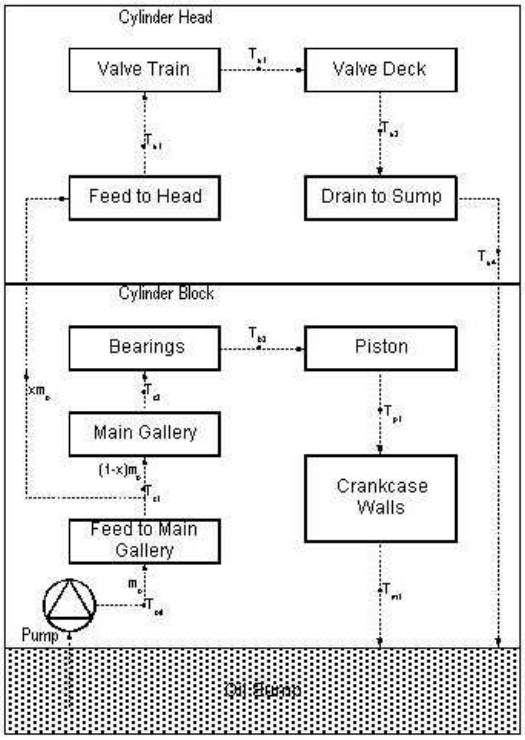

Figure 5.1 Oil Circuit for the CVH engine representation

5.2 VIPER oil circuit layout

Figure 5.2 is a CAD drawing of the VIPER oil circuit with pressurised and unpressurised flows highlighted The layout follows that of a conventional wet sump system. A crankshaft driven fixed displacement gear pump draws oil from the sump through a short pick-up tube and delivers it though a filter assembly integrated with an oil coolant heat exchanger. From here the oil flows through a short internal gallery though the block before a feed to the balancer shaft splits from the main flow. After this split the oil reaches the main gallery at the rear of the engine. The main bearings are lubricated through five feeds from the main gallery, with the big end bearings receiving oil through passages in the crankshaft from the main bearings. Piston cooling jets are used to supply oil when main gallery pressure exceeds 2.7 bar absolute to cool the piston, and for lubrication of the rings and skirt. Oil from the pistons, main and big end bearings all fall back to the sump unpressurised. There are two galleries that lead from the main gallery. A gallery running across the front of the engine provides oil to the turbocharger and timing chain tensioner before a channel up to the cylinder head provides oil to pressurise the variable valve timing actuators. The other gallery leaving the main gallery carries the oil straight to the cylinder head from approximately half way along the block. This provides the oil required to lubricate the camshafts via two parallel head galleries with feeds to the bearings. The valves and valve buckets are splash lubricated. Oil from the head collects on the head deck and returns to the sump through passages cast in the block that open out into the crankcase. The instrumentation of the oil circuit is shown in Figure 5.3. K type thermocouples are used in all locations, and are accurate to ±1º.

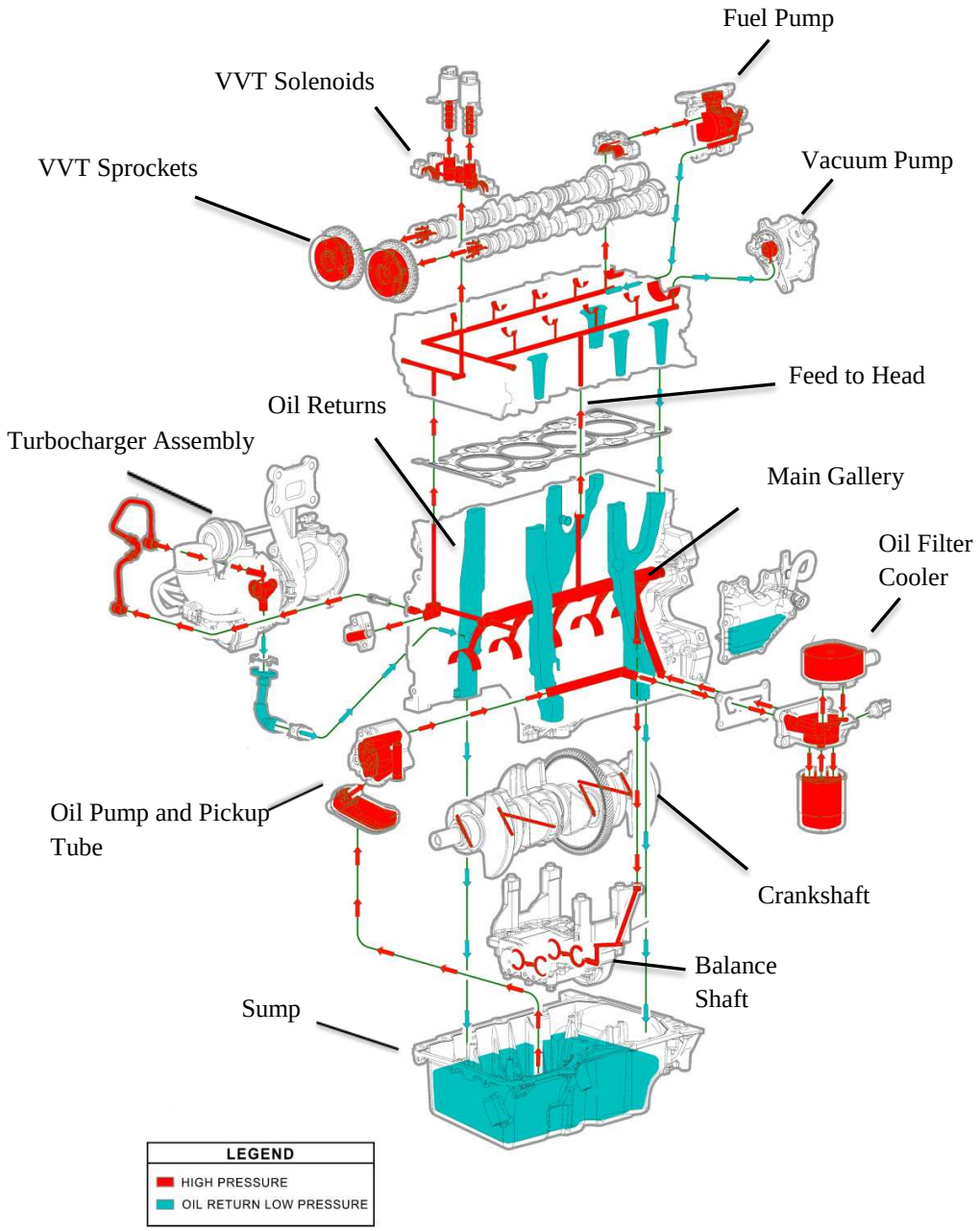

Figure 5.2 CAD Drawing of the VIPER Oil Circuit

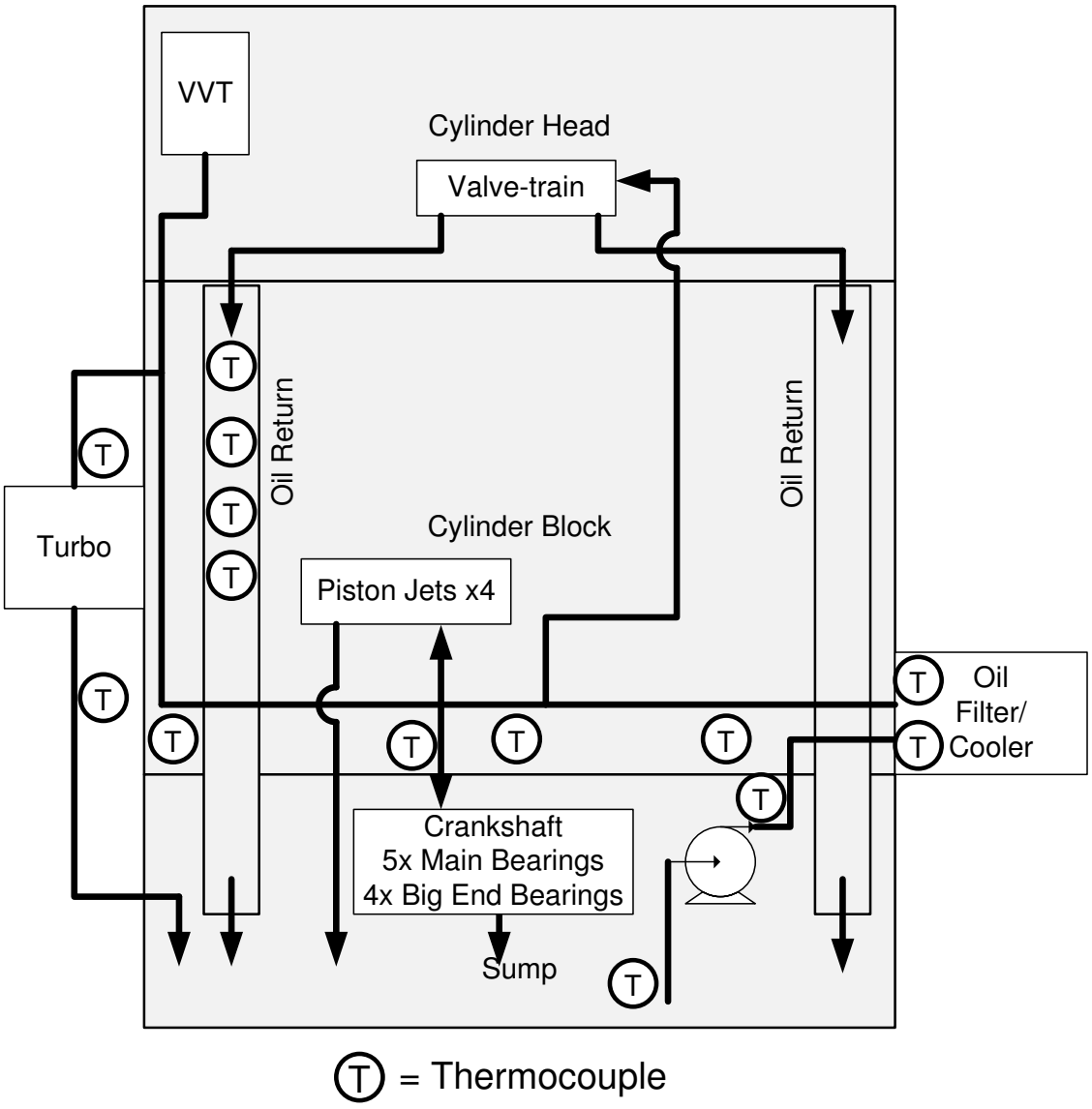

Figure 5.3 Thermocouple locations on the VIPER engine [15]

5.3 Oil circuit updates for modelling the VIPER engine

There is much commonality in the elements and system configuration used in the CVH and VIPER engines, allowing the majority of equations used to evaluate heat transfer to and from the oil circuit in previous work to be used without modification. Where possible, the equations used in Chapter 3 have been retained, albeit in a different sequence in some instances. The updated oil flow path in the PROMETS model is shown in Figure 5.4.

The major differences between the oil circuits and additions made are as follows. Firstly, a distinct sump location has been added. This was previously calculated by considering the net heat transfer to the oil around the entire circuit, and was not a discrete node. This has required estimation of the flow rates though the main bearings and piston cooling jets to complete the energy balance of oil returning to the sump. Heat transfer in the filter cooler assembly was previously evaluated before the oil returned to the sump. This has been added as a node in the oil circuit immediately after the oil leaves the sump.

Where the feed to the head leaves the main oil flow before the main gallery in the CVH engine, it is taken from the centre of the main gallery in VIPER. Heat transfer from the engine structure in the front and main gallery is required to be calculated before the oil diverges from the main flow.

The CVH engine had no piston cooling jets, so the pistons were assumed to be lubricated via splash from the main bearings. Consequently in the model for this engine, the bearing and piston heat transfer calculations were arranged in series. The piston cooling jets in the VIPER engine are supplied directly from the main gallery, and so heat transfer calculation must be done in parallel with that in the main bearings. Heat transfer pathways to the oil have also been added to the parts of the cylinder liner which will be exposed throughout parts of the stroke.

The main gallery is located directly beneath the cooling jacket in the VIPER engine, instead of in the crankcase walls. This will alter the nature of heat transfer in the galleries. The crankcase metal lags the rest of the engine in rate of warm up

due to its large thermal inertia, meaning that oil running through this metal will lose temperature. Having the gallery near the liner and the cooling jacket will mean that oil flowing through the gallery will gain energy. Figure 5.5 shows the heat inputs from the gallery to the oil. Due to the location of the main gallery in the VIPER engine, the approach of main gallery insulation outlined in [47] would not be suitable for raising the oil temperature.

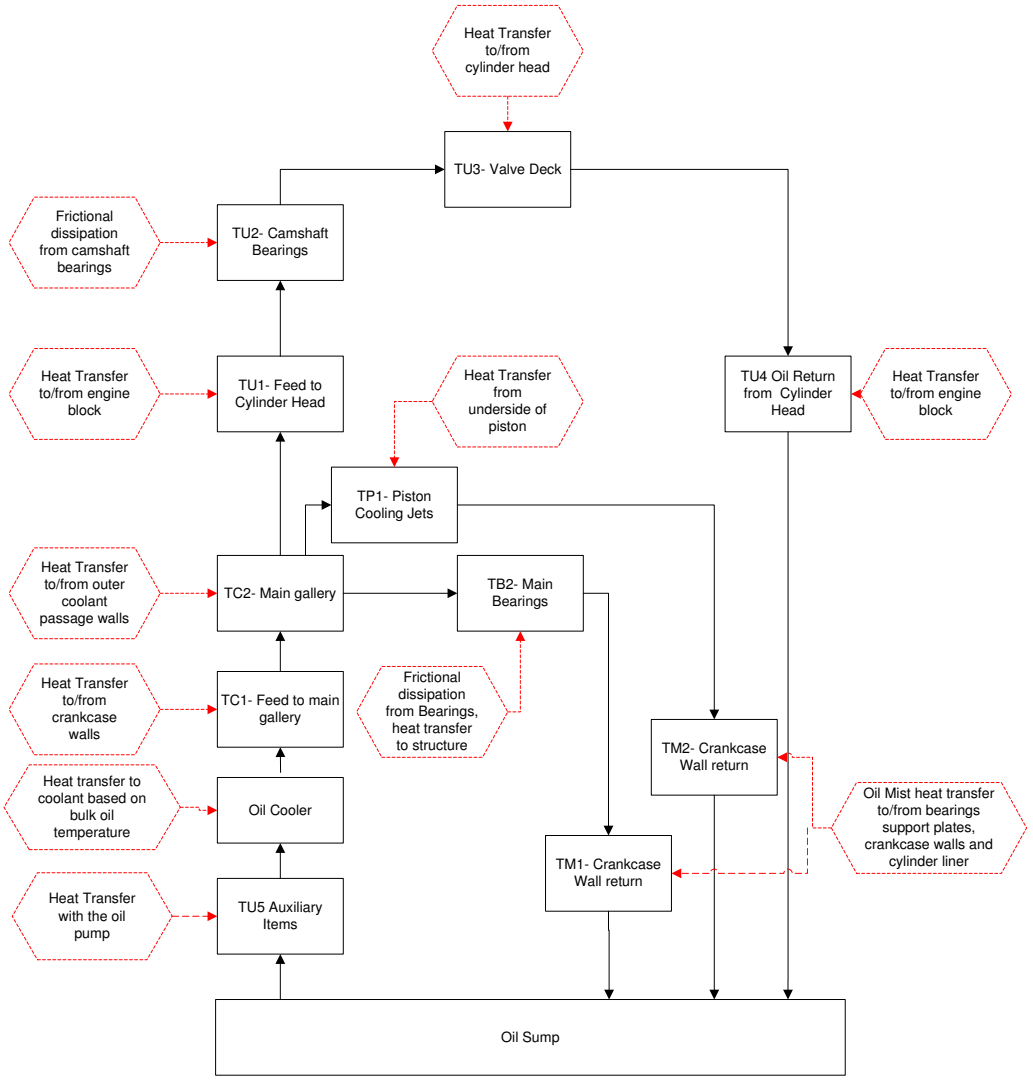

Figure 5.4 The PROMETS representation of the VIPER oil circuit

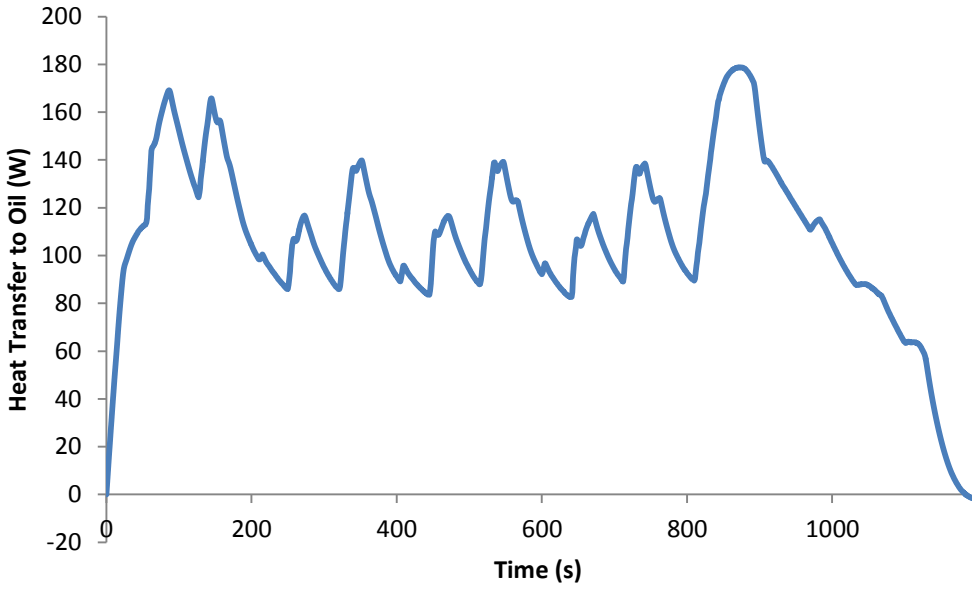

Figure 5.5 Predicted heat transfer to the oil in the main gallery during the aNEDC

5.4 Oil sump temperature

Bulk oil temperature is evaluated based on the sum of heat flows in and out of the circuit acting on a constant mass of oil. Bulk oil was previously been used as an approximation of the oil sump temperature, and has been useful in providing a temperature with which to evaluate an average oil viscosity for use in the PNH friction model.

With the move to a local temperature based friction model, a bulk oil temperature is no longer required, and the oil circuit has been reconfigured to include a representation of an oil sump temperature. This is more physically descriptive of the oil circuit.

Although work by Law [46] has shown large temperature gradients within the sump during early engine running, the sump oil has been assumed to be isothermal for the purposes of simulation. Experimental data from thermocouples located in the oil pickup in the sump does not show large temperature fluctuations as the oil enters the engine.

Based on an assumed mass continuity for the sump, the following energy balance has been made for sump oil:

$$m_s c_p \frac{dT_s}{dt} = \dot{m}_1 c_p (T_1 - T_s) + \dot{m}_2 c_p (T_2 - T_s) + \dot{m}_3 c_p (T_3 - T_s) + h_s A (T_a - T_s) \quad (5.1)$$

Where the subscript 1 refers to the oil in the bearing loop, 2 refers to oil in the piston cooling jet loop and 3 refers to oil in the cylinder head loop. T_s and T_a are sump and ambient temperatures. By using the temperature of sump inputs to evaluate sump temperature, the location can be represented within the oil circuit.

The heat transfer to ambient has been retained from the previous model, and is based on the assumption that the conductive heat transfer to the sump metal is insignificant when compared to the convective losses to ambient.

Oil consumption has been estimated for the main bearings, big end bearings, and the piston to determine the proportion of the pump oil flow that is in each of the loops and the energy which they will carry to the sump. Equations from Martin [94] [95] have been used to predict oil flow rate through journal bearings with a 180° groove. The flow rate is calculated as the sum of the hydrodynamic and pressure driven flow rate. Hydrodynamic flow describes the flow due to the pumping of oil through the bearing as a result of journal eccentricity, clearance, and rotation. The pressure flow results from the pressure difference between the main gallery and the ambient conditions at the outlet of the bearing. Hydrodynamic flow is given in [94]as:

$$\dot{Q}_h = \pi N D \varepsilon C L \left[1 - 0.22 \left(\frac{L}{D}\right)^{1.9} \varepsilon^{0.02}\right] \tag{5.2}$$

Here, N is the relative speed between the shaft and the journal, C is the radial clearance, L is the bearing length, D is the bearing diameter, and ε is the eccentricity ratio. Bearing eccentricity is set to a value of 0.8 which is typical of loaded journal bearings [33], and clearance is assumed to be 30 microns. This equation is valid for bearings of $0.25 \leq \left(\frac{L}{D}\right) \geq 1.0$ and $0.2 \leq \varepsilon \geq 0.9$

The pressure flow component is calculated as described by Martin [95] as:

$$\dot{Q}_p = \left(\left(\frac{1.23 - 0.25\left(\frac{a}{L}\right)}{6\left(\frac{L}{a} - 1\right)^{\frac{1}{3}}} \right) f_1 + \left(\frac{\frac{D}{L}}{6\left(1 - \frac{a}{L}\right)} \right) f_2 \right) \mu C^3 P \tag{5.3}$$

With:

$$f_1 = \left(1 + \varepsilon(cos\varphi_1)\right)^3 + \left(1 + \varepsilon(cos\varphi_2)\right)^3 \tag{5.4}$$

And

$$f_2 = \left[\varphi_2 + 3\varepsilon(sin\varphi_2) + \varepsilon^2\left(1.5\varphi_2 + \frac{(3(sin2\varphi_2))}{4}\right) + \varepsilon^3\left((sin\varphi_2) - \frac{(sin\varphi_2)^3}{3}\right)\right] - \left[\varphi_1 + 3\varepsilon(sin\varphi_1) + \varepsilon^2\left(1.5\varphi_1 + \frac{(3(sin2\varphi_1))}{4}\right) + \varepsilon^3\left((sin\varphi_1) - \frac{(sin\varphi_1)^3}{3}\right)\right] \tag{5.5}$$

In these equations a is the groove length, μ is the dynamic viscosity of the oil and P is the feed pressure to the bearing. The terms f_1 and f_2 are flow rate functions described in the reference and are dependent on the geometry of the oil feed groove. φ_1 and φ_2 are the angles of the beginning and end of the oil feed groove in relation to the attitude angle of the bearing. The attitude angle is the angle which arises if the centre of the bearing and the centre of the journal are joined by a line. In the case of an assumed eccentricity of 0.8, the attitude angle is 32°. Results from these equations for five main bearings at a range of speeds are shown in Figure 5.6. The dimensions used in are given in Table 5.1.

Table 5.1 Bearing properties for flow rate prediction

Eccentricity (-)	0.8
Attitude angle (°)	32
Feed Pressure (Pa)	400000
Length (m)	0.018
Diameter (m)	0.053
Groove Length (m)	0.004

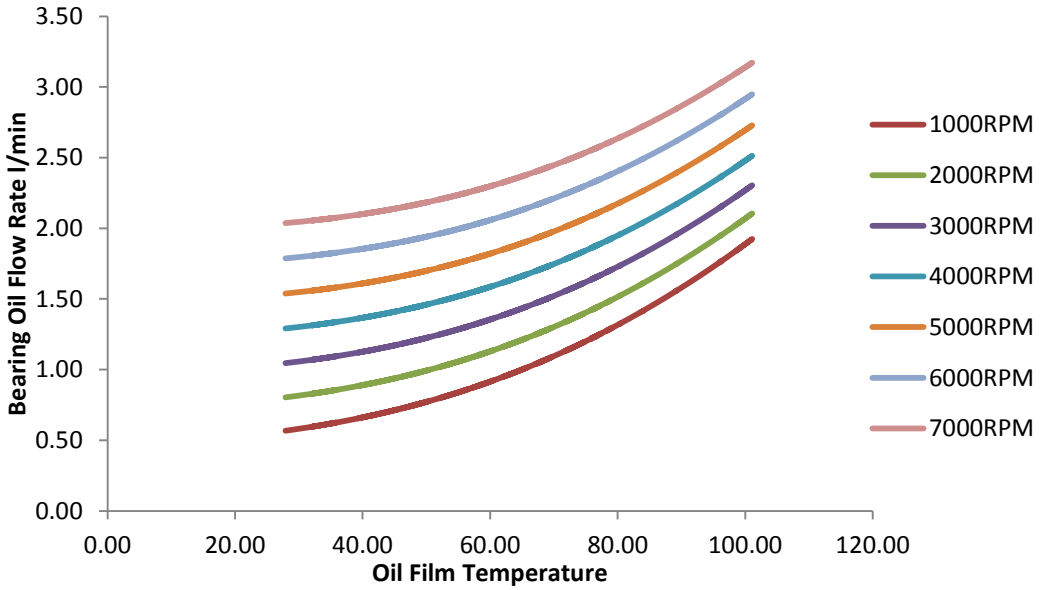

Figure 5.6 Summed flow rates for five crankshaft main bearings with a 180° groove using 5W30 oil

Big end bearing calculations are adopted from Mian [96]. This equation is suitable for a simple bearing with a single oil feed hole, and no oil supply groove in the bearing. These constraints are appropriate to big end bearing design.

$$\dot{Q} = 0.675\left(\frac{C^3 P}{\mu}\right)\left(\frac{D}{l} + 0.4\right)^{1.75} \tag{5.6}$$

Piston cooling jet flow rate was calculated based on empirical equations presented by Mian [96] which was itself based on work on discharge coefficients from Lichtarowicz et al. [97]. The discharge coefficients C_d were calculated by treating the piston cooling jets as long orifices, with a $\left(\frac{L}{D}\right)$ over 2.0. C_d is a ratio of the actual flow through the orifice, to the flow which would be produced if a stream of the same area was accelerated from the conditions at the supply of the orifice, for a given pressure drop.

The flow rate through the orifice is:

$$\dot{Q} = \frac{C_d A_o}{(1 - m^2)^{\frac{1}{2}}}\left(\frac{2\Delta P}{\rho}\right)^{\frac{1}{2}} \tag{5.7}$$

A_o is the area of the orifice, m is the ratio of diameters of the orifice supply pipe and the orifice, P is the pressure and ρ is oil density.

A hydraulic Reynolds number, which is based on orifice diameter and pressure drop (as opposed to flow velocity) is used to calculate discharge coefficient:

$$Re_h = \frac{d_o}{v}\left(\frac{2\Delta P}{\rho}\right)^{\frac{1}{2}} \tag{5.8}$$

Where v represents the kinematic viscosity. Two calculations are presented for the value of the discharge coefficient to distinguish between the changes in flow

characteristics. For turbulent flow, with Reynolds numbers greater than 20000, the upper limit of the discharge coefficient was expressed as:

$$C_{du} = 0.827 - 0.085\left(\frac{l}{d_o}\right)^{\frac{1}{2}} \tag{5.9}$$

However, at the operating conditions commonly seen in internal combustion engines, Reynolds numbers more in the region of 2000 are expected [46]. With a pressure drop of 4 Bar between the main gallery and the jet outlet, the oil viscosity would have to be an order of magnitude lower than the viscosity of a 5W30 oil at fully warm engine temperatures to reach the turbulent threshold. Therefore, for cases below the 20000 Reynolds number threshold, the following relationship is used: Flow through the piston cooling jets is shown in Figure 5.7.

$$\frac{1}{C_d} = \frac{1}{C_{du}} + \frac{20}{Re_h}\left(1 + 2.25\frac{l}{d_o}\right) - \frac{0.005\frac{L}{d_o}}{1.75(log 0.00015 Re_h)^2} \tag{5.10}$$

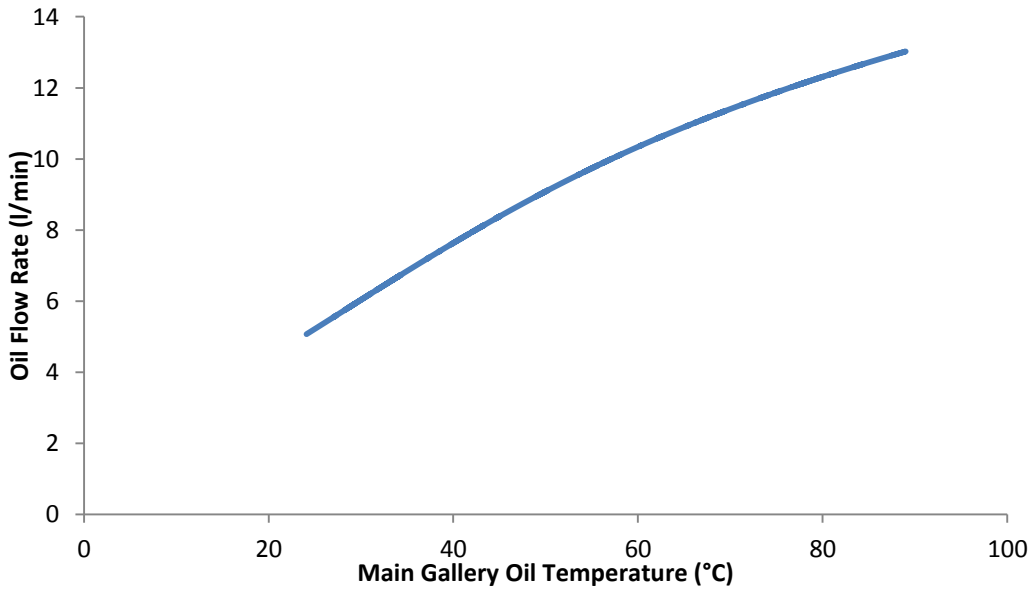

Figure 5.7 Total Piston cooling jet flow rate for four jets

Table 5.2 Piston Cooling Jet Properties

l (m)	0.05
d_o (m)	0.002

The final consumption of the piston cooling jets, main and big end bearings at fully warm conditions over a range of engine speed is shown in Figure 5.8. Piston cooling jet flow rate is independent of engine speed, and its contribution remains fixed, varying between 76-83% of total non-head main gallery oil flow, at fully warm conditions as engine speed changes. At lower temperatures however, this proportion changes, as both the piston cooling jets and the bearing flow rates are affected by changes in oil temperature. At 30°C oil temperatures, the piston cooling jets account for 91% of block oil flow when the engine speed is 500RPM, and this falls to 67% at 7000RPM. As the average engine speed of the NEDC is around 1000RPM, an 80% weighting in favour of the piston cooling jets has been adopted.

Once the mass flow rate splits between the piston, bearings, and the flow from the head have been evaluated, and the energy input to the sump oil calculated, the sump temperature is then given as:

$$T_1 = T_0 + \frac{Q}{\dot{m}C_p} \tag{5.11}$$

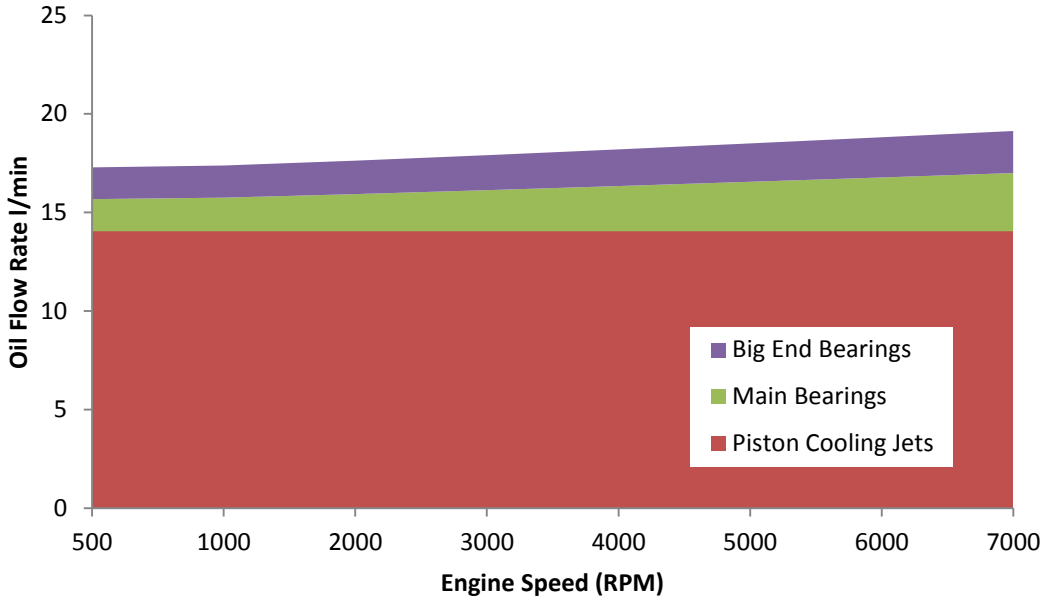

Figure 5.8 Flow rate comparison between bearings and jets at fully warm. Gallery pressure is constant at 4 bar

5.5 Filter cooler heat transfer

After the sump temperature has been calculated, the oil is thermally linked to the ancillary components with which it is in contact. This step was previously done after the oil had returned from the cylinder head and was not representative of an actual oil circuit.

After the pump, the oil flows through a small gallery to the filter cooler assembly. As with the ancillary heat transfer, this was previously conducted at the end of the oil circuit. This location has been moved to match the VIPER oil circuit.

The oil cooler is a device fitted to engines that facilitates heat dissipation from the oil to the coolant at fully warm conditions in order to prevent excessive temperature in the oil which gives rise to premature oil degradation. Conversely, during engine warm up, the oil cooler allows the coolant to act as a heat source for the oil, as the coolant temperature tends to lead the oil temperature, generally until the thermostat opens.

The oil cooler fitted to the VIPER engine has an effectiveness of around 20% when analysed using the Number of Transfer Units (NTU) method of dividing the actual heat transfer achieved by the cooler, by the maximum possible heat transfer achievable with an exchanger of infinite length as shown in Equation 5.12.

$$\varepsilon = \frac{Q}{Q_{max}} \tag{5.12}$$

Q is given as:

$$Q = C_p(T_1 - T_2) \tag{5.13}$$

Q can be calculated using the specific heat capacity and temperatures for either fluid, as the heat transfer to one fluid will equal the heat transfer from the other.

Q_{max} is calculated by taking the smaller value of the two fluid's specific heat capacities, and the temperature difference between the hot and cold fluids at the entrance to the heat exchanger:

$$Q_{max} = C_{min}(T_h - T_c) \tag{5.14}$$

The heat transfer in the oil cooler is then modelled as:

$$Q = \varepsilon\left(\dot{m}C_p\right)_{min}(T_c - T_o) \tag{5.15}$$

Where ε is the effectiveness, a number between 0 and 1. $(\dot{m}C_p)_{min}$ is the heat capacity multiplied by the flow rate. The value of this calculated for each of the fluid and the lower of the two results is taken. T_c is the coolant temperature, and T_o is the oil temperature. These values were measured during engine operation, and used to evaluate the effectiveness. Figure 5.9 shows oil cooler effectiveness calculated using experimental temperature data from three sets of fixed speed running conditions at engine speeds and loads representative of NEDC running conditions. The initial transients shown on the chart are a result of the flow rates of the oil and coolant establishing themselves, and the temperature of the oil feed stabilising.

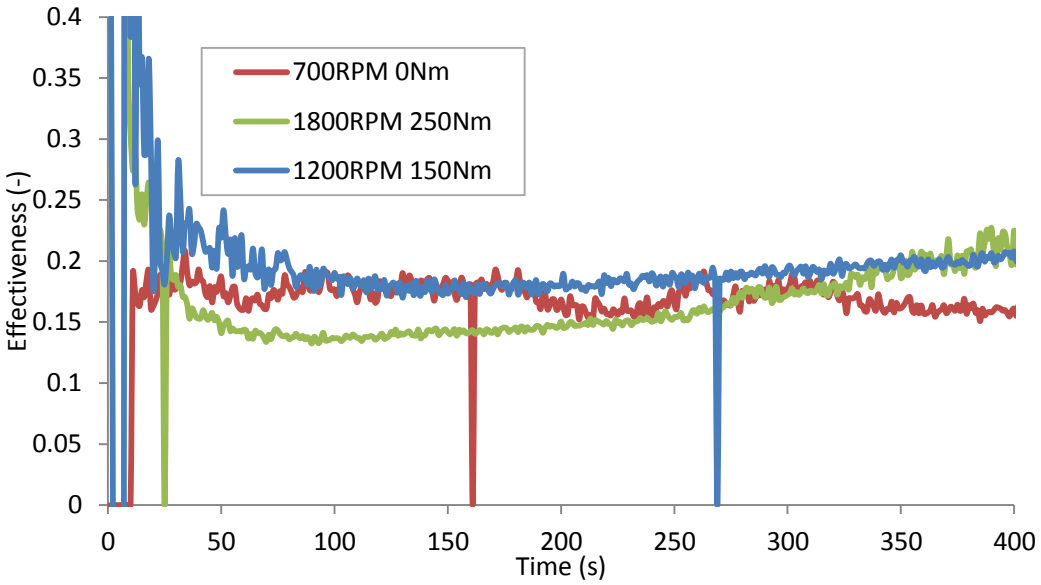

Figure 5.9 Experimental Oil cooler effectiveness data from NTU analysis. Tests were performed at constant speed load, and from cold start.

5.6 Main bearing model

The friction contribution from the main bearings is predicted to account for 13% of total engine friction power throughout an aNEDC, making it a significant contributor to the fuel consumption of the engine. In addition to this, the frictional dissipation here is one of the heat sources for the oil, accounting for around 10% of the total heat transferred to the oil during the aNEDC. Figure 5.10 shows the cumulative heat transfer to the oil in the model from all of the heat sources over an aNEDC. Heat transfer from the structure is the dominant mechanism for oil warming, but frictional dissipation is still a significant source of energy. The correct treatment of the balance between the dissipation of friction power to the oil and the heat conduction from the oil to the structure is critical when examining local thermal behaviour.

Previously, handling of the thermal friction interaction around the bearings in the PROMETS model assumed that a fixed proportion of the power dissipated as friction is transferred to the oil as heat. However, a paper by Jarrier [98] predicted this proportion to vary between 20% of friction power being used to heat the oil at engine start where the engine structure remains cold and therefore acts as a significant energy sink. This rises to 90% after 40 minutes of simulation when the engine is fully warm and most of the friction power is transported away from the bearing in the oil.

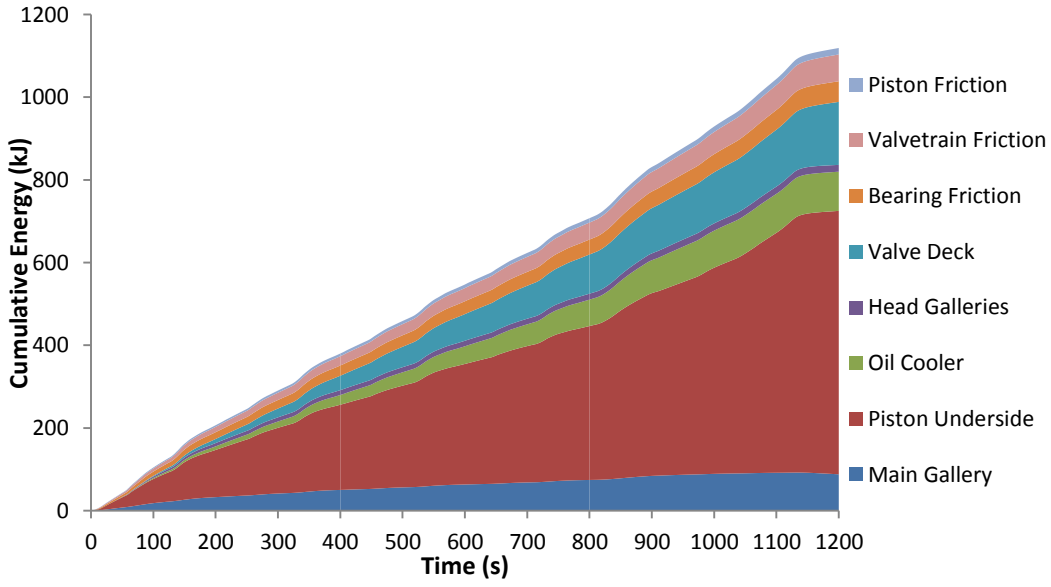

Figure 5.10 Predicted oil energy sources throughout the aNEDC

A simplified lumped capacity representation of the lower part of the engine block surrounding the crankshaft bearings was employed in older versions of the PROMETS model. Two large elements were used to represent both the bearing support plates, and the crankshaft journal, a mass which, in the VIPER engine accounts for around a fifth of the total engine.

An updated friction model has been developed where calculations are based on local temperatures, and an increased number of elements along with a description of the thermal-friction interaction in the bearing synergises well with this. This model is a continuation of the work done by Law [66] and Zammit [70] to describe the thermal interactions between the oil film, journal bearings and the metal surrounding the bearings in diesel engines, with the concept extended to further increase the number of elements that describe the bearing support plates and the addition of a shell element.

An additional three elements have been added to the model to represent the crankshaft, bearing shell and main bearing caps. The bearing support plate elements have been increased in number from two to four elements to increase the fidelity of radial heat transfer predictions. The new elements are shown in Figure 5.11 along with the previous layout. Table 5.4 gives the properties of the new elements.

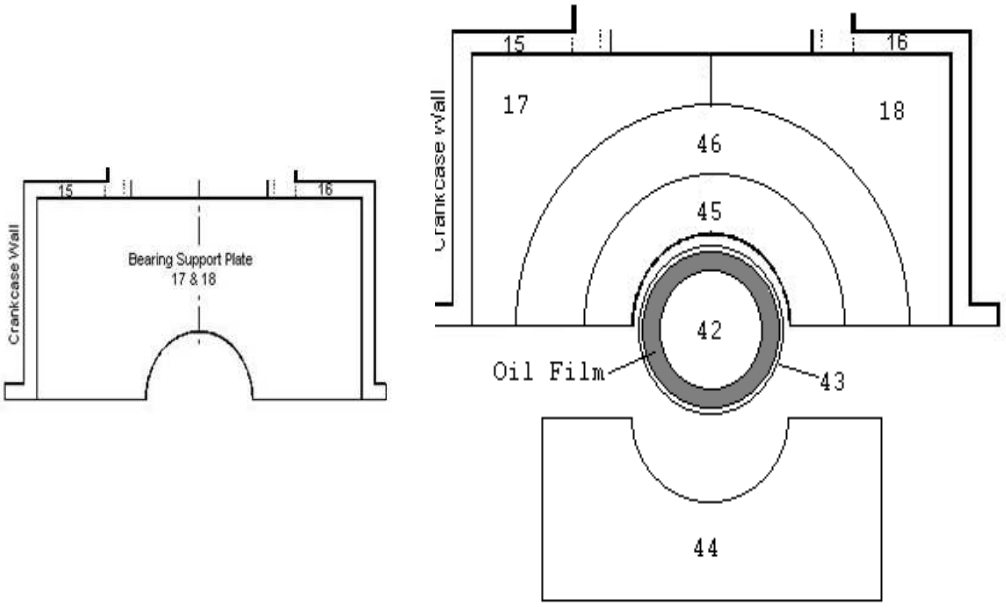

Figure 5.11 New lumped capacity elements surrounding the main bearings.

Table 5.4 Element Properties and Dimensions for the bearing model

Element	Material	Volume (m^3)	Thermal Conductivity ($W.m^{-1}.K^{-1}$)	Specific Heat Capacity (J/Kg.K)	Density (kg/m^3)
Outer Bearing Support Plate	Aluminium	$1.3x10^{-4}$	162	871	2660
Inner Bearing Support Plate	Aluminium	$6.3x10^{-5}$	162	871	2660
Bearing Carrier	Aluminium	$8.6x10^{-5}$	162	871	2660
Main Bearing Shell	Steel	$4.16x10^{-6}$	26	420	8700
Main Bearing Shaft	Cast Iron	$3.82x10^{-5}$	54	460	7570

The model assumes that all of the bearing friction work is dissipated into the oil film initially, before being transferred to either the crankshaft element, or the bearing shell element, both of which are assumed to be at a spatially uniform temperature for the purposes of the model. This heat transfer is assumed to be distributed equally around the bearing to the two elements.

Given this, the energy balance for the friction work $\dot{P}_f$, element and oil temperatures is given in [70] as:

$$\dot{P}_f = \dot{m}_o c_p (T_o - T_i) + \dot{Q}_{shell} + \dot{Q}_{journal} \tag{5.16}$$

This can be rewritten as

$$\dot{P}_f = \dot{m}_o c_p (T_o - T_i) + \frac{(T_f - T_s)}{R_{th,s}} + \frac{(T_f - T_j)}{R_{th,j}} \tag{5.17}$$

Here, the subscript i denotes oil inlet conditions, o denotes oil outlet conditions, f is the film, s the shell and j the journal. The thermal resistance between the film and the metal elements was shown in [70] to best represent experimental data for

oil film, and the surrounding metal temperatures when set to a value of 0.07 K/W. A value of 0.035K/W was found to give much better agreement with experimental data. Using this lower value, the initial temperature rise over the gallery temperature is reduced. Sensitivity studies carried out by Zammit [70], showed the influence of the thermal resistance on the film temperature to be high during early running, with a large effect on the initial temperature rise seen in the film, but making a diminishing impact on the film temperature as the oil warmed.

The model is run in an iterative loop written in an embedded M file. After receiving the user inputs of engine speed, oil starting temperature and bearing dimensions, the model uses the Vogel Equation (4.12) and oil temperature from the previous time step to calculate viscosity. This provides the correction needed for Equation 4.5 to calculate main bearing friction. Using the value for friction power, the film temperature is then re-evaluated, and heat transfer to the metal elements is calculated. The iterative process is halted when a difference of less than 0.5°C is achieved between current and subsequent oil film temperature predictions.

The destination of the heat dissipated as friction in the bearing is shown in Figure 5.12 for a constant speed test at 3000RPM. In the early seconds of running, the majority of the heat is transferred to the structural elements in contact with the oil and 20-30% of the total heat is used to raise the temperature of the film here. As the oil warms, it exceeds the temperature of the structure at the bottom end of the engine, and by approximately the 600 second mark, the oil entering the bearing from the main gallery is being cooled in the bearing due to the strong thermal link between the oil and the structure in this location. This can be seen in the Q_{conv} term as it reduced to zero at this point. The engine structure at the lower end of the engine eventually reaches its normal operating temperature, in the test this occurs at between 800 and 900 seconds, and at this point, the majority of the frictional dissipation is being carried out of the bearing in the oil, as is shown by the dominance of the convective heat flow at the end of the test. These results stress the challenges encountered when attempting to manipulate the engine's thermal state. In order to maximise the impact of feeding the bearing

with warmer oil, the thermal links between the oil and the lower structure of the engine must be weakened or broken so that as much of this temperature increase as possible is preserved in the bearing. This would allow for a larger proportion of energy to be retained in the film in during early running, and help mitigate the detrimental effect seen between 600 and 700 seconds in this test where the oil is losing energy.

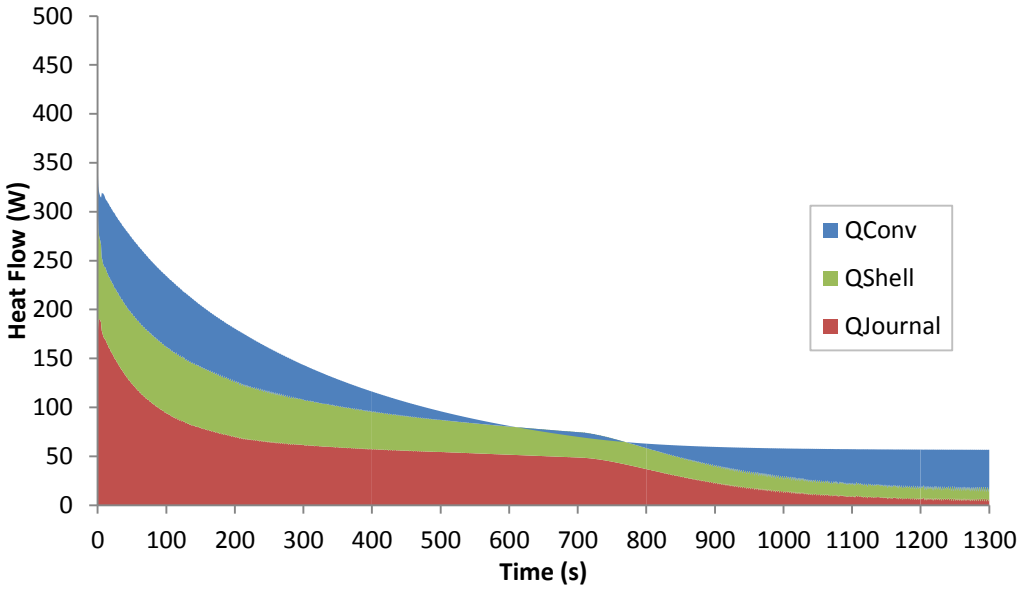

Figure 5.12 Predicted heat transfer in the main bearings for a 3000RPM warm up

5.7 Bearing model results

Results from the bearing model are shown below. The model captures the thermal behaviour of the bearing film in greater detail than the fixed proportion of friction solution did. Rapid responses to changes in friction throughout the aNEDC can be seen in Figure 5.13. The old prediction followed the temperature trends in the main gallery very closely whereas the new bearing model allows for additional temperature transients to be captured. Figure 5.14 shows the heat flows in the bearing during the final phase of the first UDC. The rapid changes in the levels of frictional dissipation to the film, the journal and the shell can be clearly seen. Fixed speed warm-up results are shown in Figure 5.15. The model captures the fast rise in temperature at the bearings, over the temperature rise purely from the increase in feed temperature, but over-predicts the effect at the end of the cycle. The previous model input similar levels of power to the oil, but did so to a mass flow rate that was estimated as a flat multiplier of the total engine oil flow, which reduced the sensitivity of the temperature predictions at this locations. The response to the same coolant plunge test as described in Section 4.8 is shown in Figure 5.16. Here, the temperatures follow the experimental oil response very well. This ability to predict the response to unusual transient events highlights the robustness of the model.

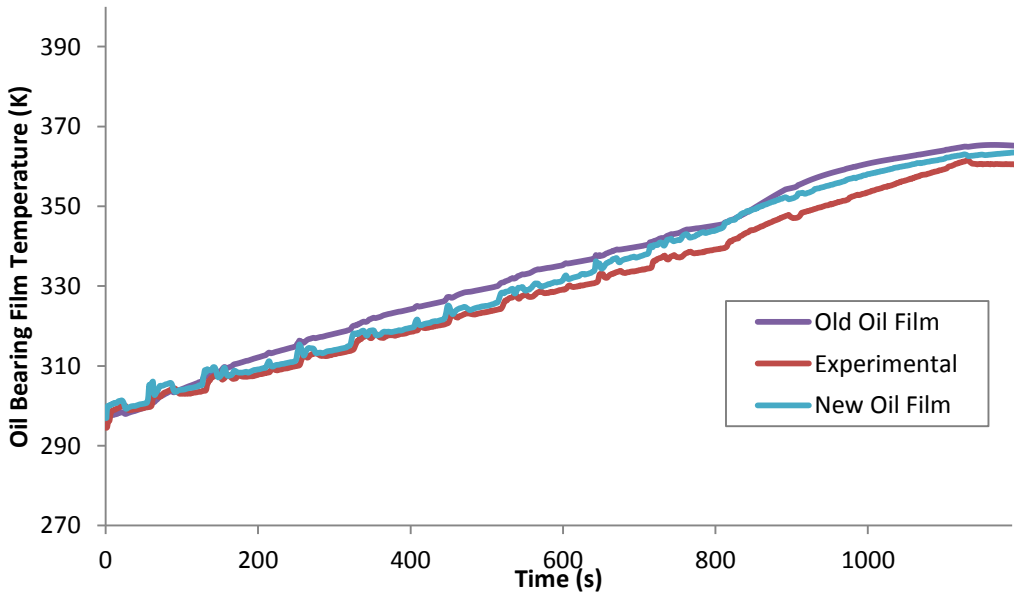

Figure 5.13 Warm up comparison between old and new bearing temperature prediction, and experimental data for the aNEDC

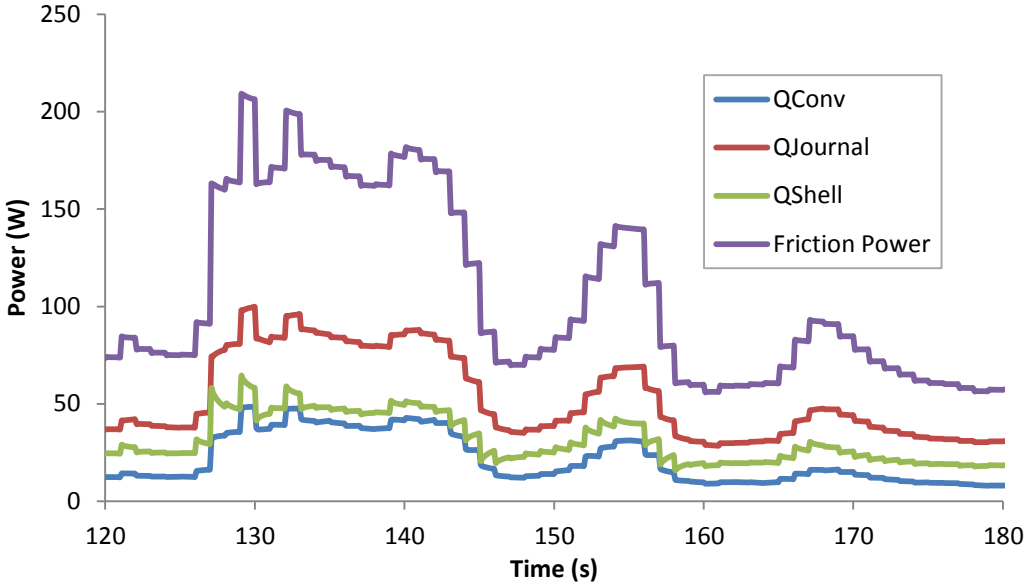

Figure 5.14 Predicted bearing heat flows over a single acceleration during the NEDC

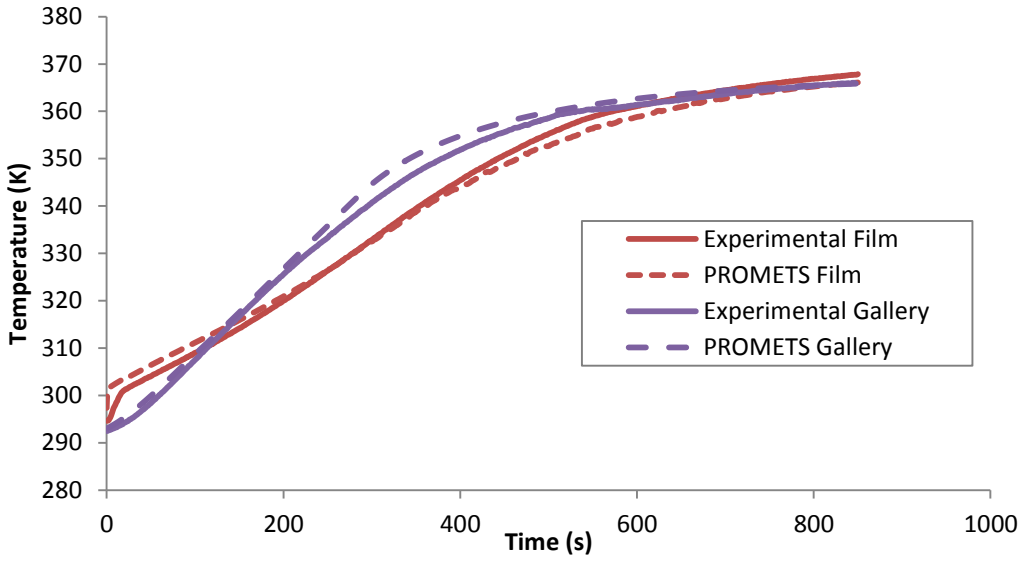

Figure 5.15 Warm up comparison between bearing and main gallery temperature predictions, and experimental data for the a fixed speed warm up at 1800RPM 90Nm

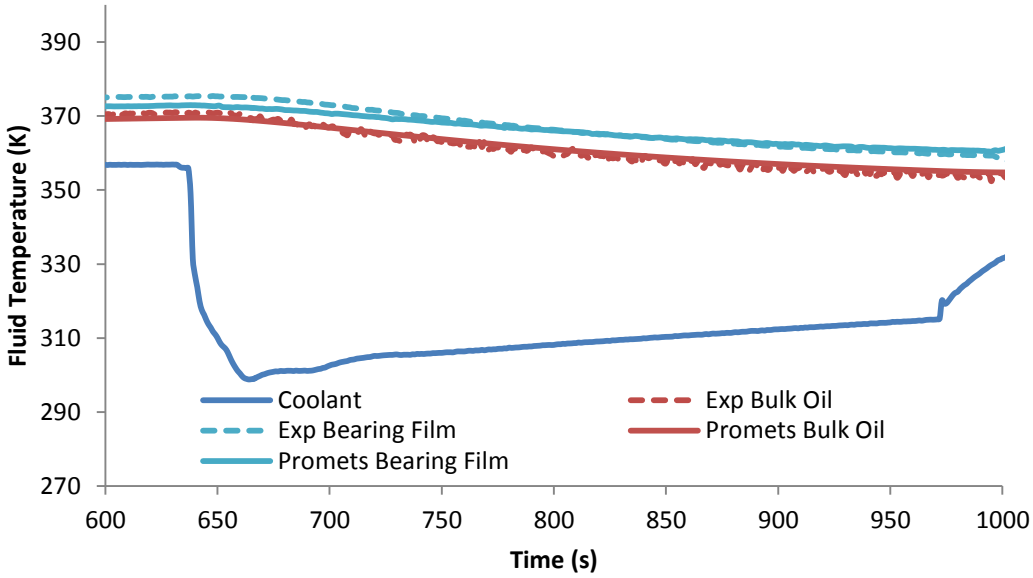

Figure 5.16 Coolant plunge test results for film and bulk oil temperatures.

5.8 Piston cooling jets

Piston cooling jets are devices, usually fitted to the main galleries which direct a stream of oil to impinge on the underside of the piston to increase cooling in this area. Increases in internal combustion engine performance combined with a trend in downsizing, has led to higher thermal loading on the piston. Passive splash cooling by the oil in the crankcase has been sufficient in the past to keep piston temperatures within an operating window where thermal efficiency and material safety are not jeopardised. Newer, more powerful and often turbocharged engines now require dedicated cooling of the pistons. The use of piston cooling jets in an engine will alter the distribution of heat in the engine. In an engine with no jets installed, the final destination of the thermal energy in the piston is the coolant via the cylinder liner. The addition of piston cooling jets will redistribute a proportion of this to the oil. Zammit [70] predicts this proportion as being between 40% and 60% of the energy input to the piston crown in a diesel engine. There will be an increase in the volume of oil present in the crankcase when jets are installed, which will cause additional resistance on the crankshaft as it moves through the oil mist [75]. This has not been modelled.

The PROMETS oil circuit used the temperature calculated in the main bearings as the source of oil being used to cool the piston skirt in the old model, and the heat transfer coefficient was based on an oil mist in contact with the metal. A value of $50 W/m^2.K$ was used in this version of the model. The heat transfer coefficient produced with a high flow rate directed jet of oil impinging on the underside of the piston has been shown to be orders of magnitude higher than this, as demonstrated in [99].

In work done by Easter et al. [100], a Nusselt number correlation was sought. The form of this is given in Equation 5.10. This work is some of the most recent focussing specifically on jet heat transfer with the piston. This correlation has been integrated with the PROMETS oil circuit to predict the heat transfer coefficient with the back of the piston. Other models have been presented in [101] and [102] but these focus on diesel engines, which often have cooling galleries within the piston.

$$Nu_{avg} = h_{avg}\, {}^{d_o}/_{k} = W\left({}^{z}/_{d_o}\right)^{X} Re_o^{Y} Pr_o^{Z} \tag{5.10}$$

This is rearranged to give the average heat transfer coefficient for the piston underside and the oil jet:

$$h_{avg} = {}^{k}/_{d_o}\, W\left({}^{z}/_{d_o}\right)^{X} Re_o^{Y} Pr_o^{Z} \tag{5.11}$$

In this equation d_o is the diameter of the jet outlet and z is the distance between the piston and the jet. The constants W, X, Y and X were empirically determined for a nozzle of a diameter of 1.7mm and are given in Table 5.4. The nozzles fitted to the VIPER engine have an outlet inner diameter of 1.4mm. Consequently it is expected that the constants used reported in [100] will cause a slight under prediction of heat transfer coefficients.

Table 5.4 Constants for equation 5.11 [100]

Constant	**W**	**X**	**Y**	**Z**
Value	0.028	-0.034	0.652	0.4

Reynolds number is calculated in equations 5.10 and 5.11 as:

$$Re_o = \rho_o v_o\, {}^{d_o}/_{\mu_o} \tag{5.12}$$

The velocity was determined by using the mass flow rate calculation in equation 5.7 and assuming no reduction in flow speed across the distance between the piston underside at the mid-stroke position and the jet outlet. Oil viscosity is calculated using the Vogel equation (4.12).

Predicted heat transfer coefficients using Equation 5.11 can be seen in Figure 5.16. Results agree with values reported in [99] as well as from the source research [100].

Implementation of the piston cooling jet model has added a significant extra heat source for the oil. During the aNEDC, this peaks at 350W per piston. In Figure 5.17, the heat transfer between the oil from the piston cooling jet, and the heat

transfer between the crankshaft oil mist and the piston skirt are shown. Jet heat transfer can be seen to be significantly greater than mist heat transfer.

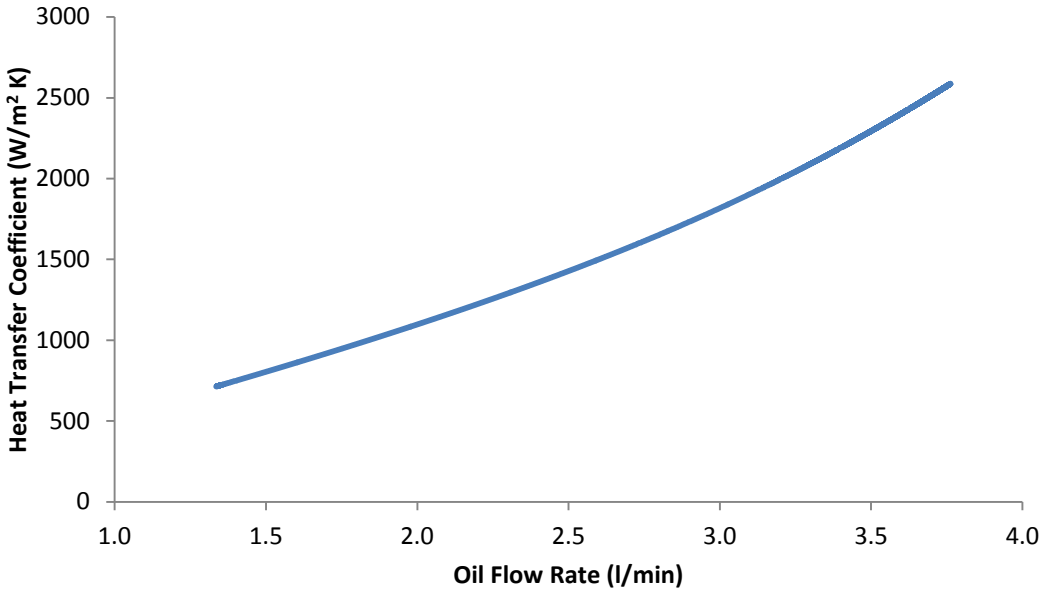

Figure 5.16 Heat transfer coefficient variation with oil flow rate for the piston cooling jets

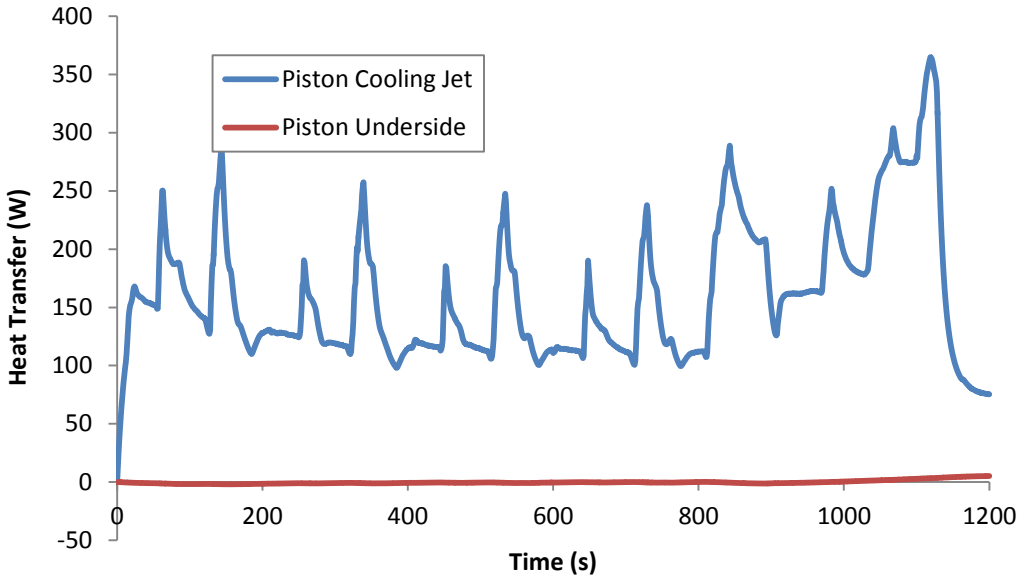

Figure 5.17 Comparison between predicted heat transfer achieved with piston cooling jets and that achieved with splash cooling of the piston underside for a single cylinder

5.9 Oil circuit predictions

The oil circuit temperature predictions have been compared to transient and fixed speed running conditions in this section. Sump oil temperature predictions have been compared with the measurements from a thermocouple located at the intake to the oil pump. This thermocouple provided a much less variable signal than the mid-sump thermocouple and is more representative of the oil temperature that the engine experiences. Full details of the engines instrumentation can be found in [92]

Oil temperatures agree well with experimental data for aNEDC tests and for constant speed warm up. In Figure 5.18, a warm up prediction over the aNEDC is shown. The predictions for two other fixed speed warm ups are shown plotted against their experimental equivalents in Figure 5.19. The dotted lines in this figure represent ±10°K from the experimental, and shows that the predictions fall within these limits in all cases.

The temperature distribution along the lower loop of the oil circuit is shown in Figure 5.20. This gives the experimental temperatures as the oil leaves the sump and flows through the main gallery to the bearings. Additional nodes are represented for the predictions of oil at the piston cooling jets and the crankcase mist, although these values are not available experimentally. The ability to predict temperatures that are difficult to measure is a strength of this model. The temperature distribution along this loop is established early as can be seen in Figure 5.20 which shows the temperatures 10 seconds into an aNEDC warm-up. This temperature distribution is maintained throughout the warm-up as can be seen at 200 and 1000 seconds. The PROMETS model tends to over-predict sump temperatures and therefore under-predict heat transfer seen in the galleries, as can be seen by the temperature rise between the bulk and the gallery being lower than that seen experimentally.

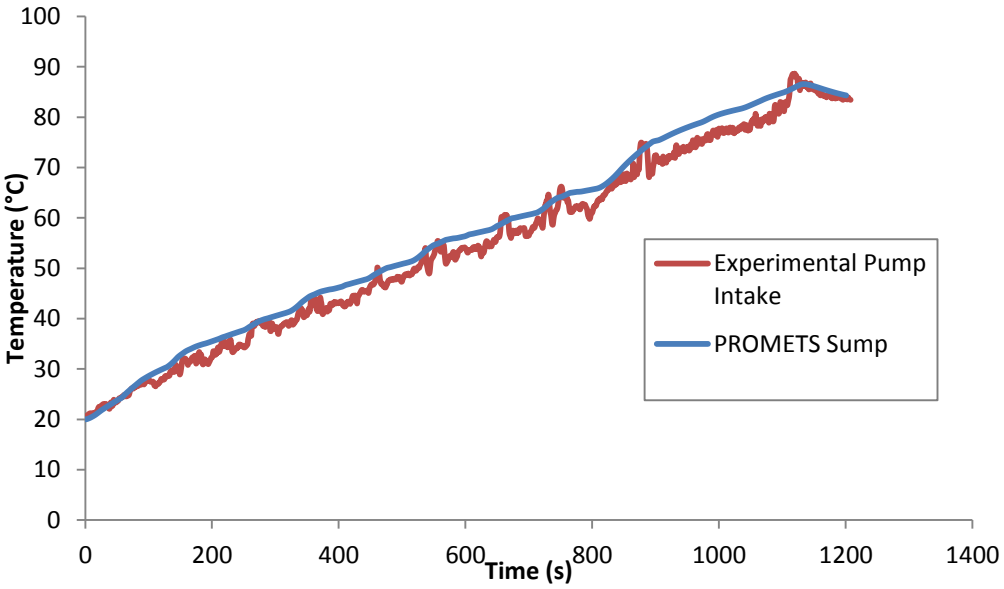

Figure 5.18 aNEDC experimental and predicted results

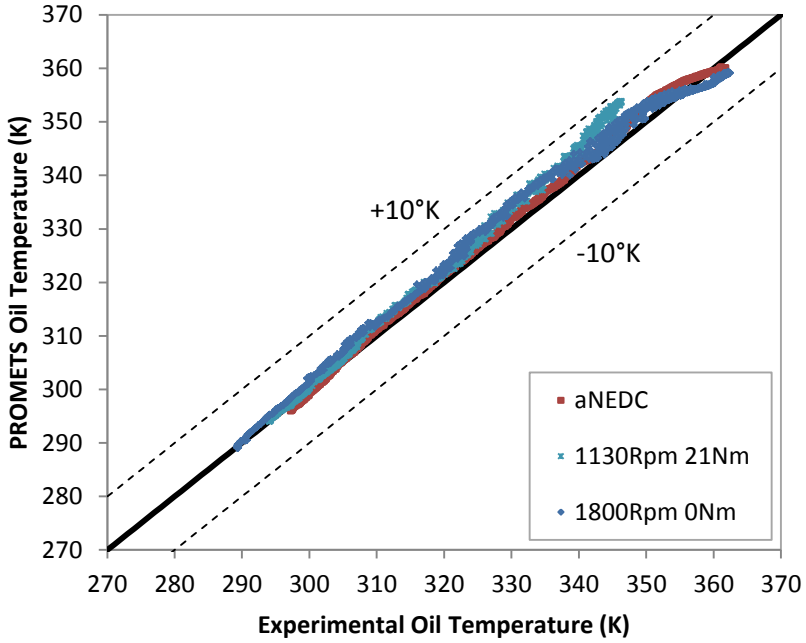

Figure 5.19 Predicted vs Experimental sump oil temperatures

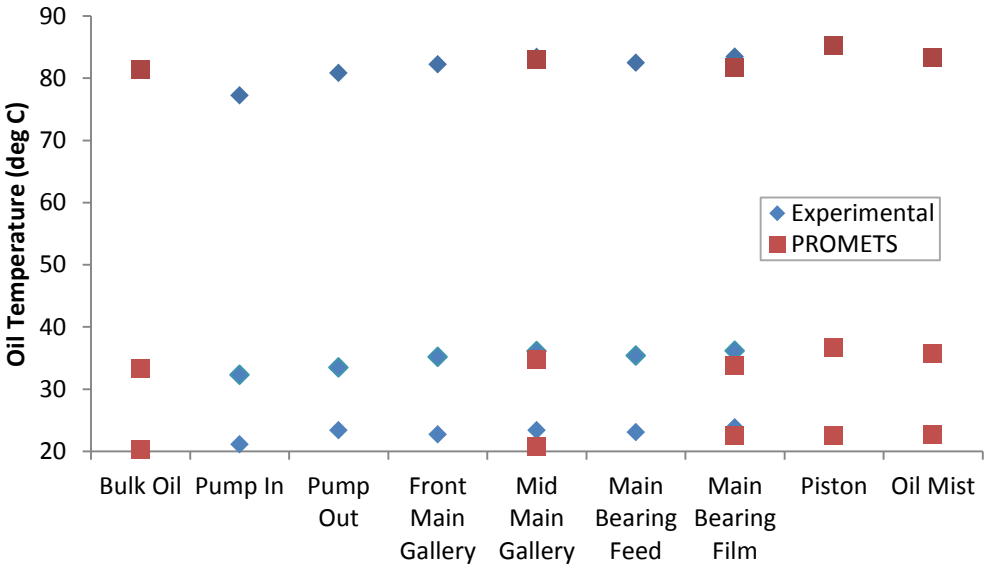

Figure 5.20 Lower oil circuit loop at 10, 200 and 1000 seconds into an aNEDC test.

5.10 Discussion

The oil circuit model in the SI PROMETS has been strengthened in its representation of a modern SI engine. An iterative model which solves the energy balance in the main bearings has been added to replace an assumption of a fixed proportion of frictional dissipation being driven to both the structure and the oil. A Nusselt number relationship has been used to predict the heat transfer coefficient for an oil jet impinging on the piston crown underside. The main gallery has been relocated to sit next to the cylinder. The sequence in which heat transfer calculations are carried out has also been modified to match the VIPER engine.

Results from the bearing model show strong coupling of the oil film temperature to the temperature of the surrounding metal, as illustrated by the high heat transfer rates to the structure during warm up. Reduction in bearing friction through increasing the oil feed temperature would therefore be difficult without insulation of the bearing to weaken this coupling.

In terms of thermal characteristics of the oil circuit, the single most significant source of difference between the representations of the engines oil circuit is the addition of piston cooling jets. These have not been simulated in SI engines in PROMETS. The effect of piston cooling jets on diesel engines was seen in [103] as being beneficial to emissions levels, but had a negligible impact on fuel economy. Simulation of oil circuit warm up shows an additional 780KJ of energy being transferred to the oil over the course of the aNEDC via the heat transfer from the piston to the oil. This energy would previously have been conducted through the piston rings to the liner, and eventually the coolant. A small proportion of this would have eventually reached the oil through the oil filter cooler. When comparing net heat transfer to the oil between the two cases, of the original 780KJ of extra energy transferred to the oil from the piston cooling jets, only 260KJ appears in the net value. A full break down of the changes to net heat transfer to the oil from the structure can be seen in Figure 5.21. The majority of the effects that prevent the piston cooling jets having as much impact as they could on the oil temperature are the reduction in heat transfer due to warmer oil in

the galleries during PCJ operation, reduced heat transfer from the coolant in the oil cooler, the increased heat loss in the oil mist.

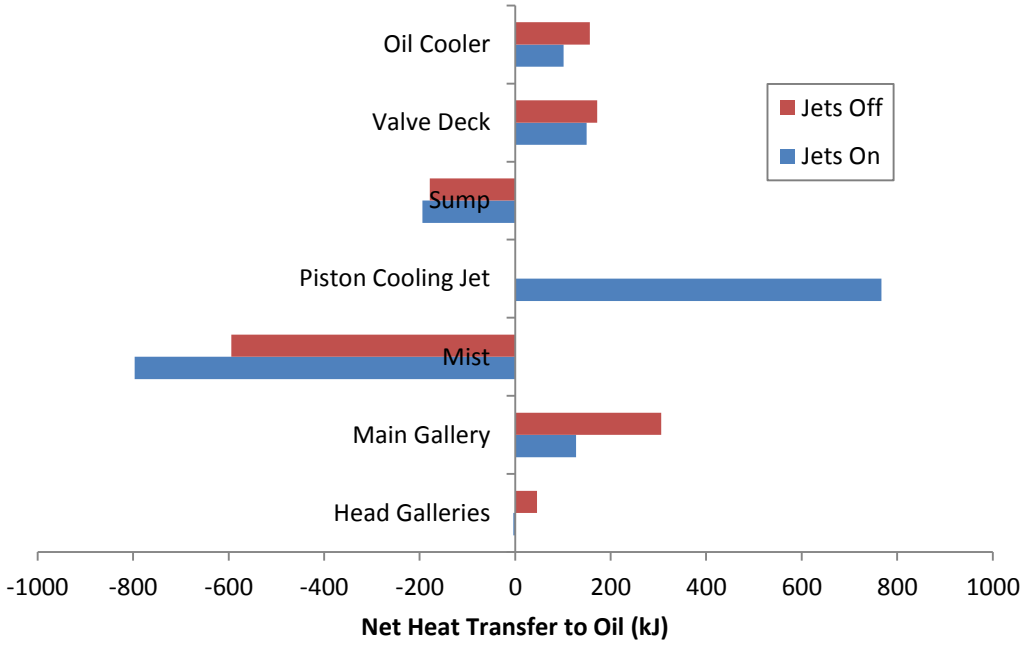

Figure 5.21 The predicted changes in heat transfer between the oil and the engine structure when using piston cooling jets.

The mitigating effects of the other heat transfer pathways on the addition of a heat source in the piston cooling jets would be applicable if other heat sources were used. Minimising the increases in heat loss in the mist or through the sump by insulating these areas would not only reduce the dampening effect on the introduction of external power, but also be beneficial in and of themselves. The problem of added power being "wasted" through reduced heat transfer in the galleries however is more difficult to solve. The gallery heat transfer is beneficial when considered alone, and so insulating the oil from these locations would have a negative effect on the warm up rate. Energy added directly at the feeds to the rubbing surfaces would have the greatest impact, as the balancing effects of the rest of the oil circuit would not have an effect on the temperature before friction benefits could be realised. If a method of providing an external power supply to provide heating of the oil is to be best utilised, these observations should be useful.

This work has focussed on the lower loop of the oil circuit, i.e. the flow through the main gallery and around the bearings and piston cooling jets. The head circuit representation remains unmodified from previous iterations of the model. The flow around the cylinder head remains poorly understood, as does the nature of the flow returning to the head. This area of the engine provides a significant heat source to the oil. Results from experiments on increasing the flow rate to the cylinder head in [104] showed a temperature increase of 10°C in the main gallery when flow rate to the cylinder head was doubled, and predicted a 2°C increase if this measure was implemented over a single urban section of the NEDC.

Improvements to the oil circuit model in PROMETS have made the predictions of changes to engine thermal state stronger due to better representation of the thermal connections present within the engine. This is important when considering thermal management of an engine, as in many cases the heat transfer between fluids and the structure can act to reduce the benefit that might be expected when energy is added to the oil.

The influence of the turbocharger on oil temperature has been neglected in the current work. This is an area in which the oil circuit could be improved in the future. Based on the size of the restriction at the oil feed to the turbocharger, the oil flow rate can be assumed to be relatively small. However, it is expected that the large temperature difference between the oil and the turbocharger may cause a reasonably significant amount of heat to be driven to the oil here.

Chapter 6. Assessing engine performance over the NEDC

6.1 Introduction

Having made improvements to the oil and friction model as described in previous chapters, the focus in this chapter will be on the behavior of the engine under NEDC and aNEDC running conditions. The way in which the model calculated pumping losses will be revised for more accurate prediction during the drive cycle. Other modifications to the model to improve the predictions for these running conditions will also be presented. Apart from friction and brake work, the pumping loss of the engine is the other main contributing factor to engine fuel consumption, and so the method of predicting these has been examined and modified for NEDC conditions. The indicated thermal efficiency of the engine has also been determined experimentally in order to improve the accuracy of the fuel consumption calculations. In order to identify the area of targetable savings, the way in which the VIPER engine uses fuel throughout the aNEDC has been described, and ways in which thermal management and reductions in parasitic losses can be used to improve fuel economy are discussed.

6.2 Pumping losses

Pumping work is defined as the work transfer between the piston and the cylinder gases during the inlet and exhaust strokes. It can generally be further divided into two parts: throttling work and valve flow work [16]. The throttling work is the work required to draw the cylinder charge through the air paths upstream of the intake valves, and downstream of the exhaust ports. This includes components such as the throttle, air filter, turbocharger, intake manifold, exhaust manifold and after treatment systems. The valve flow work is that attributed to flow through the intake and exhaust valves and ports. SI engines will typically experience high pumping losses at low engine load, as heavy throttling increases the amount of work required to bring air into the cylinder, with work reducing as the load is increased and the throttle opened. Conversely, the valve flow work is higher with increased engine load.

In the course of the project, it was decided to develop a simple empirical solution to provide PMEP values for NEDC running conditions. Previous versions of the spark ignitions PROMETS model have, to date, only modelled naturally aspirated engines when evaluating PMEP. Having a turbocharger in the air path will alter the pumping losses across the engine; whilst the turbocharger is providing a high pressure charge, pumping losses will be low, and vice versa. This will alter the fuelling requirement of the engine, and so should be taken account of in the PROMETS fuel consumption model. Turbocharger models developed for the compression ignition version [64] [91]are unsuitable due to the lack of a throttle in these engines.

Having a turbocharger present in the air path will alter the pumping losses across the engine, as the work required to move gases in and out of the cylinder will depend on the mode of operation of the turbocharger. Whilst the turbocharger is providing a high pressure charge, pumping losses will be low, and vice versa. This will alter the fuelling requirement of the engine, and so should be taken account of in the PROMETS fuel consumption model.

With the main emphasis of this project being on the thermal state, and fuel consumption of the engine, the decision has been made to focus on the effects on pumping losses of the turbocharger, as opposed to modelling the turbocharger physically, and to this end, a simple relationship linking the mass flow rate of air into the engine to the pressure drop across the engine intake has been sought. The following assumption has been made to approximate the pressure drop across the engine:

$$P_{ex} - P_{man} = \Delta P_{eng} \tag{6.1}$$

Here, P_{amb} is the ambient pressure in the laboratory, P_{man} is the pressure in the intake manifold of the engine, which is measured after the throttle and the compressor, and P_{ex} is the pressure in the exhaust manifold, measured before the turbine and after-treatment.

By evaluating the pumping losses in this manner, the complex interactions between the compressor and throttle, and waste-gate and turbine can be simplified, with their effects expressed as a function of the pressures observed in the inlet and exhaust manifold. The evaluation of the pressure drops over these components would have been difficult to evaluate given their complexity, and is not in the scope of this project.

To evaluate the intake manifold pressure from known temperatures and densities, the ideal gas law for mass flow rate was used, where:

$$\frac{\dot{m}}{v} = \rho = \frac{P}{RT} \tag{6.2}$$

Rearranging for P then gives:

$$P = \rho RT \tag{6.3}$$

The density of the intake air can be expressed as:

$$\rho = \frac{\dot{m}}{V_s \frac{N}{120} \eta_v} \tag{6.4}$$

The volumetric efficiency, η_v has been estimated from experimental data, and a fixed value of 75% has been used in the calculation. The resulting calculated values of inlet manifold pressure pressures over an aNEDC cycle can be seen below in Figure 6.1, and show good agreement with experimental values.

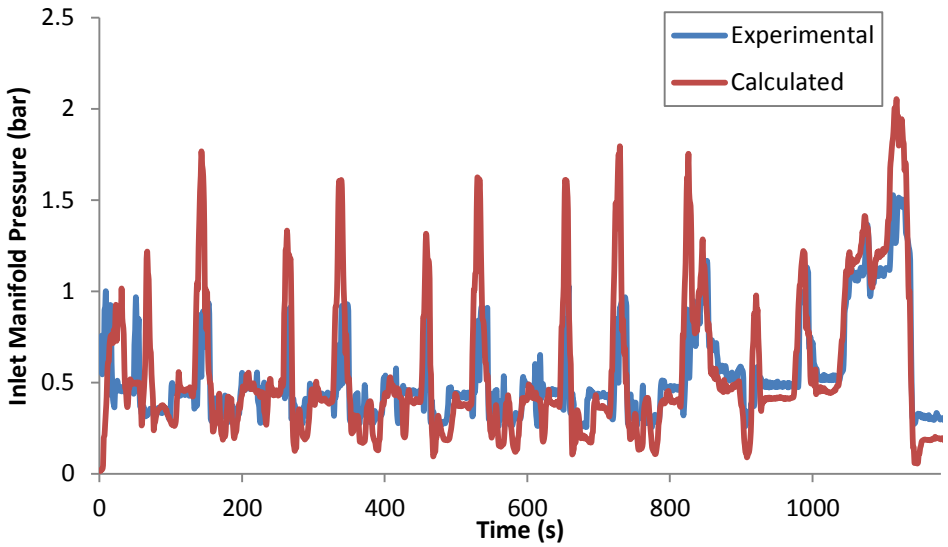

Figure 6.1 Inlet manifold pressure calculated with assumed volumetric efficiency

The pressure in the exhaust manifold was seen to be well correlated to the mass flow rate of air and fuel. The quadratic 6.5 correlated well for the exhaust manifold.

$$P_{ex} = 174(\dot{m}_{air} + \dot{m}_{fuel})^2 + 0.36(\dot{m}_{air} + \dot{m}_{fuel}) + 1.1325 \tag{6.5}$$

Results from this relationship can be seen in Figures 6.2 and 6.3.

The experimental PMEP has been calculated by integrating the pumping loop of the Pressure Volume diagram which is obtained from in-cylinder pressure transducers. By approximating the PMEP as a simple function of Pex-Pin, the

assumption is made that the pumping loop forms a perfect rectangle. In reality, this is not the case, and a further correction has been made in the form of a correlation with relation to inlet pressure:

$$PMEP = 0.3(P_{ex} - P_{man}) + 0.03\frac{P_{amb}}{P_{man}} + 0.2 \tag{6.6}$$

Final predicted results are shown in Figure 6.4. The model shows good agreement for a simple model that attempts to predict the results of a complex series of interactions. This approach has been taken to improve the accuracy of fuel consumption predictions, and was done in the absence of turbocharger maps that often form the foundation of PMEP prediction in turbocharged engines. The model is however, quite specific to the NEDC, and has less success predicting PMEP values when running at other conditions, especially at higher speeds and loads, given that the NEDC is a mainly low load. At higher load conditions, the effects of the turbocharger become more apparent; the intake manifold pressure is boosted over ambient and the waste gate on the compressor will influence exhaust manifold pressure. These interactions are complex, and without further information about the behaviour of the turbocharger, would be time consuming and difficult to evaluate. The need for further work to describe the influence of the turbocharger would revolve around a physics based model combined with turbocharger speed maps.

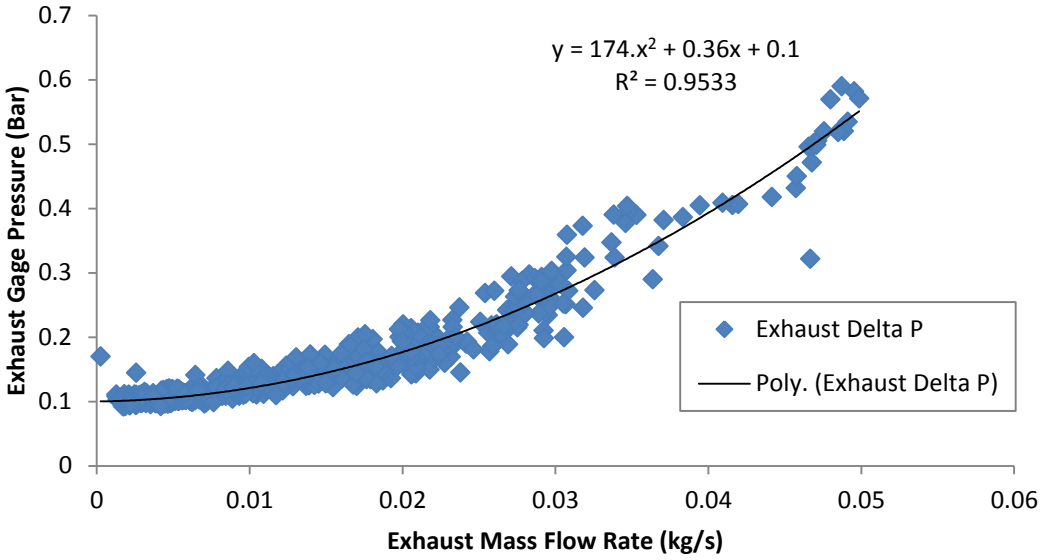

Figure 6.2 The relationship between exhaust mass flow rate and pressure

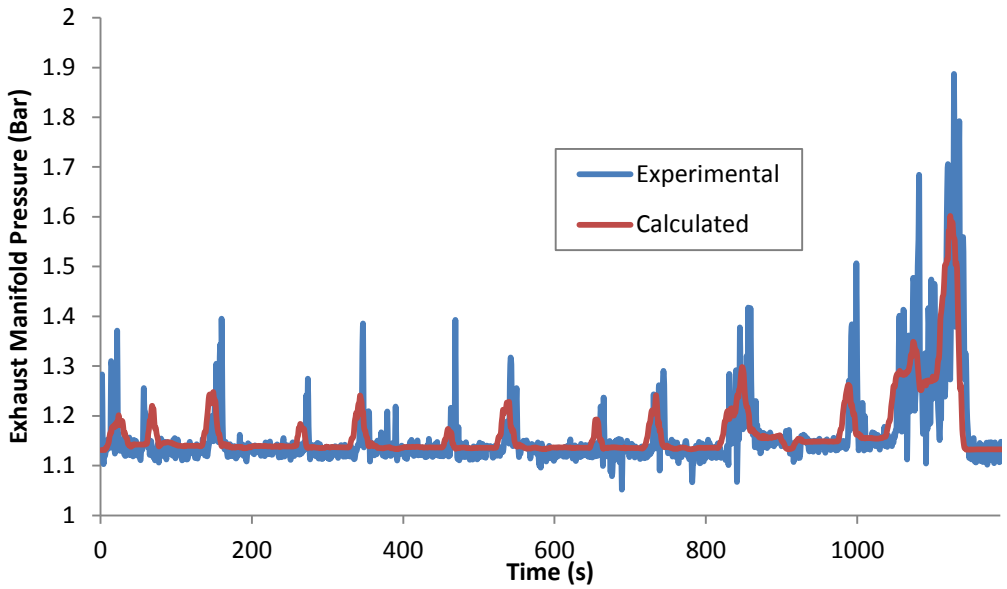

Figure 6.3 NEDC exhaust pressure as calculated using Equation 6.5

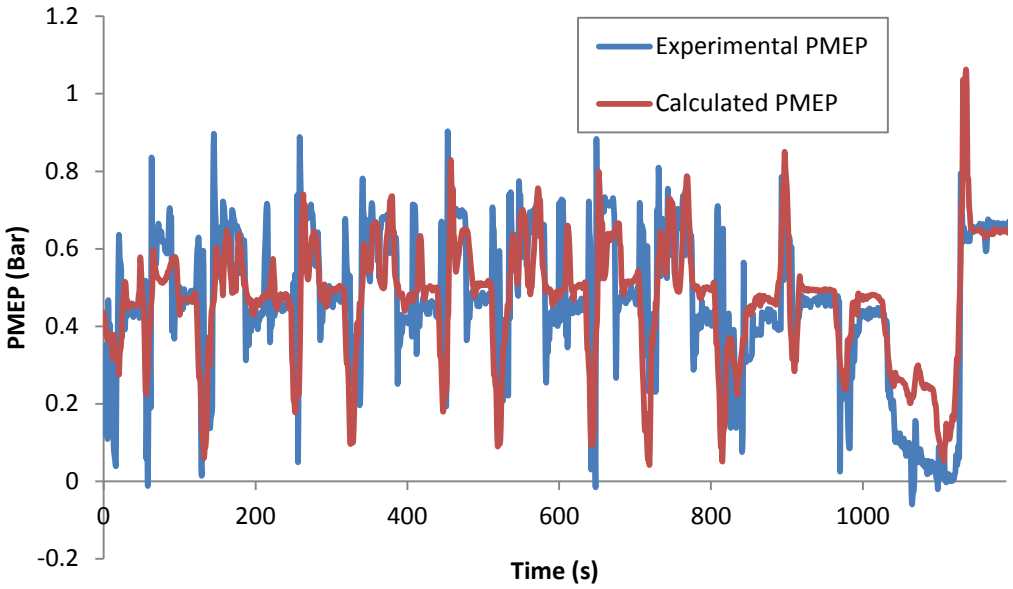

Figure 6.4 NEDC PMEP as calculated in Equation 6.6

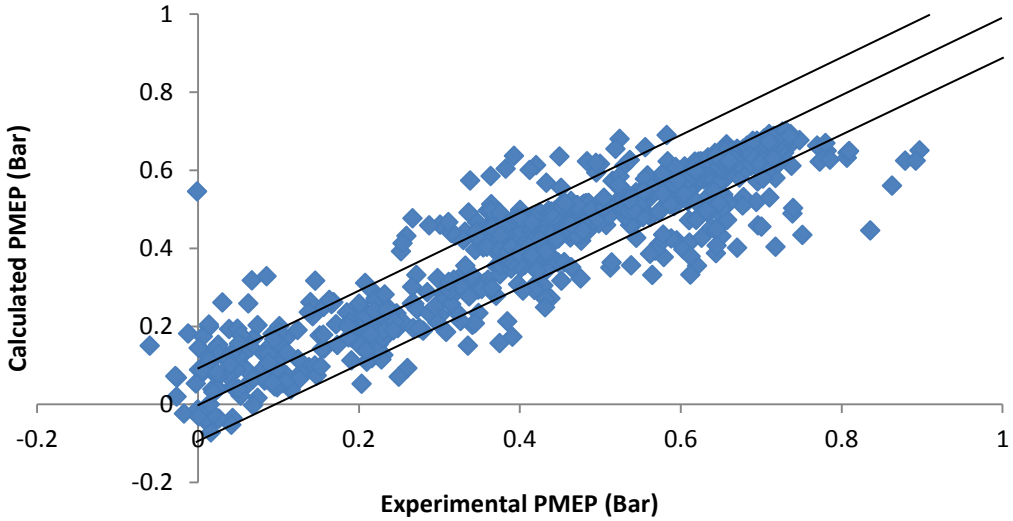

Figure 6.5 Experimental vs Predicted PMEP results. The black lines denote ±0.1 bar variation

6.3 Fuel consumption

Fuel consumption has been evaluated over the aNEDC. Initial predictions of fuel economy in the PROMETS model were low compared to experimental measurements. Indicated thermal efficiency was examined for the VIPER engine. Gross indicated thermal efficiency is a ratio of the amount of work produced to the amount of energy supplied as fuel, and is calculated as:

$$\eta_{i,g} = \frac{P_{i,g}}{\dot{m}_f Q_{LHV} \eta_c} \tag{6.7}$$

Previous versions of the SI model assumed an indicated thermal efficiency of 43%, which is more representative of diesel engines [64]. This is significantly higher than the values show in table 6.1 for a range of speeds and loads, which peaked at values around 36%. These values are still higher than reported gross thermal efficiencies for SI engine of compression ratios of around 10. [105] The lower heating value Q_{LHV} of gasoline is taken as being 44MJ/kg. The combustion efficiency η_c is a description of how completely the fuel supplied to the engine is burned. For gasoline engines running lean or stoichiometric combustion strategies, i.e $\phi \leq 1$, η_c is typically 0.98. This falls if the engine runs rich and the equivalence ratio exceed 1, where the combustion efficiency will fall according to Equation 3.38.

aNEDC data for thermal efficiency is shown in Figure 6.6. For aNEDC test, a value of 0.3 was chosen as representative for prediction of fuel flow rate based on the experimental residency time around this value. With the thermal efficiency of the engine lowered to match experimental results, fuelling predictions agreement with measured values increased. Instantaneous fuel flow rate during the aNEDC is shown in Figure 6.7. Total cumulative fuel used by the engine on the test bed was 0.75kg for the aNEDC, against a simulated value of 0.72kg.

Table 6.1 Experimental gross indicated thermal efficiency changes with speed and load.

Engine Speed (RPM)	Engine Load (Nm)								
	0	**8**	**21**	**30**	**45**	**60**	**90**	**150**	**250**
700	20	-	-	-	-	-	-	-	-
1000	-	-	-	29.3	-	29.8	32	29.9	-
1130	-	-	28	-	-	-	-	-	-
1200	-	-	-	-	-	-	-	32.5	-
1500	-	-	-	32	-	32	34.6	32.6	-
1800	-	30.5	-	32.4	31.7	33.8	34.8	-	32.9
2000	-	-	-	32.9	-	34.4	35.2	-	-
2500	-	-	-	-	-	-	35.4	-	-
3000	-	-	-	-	-	-	35.6	-	-
3500	-	-	-	-	-	-	36.4	-	-
4000	-	-	-	-	-	-	36.1	-	-
4500	-	-	-	-	-	-	36.5	-	-

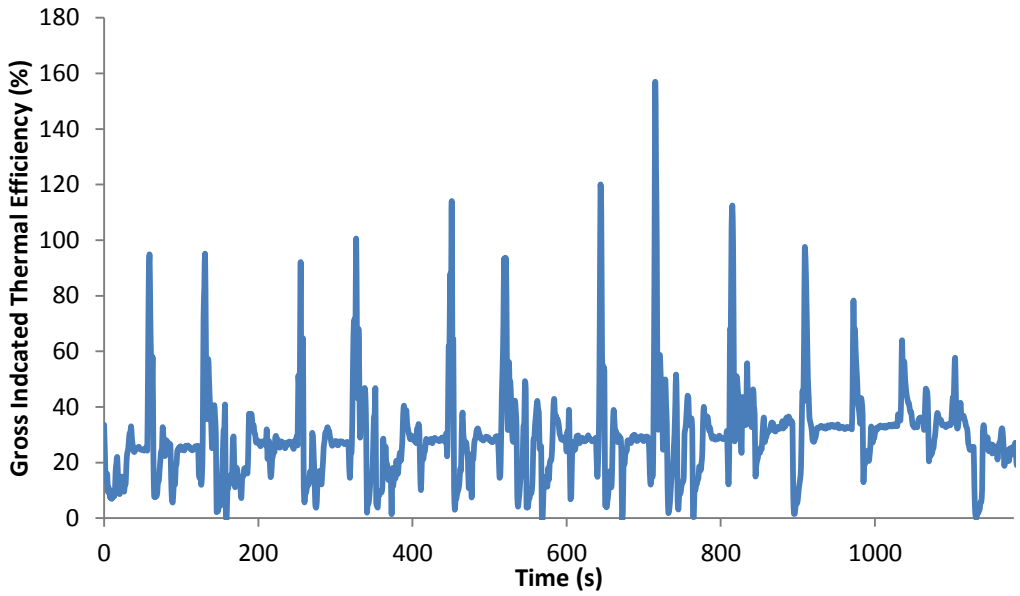

Figure 6.6 Indicated thermal efficiency of the VIPER engine through an aNEDC

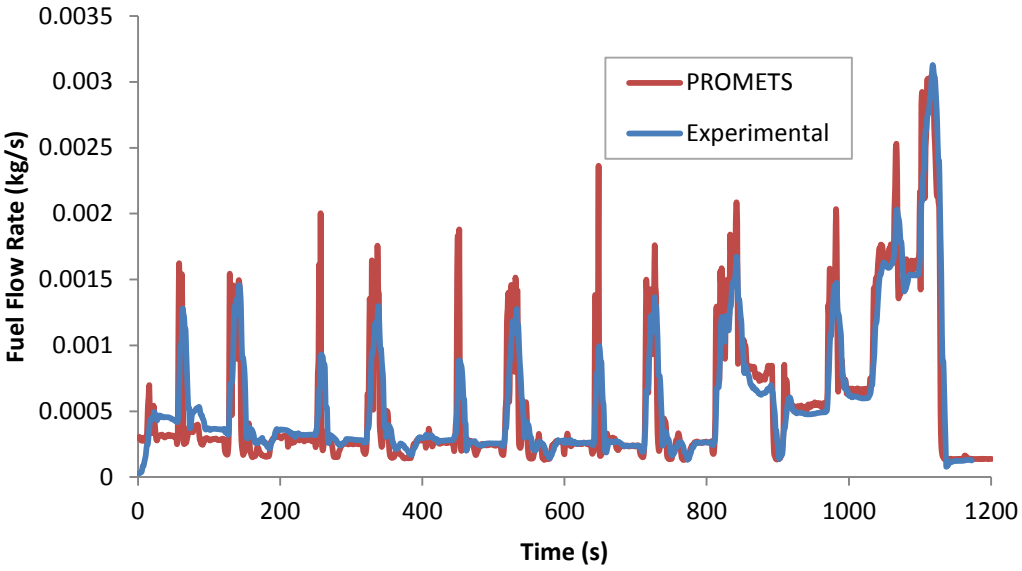

Figure 6.7 Instantaneous fuel consumption measured and predicted values for the aNEDC

6.3.2 The cold start fuel consumption penalty

To evaluate the maximum potential savings that could be realised through thermal manipulation of the engine, comparisons between the fuel consumptions of aNEDC tests starting at ambient temperatures, and when fully warm were made. By starting at a fully warm condition, the penalty to friction from high viscosity in the fluid films is reduced to the lowest level experienced during running, making this the best case fuel consumption. Total fuel used when the cycle was performed under fully warm conditions was 0.69kg, which represents a 4.4% reduction in fuel used compared to the result of 0.72kg for an ambient temperature start. Instantaneous fuel consumption for the hot and cold start tests is shown in Figure 6.8. The corresponding friction predictions are given in Figure 6.9. This is significantly lower than the penalty assigned to ambient start cycles reported elsewhere in the literature [45] [60], and this can be attributed to both the larger displacement of the engines used in these studies, and the fact that the effects of pre-heating both the gearbox and the transmission oil was included. Additionally, no mention of the lubricant grade used for the test was made. A lubricant with a wider range of viscosity, for example a 0W40 rated oil, would cause a greater change in engine friction when comparing cold and hot start fuel consumption. The ideal lubricant would have a low and flat temperature viscosity profile, and this would experience no change in friction between hot and cold start outside of the effects of clearance. This would eliminate the requirement for improved thermal management from a fuel consumption point of view. With the trend towards downsizing, the maximum savings targetable by thermal management will fall, as the proportion of the engine's power that is dissipated in friction relative to the brake output is reduced. This would lessen any efficiency gains due to improved thermal management with the intention to reduce friction in smaller engines.

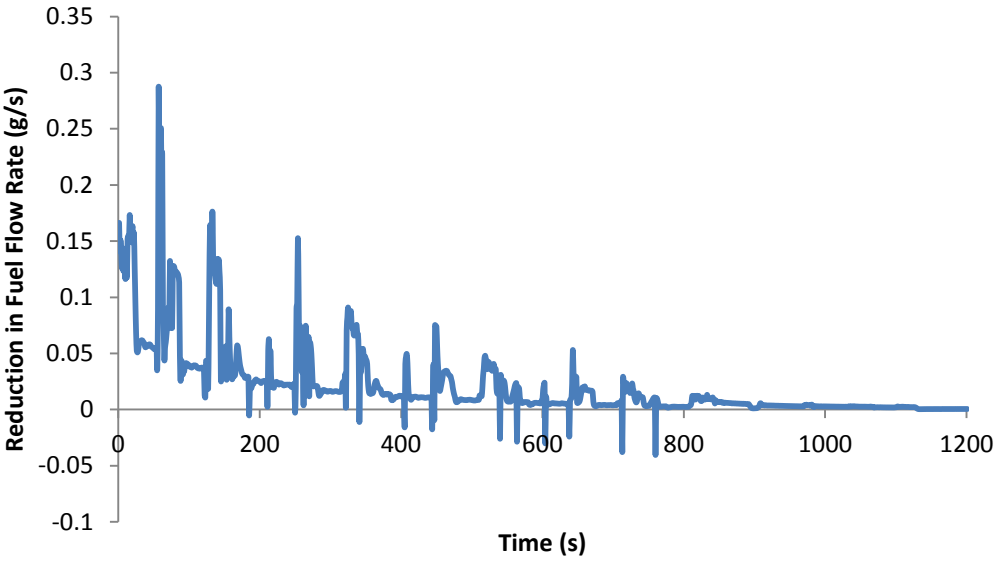

Figure 6.8 The predicted reduction in fuel consumption when performing an aNEDC test from a fully warm start

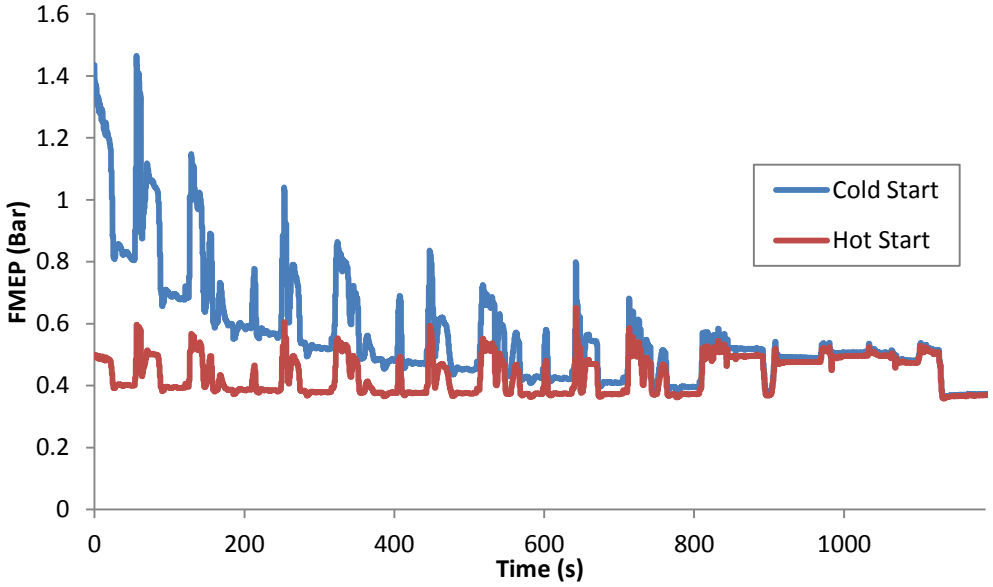

Figure 6.9 The predicted friction penalty incurred due to cold start running during the aNEDC

6.3.3 Fuel energy utilisation

An audit of how fuel supplied to the engine is used during the aNEDC cycle was conducted in PROMETS.

By subtracting the total brake, friction and pumping work from the total fuel energy input to the engine, a value for inefficiencies, or the energy lost in the structure, coolant and exhaust was found. The predicted balances of fuel usage as well as the experimental equivalent are given in Figures 6.10a and 6.10b. The amount of fuel energy used to overcome friction throughout the cycle was also calculated and is shown in Figure 6.11. While the instantaneous percentages would suggest that friction accounts for significantly more fuel than the 4% shown in Figure 6.10a, it should be noted that the engine consumes more fuel in the final 400 seconds in the extra urban portion, using 0.41kg of fuel, than in the first 780 seconds of the urban cycles, in which 0.32kg of fuel is used.

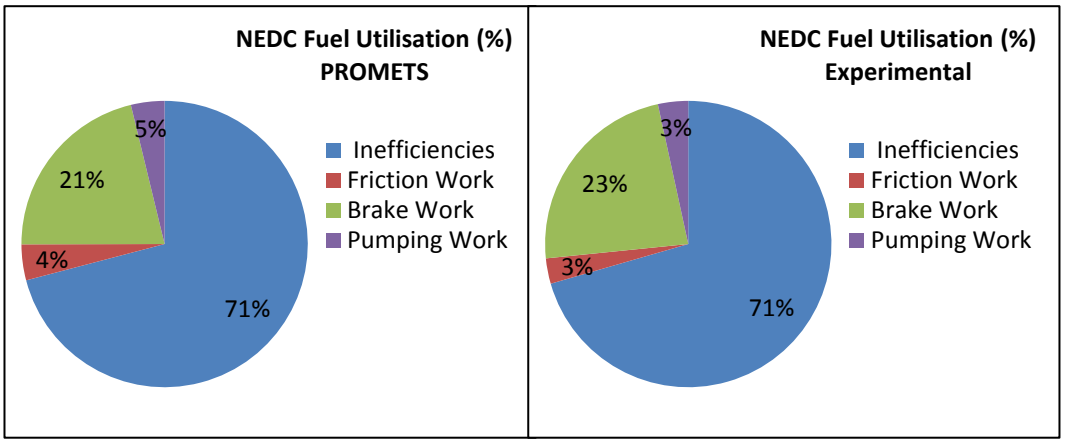

Figure 6.10a and 6.10b Fuel usage over the aNEDC. The inefficiencies area accounts for the energy lost to the exhaust or transferred to the fluids or the structure.

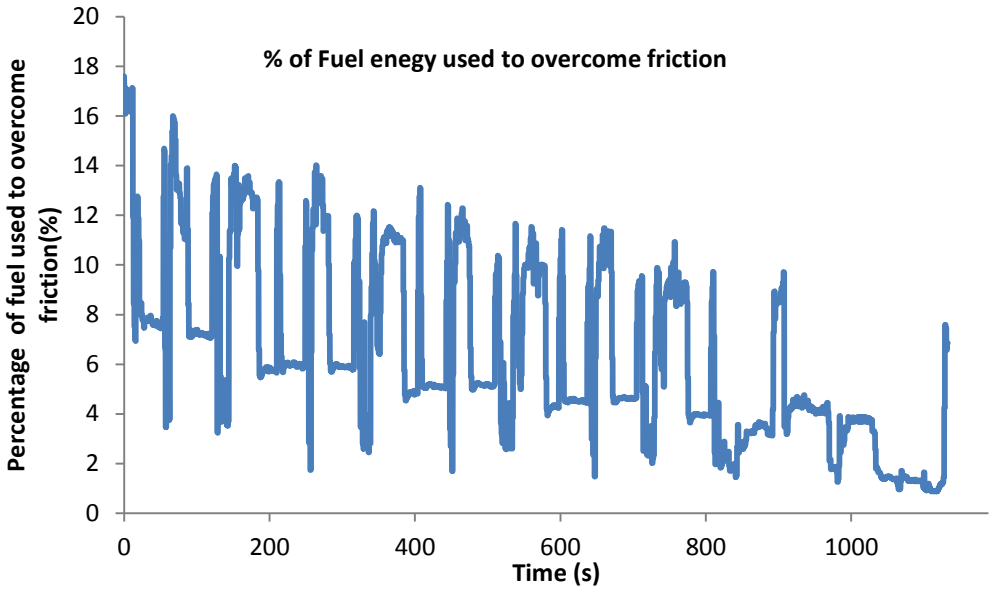

Figure 6.11 Instantaneous prediction of the fuel required to overcome engine friction

As can be seen in Figures 6.8 and 6.9, large reductions in friction work translate to relatively small reduction in fuel consumption. Because thermal and combustion efficiencies must be taken account of when converting the fuel power supplied to the engine to the gross engine power, any reduction in friction does not translate to a fuel saving on a like for like basis. The amount of friction work that would be required to be saved in order to make a 1% saving in fuel used throughout the cycle was examined.

The engine energy balance is given as:

$$m_{fuel} Q_{LHV} \eta_c \eta_{th} = W_f + W_b + W_p \tag{6.8}$$

If the efficiencies on the left hand side, and the pumping and brake work on the right hand side are assumed to be constant, then the result is:

$$m_{fuel} x = W_f + y \tag{6.9}$$

To calculate a percentage change in the mass of fuel:

$$\frac{m_{fuel1} - m_{fuel2}}{m_{fuel1}} = \frac{\frac{1}{x}\left((W_{f1} + y) - (W_{f2} + y)\right)}{\frac{1}{x}W_{f1} + y} \tag{6.10}$$

Which simplifies to:

$$\frac{m_{fuel1} - m_{f2}}{m_{fuel1}} = \frac{W_{f1}}{W_{f1} + y} - \frac{W_{f2}}{W_{f1} + y} \tag{6.11}$$

So for a 1% reduction in fuel used over the NEDC:

$$0.01\left(W_{f1} + y\right) = \Delta W_f \tag{6.12}$$

Using the predicted friction, brake and pumping work, this value was calculated at 96KJ, or 7% of the total friction work over the aNEDC cycle, run with the VIPER engine. Due to the nature of the increase in friction and the rate at which the oil rises to the fully warm value, this reduction in friction must be made in the first 800 seconds of the aNEDC.

6.4 Reducing fuel consumption over the aNEDC

Several methods of reducing fuel consumption over the aNEDC will be considered in this section, and their potential will be considered using PROMETS.

6.4.1 Stop-start

Stop start is a technology widely adopted in Europe, and is beginning to penetrate US markets. The systems typically work by monitoring vehicle speed and gear [106]. Once the vehicle stops and is placed in neutral, the ECU will check that there is sufficient charge in the battery to allow a restart before waiting a specified length of time and turning the engine off. When the clutch is re –engaged and the brake pedal is released, a strengthened starter motor is used to rapidly re-start the engine so the driver can accelerate away. Benefits of these micro-hybrid systems are reported to be between 3-10% reduction in fuel consumption [107].

To examine the effects of a stop start system on the fuel consumption of the VIPER engine, the aNEDC operating conditions were modified to include engine off sections. A total of 12 stops, of 15 second duration were inserted into the aNEDC in positions where the vehicle would be stationary. The modified engine speed and load traces are shown in Figures 6.12 and 6.13.

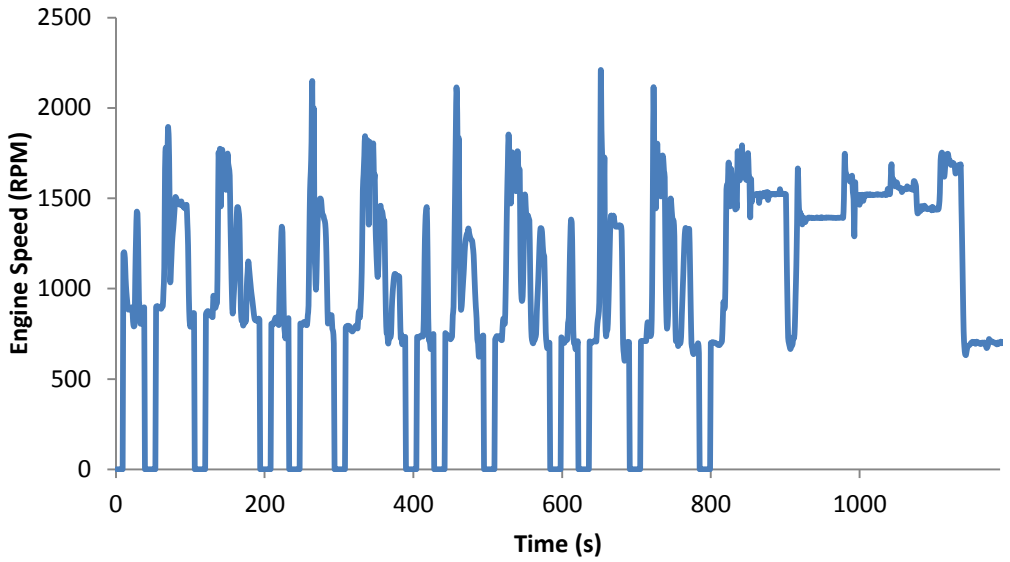

Figure 6.12 Engine Speed profile for Stop-Start simulations

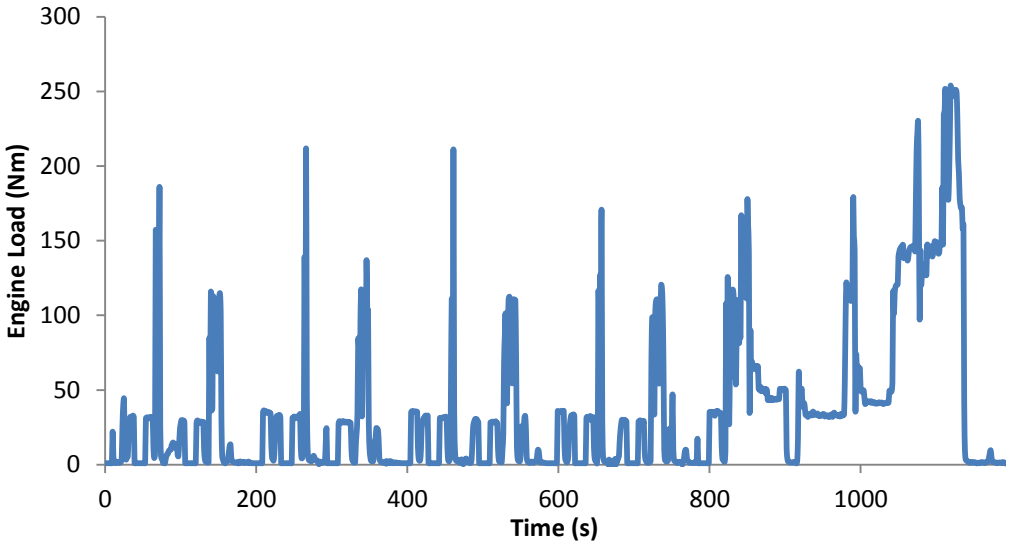

Figure 6.13 Engine Load profile for Stop-Start simulations

A reduction in fuel consumption of 5% over the aNEDC was predicted when the stop start speed and load profiles were run in place of the standard ones. The instantaneous fuel consumption predictions for both cases are shown in Figure 6.14. Figure 6.15 shows the predicted changes in work when running the stop start aNEDC. The majority of savings come from reductions in brake work. The standard aNEDC speed and load profiles were defined using data collecting from in vehicle testing, and contains idle periods in which there is a load of 30Nm on the engine, as shown in Figure 4.18. This loaded idle is required to run a combination of the automatic gearbox and the FEAD. By eliminating this during the stop periods, a large reduction in cumulative brake work is seen. This effect would be diminished in a manual vehicle, as there would be no brake work during idle periods. Additionally, the elimination of this loaded idle period may impact the ability of the vehicle to support heavy electrical loads such as the air conditioning. This calculated saving does not take into account the increase in fuel that would be required to recharge the battery after re-starting the engine. The alternator efficiency, which is around 50% at medium engine speeds [108], thermal efficiency and combustion efficiency must all be accounted for when considering this.

The next greatest saving is seen in the pumping work. Pumping losses at idle are high in gasoline engines, due to the restriction on airflow imposed by the throttle being closed.

Overall, the friction savings for running a stop-start cycle are more modest. At idle speeds friction is already low, which limits the maximum savings from this source. The benefit is eroded however due to the reduced rate of warm up caused by the decrease in fuel energy available to heat the coolant and lubricants. This translates to frictional dissipation that is marginally higher when the engine is running when compared to the standard cycle. The effect of the reduced fuel energy on the bulk oil temperature can be seen in Figure 6.16, which shows the temperature penalty incurred due to the engine not running in the first 600 seconds of the test.

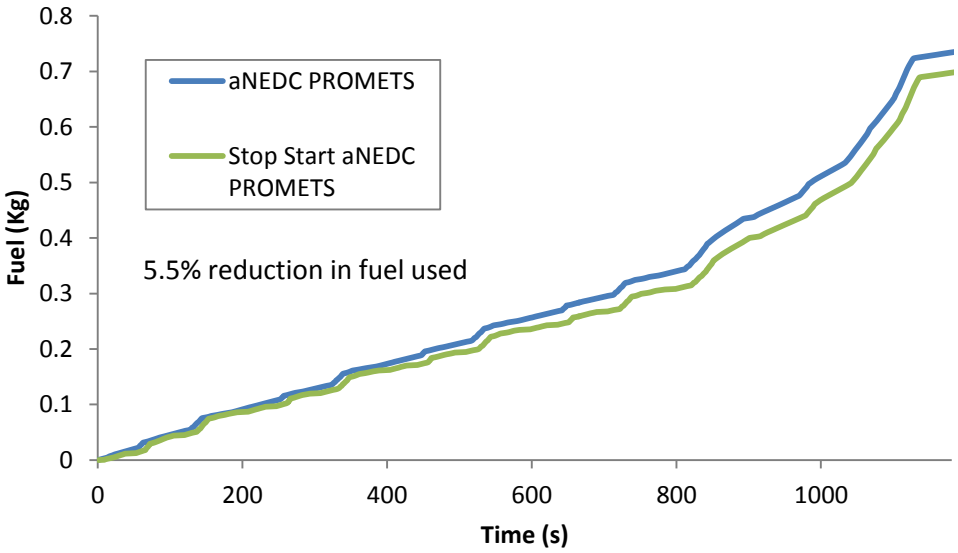

Figure 6.14 Predicted cumulative fuel consumption with and without stop-start enabled for the aNEDC

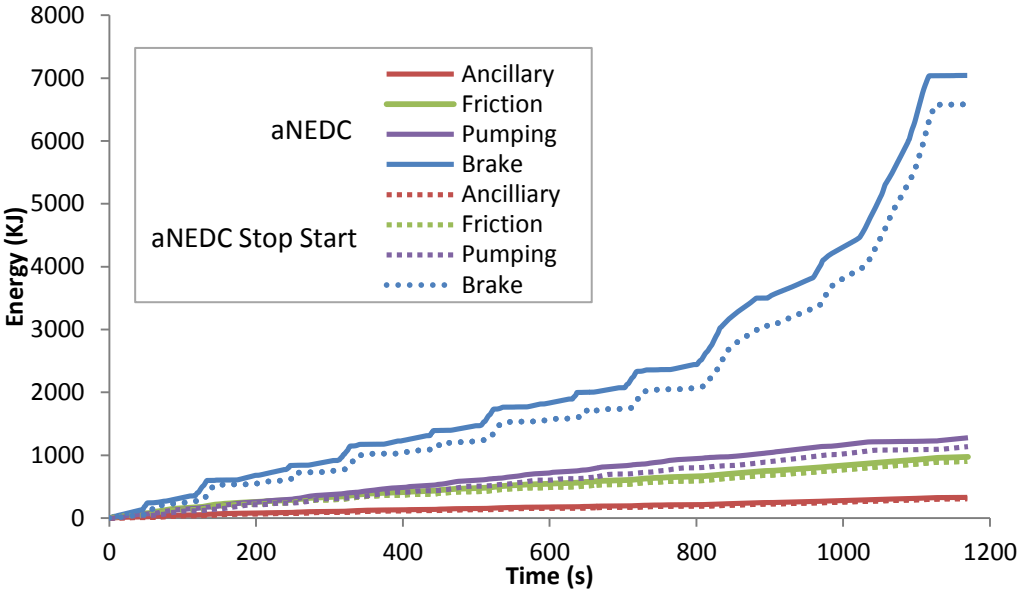

Figure 6.15 The changes to the energy usage of the engine when running the stop-start cycle

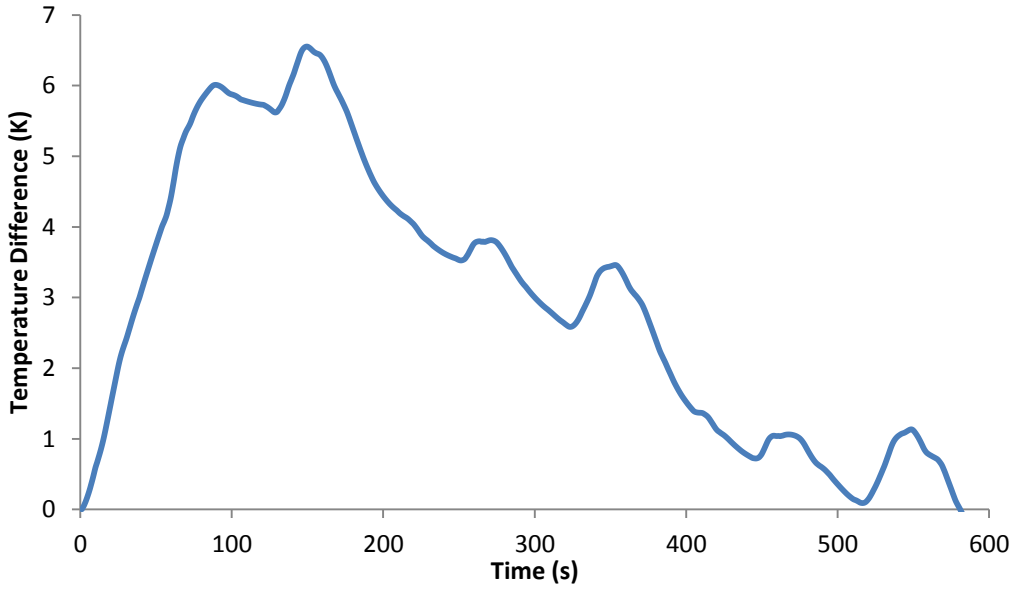

Figure 6.16 The predicted bulk oil temperature penalty due to running the Stop Start Drive cycle

6.4.2 Heat exchange devices

One method to improve the rate of oil warm up and thus reduce the friction penalty incurred during cold running has been to couple the oil to a heat source though a heat exchanger. The two most readily available fluids in an engine are the coolant and the exhaust gases. Most modern engines will have one such device present as standard in the form of the oil cooler.

The oil cooler fitted to the viper engine is described in Section 5.5 and the heat transfer rate across it given in Equation 5.15

The current oil cooler as fitted to the VIPER engine was found to have an effectiveness of around 20% when analysed using the Number of Transfer Units method of dividing the actual heat transfer achieved by the cooler, by the maximum possible heat transfer. To assess the suitability of the coolant as a source of heat for the oil, the effect on engine friction and fuel economy over the NEDC by increasing the effectiveness of the oil cooler has been examined. Increasing the effectiveness of the oil cooler to 100% will give the best case heat transfer between the fluids, and show the maximum temperature gain that can be realised in the oil through better coupling with the coolant.

The sensitivity of the model predictions to oil cooler effectiveness is shown in Figure 6.17. Increasing the effectiveness has improved the heat transfer between the two fluids as they pass through the heat exchanger, bringing the temperatures of the fluids closer together. The oil experiences a greater change in temperature than the coolant does, due to the lower specific heat capacity of the oil.

The instantaneous fuel consumption of the tests for 20 and 100% effectiveness is shown in Figure 6.18. The change in friction levels for the Valvetrain, Crankshaft, Piston and Connecting Rods are shown in Figure 6.19.

While the overall level of engine friction has been marginally reduced by improving the effectiveness, it can be seen that the piston friction actually increases due to the decrease in coolant temperature influencing the temperature of the cylinder liner. This is offset by the reduction in friction from the bearings in the crankshaft and connecting rods, because the rise in oil temperature is greater

than the fall in coolant temperature. Additionally, the equations governing the bearing friction are more sensitive to operating temperature than those describing the piston friction. Another reason that the reduction in friction is not larger can be attributed to the fact that the rubbing surfaces will not experience the full rise in oil temperature, as much of the energy will be lost to the engine structure as it is transported to the rubbing surfaces.

The reduction in fuel consumption described above is for a case where the oil cooler has an effectiveness of 100%, which would not be attainable in reality. In addition to this, the reduction in fuel consumption over the NEDC is predicted as being around 0.3% which although being fairly significant in the scope of the project, would be difficult to demonstrate with confidence experimentally. This exercise highlights two main points: that the benefit to friction levels of raising the bulk oil temperature will outweigh the penalties associated with the reduction in coolant temperature, and that the coolant does not have a sufficiently large amount of available energy which can be usefully transferred to the oil during warm-up for the VIPER engine.

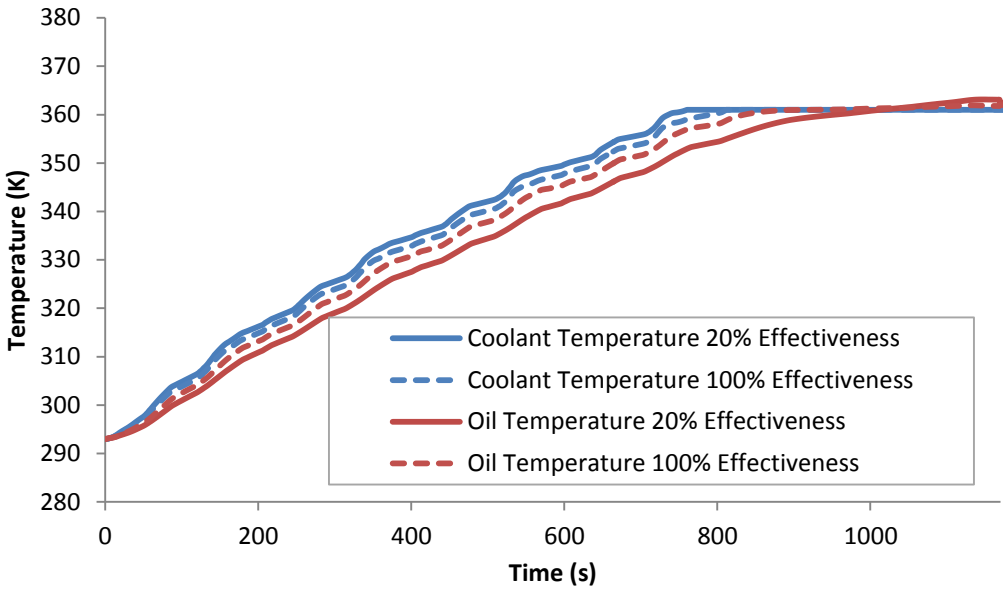

Figure 6.17. Effect on oil and coolant warm up rates of increasing the oil cooler effectiveness

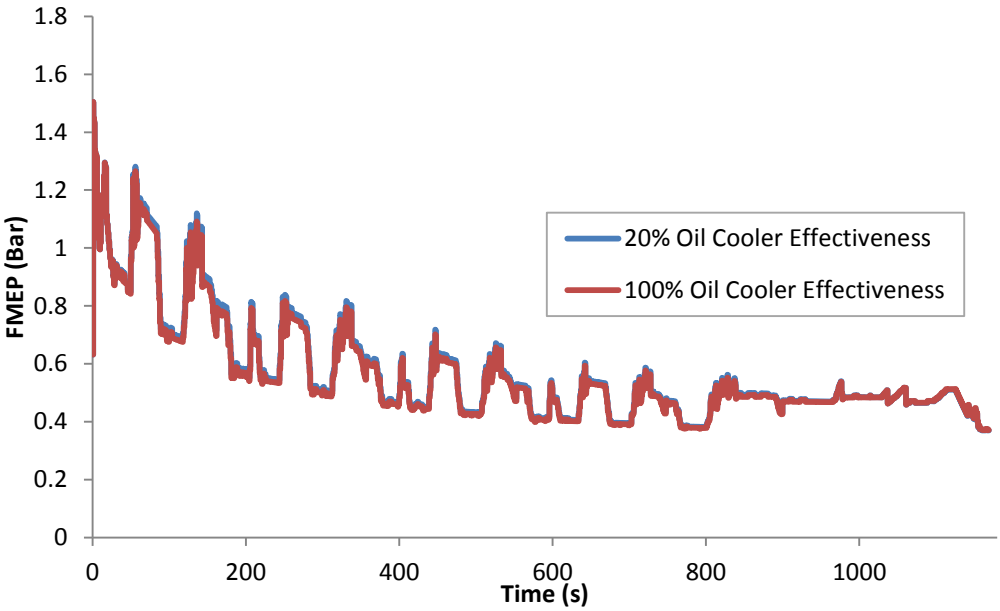

Figure 6.18. Predicted 0.3% reduction in fuel consumption as a results of increasing oil cooler effectiveness

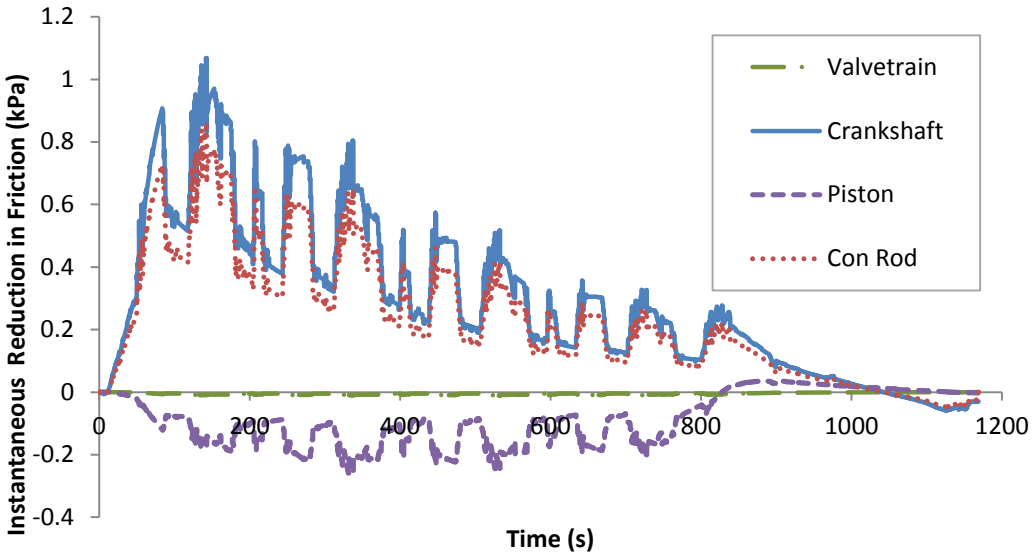

Figure 6.19. Predicted reduction in component friction during the NEDC cycle by increasing oil cooler effectiveness

6.4.3 Reduction of parasitic losses

In Section 4.2.4, the power consumption of the fuel, oil and coolant pumps was examined. The fuel consumption penalty with driving each of these pumps is given in Table 6.1.

Table 6.1 Fuel Consumed by the ancillary pumps over the aNEDC

Pump	Fuel Used (g)	% of Total Fuel used
Coolant	8.8	1.2
Oil	21	2.9
Fuel	4.3	0.6

Pump electrification is an area of growing interest. Electrically driven variable flow (VF) rate pumps are more flexible in the types strategy that can be applied. VF oil pumps would allow for the lubricating demand of the engine to be matched avoiding wasted power. VF cooling pumps would allow for the warm up strategy of the engine to be optimised.

Experiments by Bent [41] showed increases in mid stroke liner temperature of up to 10°C during fixed speed running conditions due to stalled coolant flow. This is a result of decreased heat transfer coefficients between the coolant and the structure.

If the electric pumps are powered by the alternator, then alternator efficiency must be accounted for when evaluating fuel savings, and the power is still ultimately sourced from the crankshaft. The use of wasted exhaust energy to provide power to the pumps however would remove the load from the crankshaft entirely.

As much as 30% of the fuel energy used in the engine is wasted in the exhaust [109], and power recovered from this is essentially free if potential adverse effects on catalyst performance are discounted. Thermo-electric generators (TEGs) are devices which can be fitted in the exhaust path of an engine that utilise Seebeck devices to generate electricity from the delta between the temperature in the exhaust gases, and that of a coolant. When the junctions between the

thermoelectric materials are kept at different temperatures, an electrical force will be produced which is governed by the following equation [110]:

$$V = a(T_h - T_c) \tag{6.13}$$

In this T_h and $T_c$are the hot and cold side temperatures respectively. a is the difference between the Seebeck coefficients between the leg materials which is given for each as:

$$S = -\frac{\Delta V}{\Delta T} \tag{6.14}$$

The Seebeck coefficient describes the voltage generated with a given temperature difference over a material.

A common thermoelectric material used in TEGs is Bismuth Telluride (Bi_2Te_3) [111]. This material operated best at hot side temperatures lower than 250°C. A prototype device using such TEG modules has been developed as part of the VIPER project by a member supporting the consortium, and has been tested during the aNEDC at the University of Nottingham. The device was fitted pre-catalyst in the engines exhaust path and electrical generation was measured. These values were taken, and the potential impact on fuel economy if this was used to drive the ancillary pumps was assessed using PROMETS. Measured TEG power output is given in Figure 6.20.

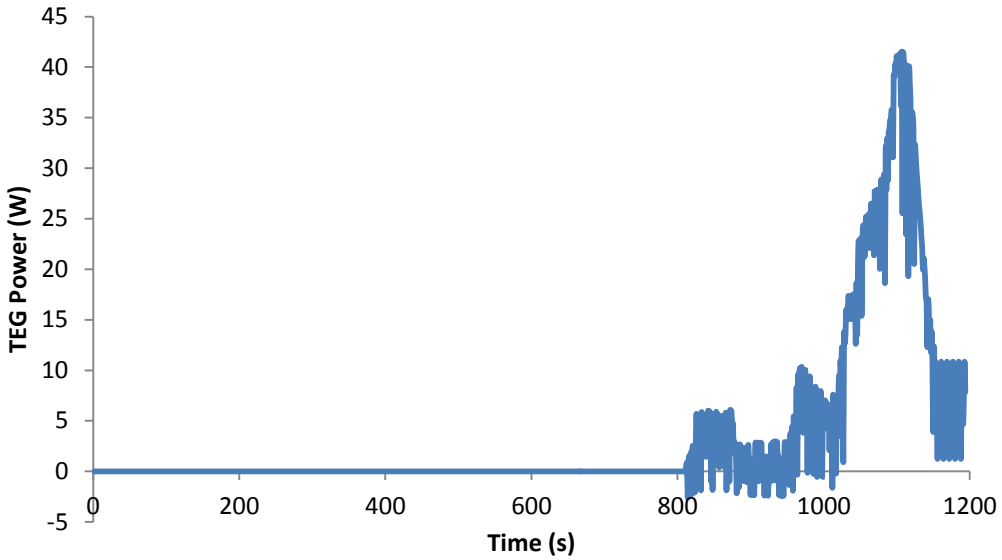

Figure 6.20. Measured TEG power output

In the first 800 seconds of the test, during the urban drive cycle conditions, the TEG unit consumed more power with its onboard electronics that it generated. This has been neglected for the current studies. The only useful energy was generated during the extra urban part of the cycle, and even then, the peak power output is less than a third of the water pump power consumption at this part of the cycle. This power generated is insufficient to account for the additional pumps required to provide coolant to the system. This data is from a very early proof of concept design used to identify the effect of features and problems with construction. More details of the TEG design are confidential at present but it is clear that the current iteration is yet to reach the potential levels of performance promised by the theoretical ideal. Predicted fuel consumption benefits were minimal using this prototype, with a 0.04% saving in fuel when only considering the power generated.

6.4.4 Supplementary oil heating

To predict the possible thermal gains from recovered energy if it was applied to heat the oil, a sensitivity study on fuel consumption to supplementary oil heating was carried out. Results from this for heat input of up to 1500W to the sump are shown in Figure 6.21. The effect on the sump oil temperature is shown in Figure 6.22. Results from the simulations show relatively modest gains in fuel economy to quite significant power inputs to the oil. To put the magnitude of the savings into perspective, in order to gain a fuel consumption benefit of just under 1% during the cycle, a heat input of 1KW is required to the sump oil. This would be more than sufficient to drive the ancillary pumps throughout most of the cycle, which account for a combined fuel penalty of 31g. This would translate to a saving of 4.7% in fuel consumption. Interestingly, it can be seen in Figure 6.23 that the proportion of the original heat input to the oil that is retained in the sump remains very similar for each of the supplementary heating values. The response of engine FMEP is shown in Figure 6.24.

The biggest heat sink for the oil in the model is the heat transfer between the oil mist and crankcase structure around the bottom end of the engine. The metal in the crankshaft, the bearing support plates and the crankcase walls lag the oil in warm-up throughout the whole cycle. The power lost from the oil in this manner is shown in Figure 6.25. The red line in Figure 6.21 shows the effect on fuel consumption if this mist was decoupled from the crankcase either through the use of baffles to collect and direct oil to the sump, or through an insulating surface finish on the crankcase and crankshaft. By insulating here, the amount of additional power supplied to the oil in order to gain a 1% reduction in fuel consumption would be reduced to around 350W. Decoupling the oil mist also increases the proportion of the additional power that is retained in the oil.

Investigations into the most advantageous distribution by Janowski [6] on full powertrains showed that when less heat is available, using it to heat the oil in the differential was most beneficial. As more heat became available, the advantages of warming engine oil became more apparent. This was due to the increased

thermal inertia of the engine requiring a larger heat input before meaningful temperature gains were seen.

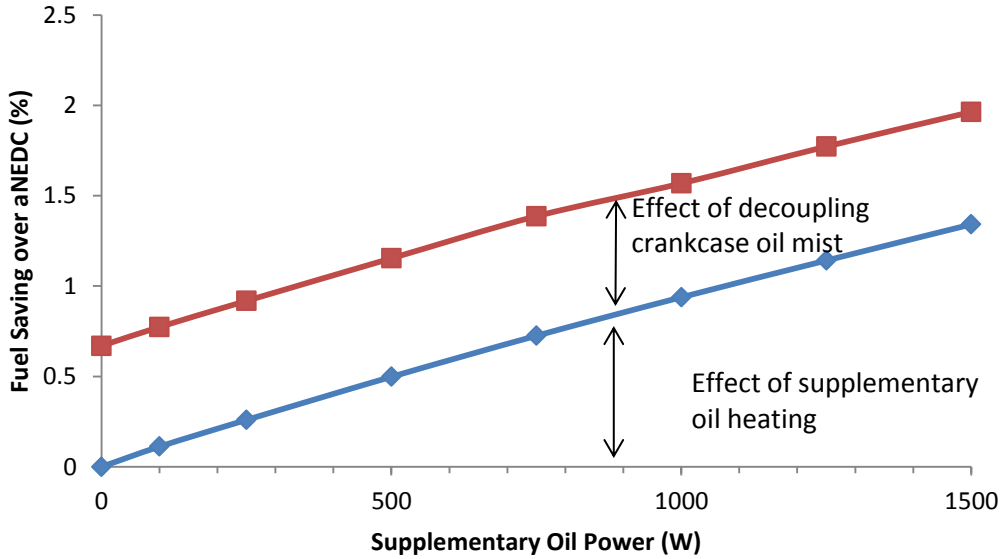

Figure 6.21 The relationship between additional heating of the oil and the fuel consumption benefit.

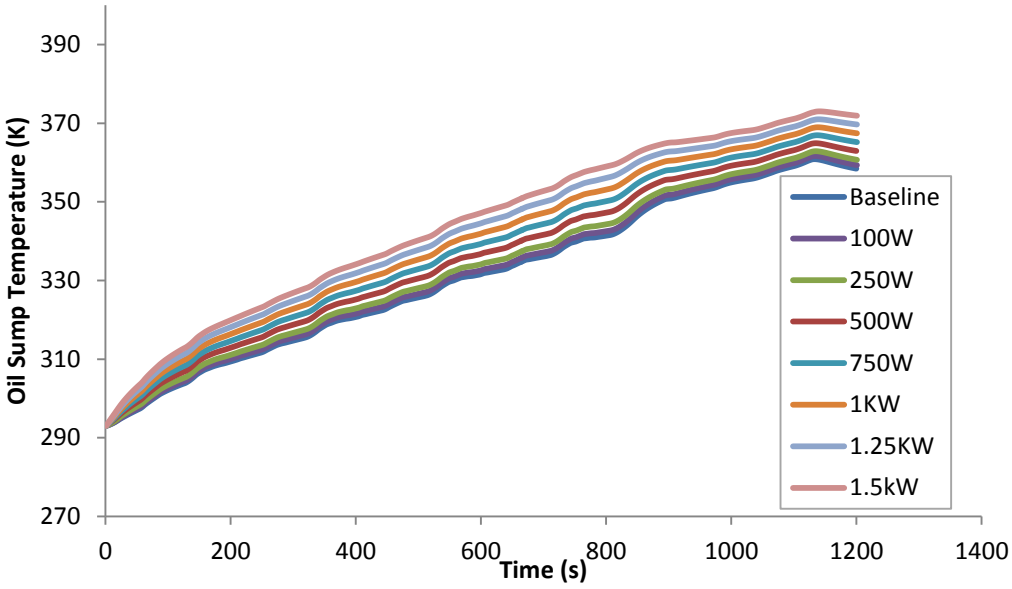

Figure 6.22 The effect of additional heating on sump oil temperature

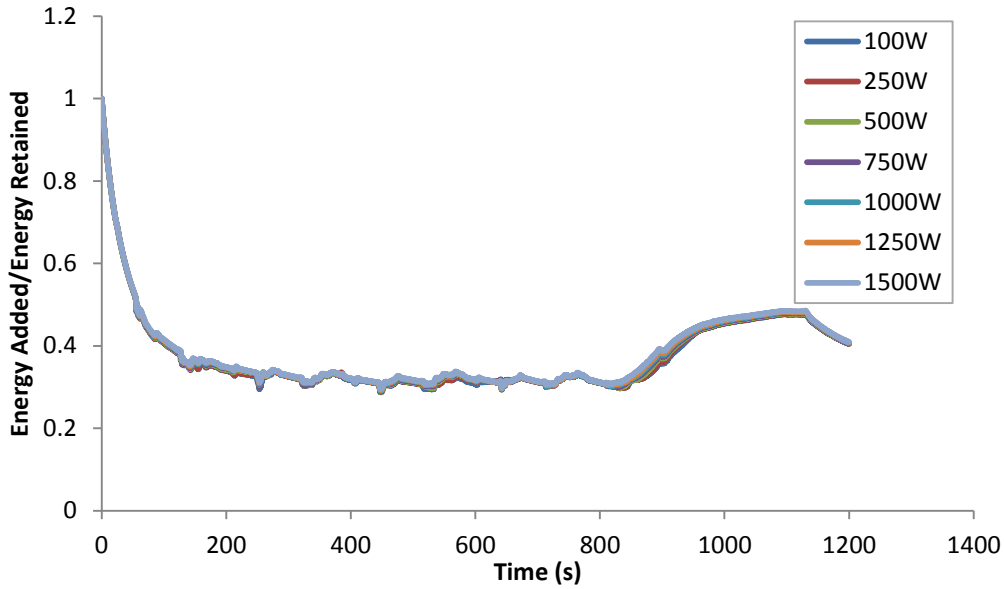

Figure 6.23 The proportion of additional energy retained in the oil

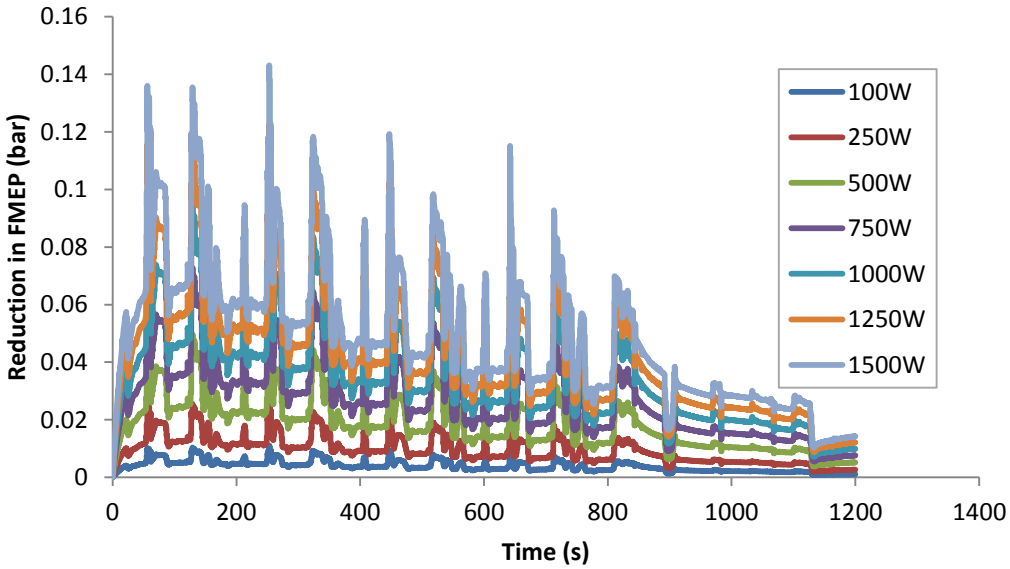

Figure 6.24 The effect of heating the oil on engine FMEP.

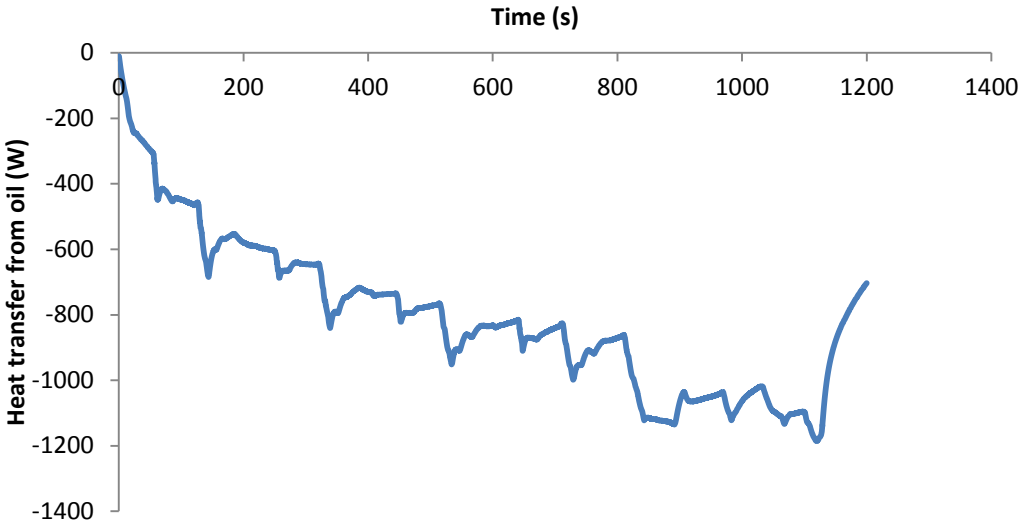

Figure 6.25 Heat lost from the oil to the engine structure in the crankcase mist during the aNEDC

6.5 Discussion

In this chapter, the performance of the engine has been examined, with a particular focus on the fuel economy of the engine and the factors affecting it, using PROMETS to expand on and complement experimental results

A simple model for calculating the PMEP of the VIPER engine has been created based on the ideal gas law for the intake manifold pressure, and a quadratic built around exhaust mass flow rate for the exhaust manifold. Results show reasonable prediction of manifold pressures and PMEP over the aNEDC compared to measured values. This solution fulfils the requirements of the current work, in which the emphasis is on the thermal management and fuel consumption of the engine over the aNEDC. Over higher load running conditions, where the turbocharger has a larger influence on intake manifold pressure, the relationships do not hold. Further information on the operation of the turbocharger, and the interaction between the turbocharger and the throttle would be required to create a more robust model.

Gross indicated thermal efficiency data was gathered experimentally over a range of operating conditions in order to improve the model's fuel consumption predictions. Results showed the value previously used in the PROMETS model was higher than it should have been, leading to under-predicted fuel consumption. A value of 30% was used as a more representative value of the aNEDC. This brought fuel consumption calculations in line with experimental data and strengthened the confidence in the models predictions.

The maximum possible saving over the aNEDC as a results of thermal effects was calculated by comparing the fuel consumption of the engine when the cycle was run from cold and fully warm starts with a saving of 4.5% seen. This is not realistically achievable in practice but it illustrates the magnitude of the targetable fuel consumption. When considering the use of power generated by energy recovery devices however, it highlights the fact that the power would be better put to use in reducing the ancillary load on the engine. If the parasitic losses on the crankshaft could be eliminated entirely, it is predicted that fuel consumption could be reduced by as much as 4.7%. This would be compounded by any fuel

consumption benefits of using electrically driven variable flow pumps to optimise engine warm-up.

This relies however on the presence of such an energy recovery device that is able to produce power that peaks at nearly 1kW at the part of the cycle in which there is not a large amount of energy in the exhaust. The TEG unit available at this time is not fit for this, with a peak power output of around 40W in the most energetic part of the cycle. Reports of other TEG devices show power generation of up to 700W on a test bed, and peak power of 250W in the US06 cycle [112]. This cycle is an aggressive cycle with periods of high acceleration and sustained cruising over 60mph [113] making it suitable to best showcase the capabilities of a TEG, as high exhaust energy is required for best operation.

The relationship between fuel consumption over the cycle and friction power for the VIPER engine has been characterised, showing that for every 1% of fuel consumption reduction, friction must be reduced by 7%. This has been shown to require a heat input to the oil of over 1kW if this effect is to be achieved thermally.

Sensitivity studies on oil cooler assembly effectiveness has shown that the coolant is not a suitable source of heat for the oil unless the coolant is able to pick up energy elsewhere. Despite raising effectiveness of the oil cooler to 100%, the enthalpy difference between the fluids is not great enough for a meaningful increase in oil temperature to be realised through greater thermal coupling. Examination of friction model results has highlighted the fact that if there is an option for greater coupling that any increase in friction due to reduced mid-stroke liner temperatures will be offset by the reductions in friction at the oil temperature critical rubbing surfaces. Work done by Andrews et al. [114] showed that by increasing the energy in the coolant through use of an exhaust-coolant heat exchanger, that the oil temperature was able to be raised significantly using an oil-coolant heat exchanger.

Chapter 7. Discussion and conclusions

The work underpinning the studies reported has updated and improved the PROMETS model for application to the latest generation of modern spark ignition engine. Upgrades have been carried out on the friction and oil sub-models to introduce a better description of friction-thermal interactions within the engine, to increase the models sensitivity to changes to the engines thermal state. The friction model has been altered from the previous form, where a bulk oil temperature correction was applied to account for increased friction during warm up, to a model in which each friction contribution is corrected using local oil temperatures. The empirical constants for each of the friction equations have been reevaluated against a combination of teardown data and fully warm complete engine friction measurements. The oil circuit has been upgraded with additions of an iterative model to predict the energy flows within the main bearings, and a piston cooling jet representation.

In Chapter 4, the use of a friction model corrected with oil viscosity evaluated at temperatures local to the rubbing surfaces is described. Earlier versions of the model included a friction model that was based on a bulk oil temperature value to evaluate viscosity at each of the rubbing surfaces. This method proved to be adequate for predicting total engine friction, but lacked any description of how the temperature of the oil at the individual rubbing surfaces would affect engine friction. The improved model now uses the temperature of the mid-stroke cylinder liner, the bearing film and the valvetrain structure to evaluate oil viscosity. Results for both fixed speed and transient operating conditions show good agreement between experimental and predicted results.

The model allows for the effect of thermal manipulation to be predicted in more detail, with the effects on individual components being easily examinable. The coolant plunge test in particular, has highlighted the quick response of the engine friction to changes in coolant temperature and predictions showed this to be due to friction at the piston-liner interface. The dependence of piston friction on the

temperature of the liner has important implications when considering thermal management. The use of partial insulation of the back of the cylinder liner from the coolant could be used to raise the temperature of the structure and reduce piston friction. Previous treatment of the friction would have over-predicted the effect on fuel consumption of gains in oil temperature.

Comparison to a limited set of teardown data has allowed for updates in the friction constants for a more modern engine. In particular, this has highlighted the fact that since the initial implementation of the model, improvements to engine design have led to a greatly reduced level of friction in the valvetrain and the constants have been reduced by 50% to reflect this. Factors that affect valvetrain friction include surface finish of the rubbing components, the spring loading, and the reciprocating mass of the valves and followers, although it is unclear as to which, if any of these are responsible for the reduction in friction.

While assumptions on the thermal conditions of the oil film on the liner have been supported experimentally, and the main bearing films have been modelled explicitly, there still remains doubt about the condition of the oil in the valvetrain. The oil flow here is poorly understood, and the assumption that the oil will follow the port metal temperatures here remains a weakness in the friction model.

An older generation of engine design, the Ford CVH engine was used as the starting point for the oil circuit in earlier versions of the PROMETS model. The oil circuit representation in PROMETS has now been revised in several key areas to better reflect current understanding of the lubrication system and this is described in Chapter 5. Predictions of flow rates through piston cooling jets and main bearings have shown that of the oil flow retained in the engine block, between 70 and 90% of the oil will flow through the piston cooling jets, making the temperature predictions for oil returning to the sump highly dependent on the accuracy of heat transfer calculations at the back of the piston. To this end, a model to predict the heat transfer coefficient between a jet of oil impinging on the back of the piston was added. The piston cooling jets now provide the largest single source of heat for the oil and redistribute heat away from the structure, but cause increased heat transfer from the oil to the structure in the crankcase mist.

These interactions show that the thermal state of the oil cannot be considered independently of the structure. Insulation of the oil mist from the crankcase as a method of decoupling the oil from the structure would increase the amount of heat that is retained in the oil.

An iterative model to calculate bearing oil temperature and friction has been included, which better represents the thermal/friction interaction in the bearing. Oil film warm up has been shown to be initially dependant on the frictional dissipation from within the bearing, but to be dependent on the surrounding structure temperature during longer running. The oil filter cooler assembly from the VIPER engine has been characterised, and the heat transfer model of the filter cooler has been adjusted to match. The current filter cooler is around half as effective at transferring heat between the oil and the coolant as was previously assumed in the model, with NTU analysis suggesting around 20% effectiveness. Strengthening the coupling between coolant and oil by increasing this effectiveness would have limited beneficial effects on engine friction. Increasing the effectiveness of the filter cooler to simulate perfect coupling showed fuel economy benefits of less than 0.5% over the aNEDC.

Comparisons between hot and cold start aNEDC, an approximation to the NEDC showed the maximum reduction in fuel consumption that can be achieved thermally, a figure that was predicted at 4.5%, and shown experimentally to be 5.4%. This gives an indication of the size of the fuel consumption reduction that can be pursued by improved thermal management. The VIPER engine exhibits low levels of friction when compared to other gasoline engines of the same displacement. If the friction were higher, then this saving would be greater. The NEDC is defined with a start temperature between 20 and 30°C, however in the case of real world driving in northern Europe, starting temperatures of 10°C are more likely, with sub-zero conditions common in the Nordic counties. With these colder starts, the benefits of thermal management would be more pronounced, and this highlights the limitations of using the NEDC for selection of fuel consumption strategies. The converse effect is expected with current industry trends towards engine downsizing. In smaller engines of a comparable brake

power the friction losses will be a smaller proportion of the indicated power, meaning that thermal management techniques would have a smaller targetable fuel penalty. Adoption of a longer, more aggressive standard cycle such as ARTEMIS would also lead to reduced importance of thermal management when considering fuel consumption. Of the 1189 seconds of the NEDC, the oil is below the fully warm state for practically the whole cycle; around 1100 seconds, emphasizing the effects of high friction due to sub-optimal temperatures. The ARTEMIS cycle last for 3143 [13] seconds so that if warm up rates were identical, the engine would only be operating at a fuel consumption penalty for approximately a third of the cycle.

The use of low viscosity lubricants has been shown to have large effects on the fuel economy of internal combustion engines. Inoue et al. [115] showed a 2.7% improvement by switching from an SAE grade 10W30 lubricant to a low viscosity 5W20 with molybdenum friction modifiers. A 1.5% fuel consumption reduction was measured when comparisons were made between 5W30 lubricants and super low viscosity 0W20 in [56]. As with engine downsizing, the reduction of friction through the use of low viscosity lubricants does not synergise well with thermal management techniques.

While targeting fuel consumption reduction over the NEDC is desirable to manufacturers both in terms of legislation, and in the marketing of their vehicles, it does exclude certain technologies that would be beneficial to drivers in the real world. Latent heat stores are not currently eligible for use during official testing due to strict starting temperature limits. Results from [45], [44] and [41] all show reductions in fuel consumption over a range of drive cycles through use of thermal stores.

The friction equivalence ratio to fuel consumption for the VIPER engine was shown to be 1:7, i.e. for every 7% of friction saved, there will be a 1% saving in fuel consumption for the NEDC. The required heat input to the oil for this to be achieved is 1kW until the engine is warmed. This is reduced if the large sinks are decoupled from the oil, and with insulation of the oil mist from the crankcase, it is estimated that only 350W would be required. This is a power level that is

achievable with current TEG technology. The usefulness of these units is again very dependent on the type of cycles under which they are tested. The NEDC is a comparatively lightly loaded cycle, which does not provide as much energy in the exhaust as would be available during ARTEMIS.

7.1 Conclusions

- The improvements made to the model, most importantly the local temperature based friction model and oil circuit upgrades including main bearing and piston cooling jet representations have allowed for additional insight into the behavior of friction during warm up. The responses of individual rubbing components to changes in the thermal state of the engine can now be separated and analysed. This additional modelling capability has allowed for the following observations to be made.

- Under fully-warm operating conditions, the 2.0lGTDI engine has a rubbing friction, fmep value of 0.56 bar at an engine speed of 2000 rev/min and light loads, distributed between piston assembly, crankshaft assembly and valvetrain in the proportions 44/15/18/23%. Friction increases with engine speed, primarily due to increases in friction at the piston-liner interface and in crankshaft and big-end journal bearings which operate in the hydrodynamic lubrication regime. Down-speeding (lower engine speeds) and down-sizing (higher IMEP values) trends move duty parameter to a lower value and contribute to constraints on viscosity if hydrodynamic lubrication is to be maintained.

- During a 2000 rev/min warm-up from start temperatures in the range 20-25°C, the friction contribution of the piston assembly shows the largest absolute reduction (0.7 bar) from a cold start, but the reduction in friction of crankshaft group is proportionally greater (6.5x).

- Using mid-stroke liner temperature appears to be more suitable for evaluating oil viscosity than bulk oil temperature. When cold coolant was introduced to the engine, the rate of friction response was not captured when oil temperature was used to evaluate the viscosity ratio for piston

friction. The oil film in this location has a low thermal capacity, and can be assumed to take the temperature of the mid-stroke cylinder liner. When this temperature was used to evaluate the viscosity ratio the friction model response matched experimental data.

- The mid-stroke liner is a better candidate for thermal efforts to raise temperatures than the main bearing feeds as a larger reduction in friction can be gained, despite the piston friction being less sensitive to temperature. In a 1500 second fixed speed test, raising the mid-stroke liner temperature by 10° over its normal temperature profile reduced friction by 2.3%, versus 1.2% seen when the same was done to the bearing feed temperature.

- Promoting bulk coolant to bulk oil heat transfer will reduce total engine friction but achieving this is impeded by thermal links of these fluids to engine structure. The effectiveness of the filter cooler assembly, typical of the size used in light duty automotive applications, is around 20%. Sensitivity studies showed a reduction in fuel consumption of 0.4% when effectiveness was raised to 100% to simulate perfect coupling. This suggests there is little scope to exploit this as a route to increase coolant-oil heat transfer with the coolant at its current energy level.

- If the oil is warmed at the expense of the coolant, there will always be a reduction in total engine friction. The reduction in friction from the main bearings and the big end bearings outweighs the small penalty to piston friction. Due to the smaller specific heat capacity of the oil, the oil will experience a temperature rise greater in magnitude than the fall in coolant temperature.

- The piston cooling jets represent the single most influential heat source for the oil, accounting for 56% of total heat transfer to the oil over the aNEDC.

- The strong thermal coupling between the oil film and the surrounding metal dominates the distribution of frictional dissipation in the main bearings.

- The location of the main gallery next to the cylinder liner provides a heat source to the oil, and therefore this location is not a candidate for oil circuit insulation.

- Starting the VIPER engine from a fully warm start will allow a 4.5% reduction in fuel consumption over an aNEDC against starting the same cycle from ambient temperature. This is attributed to the lower friction of the engine when the oil is hot.

- A 7% reduction in friction throughout the cycle is required for a 1% reduction in fuel used.

- If external power is available to the engine, it would be better used to reduce the ancillary load on the crankshaft than to heat the oil to reduce friction. 1kW of additional power would produce a reduction in fuel consumption of just under 1% if used to heat the oil. This amount of power could instead be used to drive the oil and coolant pumps, for an estimated fuel consumption reduction of 4.7%.

- Around 30% of additional energy transferred to the oil will be retained to increase the temperature. The rest is lost to the coolant via the engine structure. Due to the dependence of piston friction on the mid-stroke liner temperature, this still provides some benefit to fuel consumption.

7.2 Future work

To complement the local temperature friction model, the manner in which the PROMETS model describes the interaction between frictional dissipation and heat transfer around the piston and the valvetrain should be an area in which further model development should be focussed. This would give greater fidelity to the friction predictions during warm-up as well as the local oil temperature predictions in these regions.

Modelling work has identified the heat lost from the oil in the crankcase mist as a major sink to the oil. Predictions have shown that insulation here would have a positive effect on fuel consumption, and experimental data to verify this would be advantageous

Future developments on VIPER prototype engines will include split coolant and oil circuits for the block and cylinder head, and having this functionality in the PROMETS model would allow for greater insight into the behaviour of these features for added value during ongoing projects.

A turbocharger model that fully describes the interactions between the turbocharger and throttle would lead to better prediction of pumping losses. This would position the model to be more relevant to modern SI engines.

References

1 Department of Transport. UK Transport Greenhouse Gas Emissions. http://assets.dft.gov.uk/statistics/series/energy-and-environment/climatechangefactsheets.pdf. Accessed June 2014

2 Department of Transport. Quarterly Road Traffic Estimates: Great Britain Quater 1. https://www.gov.uk/government/uploads/system/uploads/attachment_data/file/310403/road-traffic-estimates-quarter-1-2014.pdf. Accessed Jun 2014

3 Taylor, R. I and Coy, R. C. Improved fuel efficiency by lubricant design: a review. Proceedings of the Insitution of Mechanical Engineers, Volume 214 Part J. 1999.

4 Andre, M. In Actual Use Car Testing: 70000 Kilometres and 10000 Trips by 55 French Cars under Real Conditions. SAE Paper 910039. 1991.

5 Will, F., Boretti and Alberto, A. New Method to Warm Up Lubricating Oil to Improve Fuel Efficiency During Cold Start. SAE Paper 2011-01-0318. 2011.

6 Janowski, P., Shayler, P. J., Robinson, S. and Goodman, M. The effectiveness of heating parts of the powertrain to improve vehicle fuel economy during warm up. VTMS Conference and Exhibition 10. 2011.

7 International Energy Agency. Oil Market Report May 2014. http://omrpublic.iea.org/. Accessed July 2014

8 Agency, International Energy. Oil Market Report: Annual Statistical Supplement 2012 Edition. https://www.iea.org/oilmarketreport/omrpublic/ Accessed January 2013

9 US Department of Transport. April 2014 Monthly Energy Review. http://www.eia.gov/totalenergy/data/monthly/archive/00351404.pdf. Accessed July 2014

10 European Envornment Agency. CO_2 Emissions Performance of Car Manufacturers in 2011. http://www.eea.europa.eu/publications/co2-emissions-performance-of-car. Accessed February 2013

11 United States Enviromental Protection Agency. Code of Federal Regulations Part 600- Fuel Economy and Greenhouse Gas Exhaust Emissions of Motor Vehicles.

12 European Commision. Directive 70/220/EEC.1970

13 Barlow, T. J., Latham, S., McCrae, I. S., and Boulter, P. G. A Reference Book of Driving Cycles for Use in the Measurement of Road Vehicle Emissions. Transport Research Laboratory, 2009.

14 Morgan, T.J. The Modelling of Internal Combustion Engine Thermal Systems and Behaviour. Doctoral Dissertation. University of Nottingham. 2003

15 Gardiner, R., Zhao, C., Addison, J., and Shayler, P. Investigations of the effects of thermal state changes on friction during the warm up of a spark ignition engine. VTMS 11 pp307. 2013.

16 Heywood, J. B. Internal Combustion Engine Fundamentals. McGraw-Hill, 1988.

17 Ricardo. Calculation of Friction in High Performance Engines http://www.ricardo.com/PageFiles/35412/calculationofFrictioninHighPerformanceEngines.pdf. Accessed January 2015.

18 Rezeka, S. and Henein, N. A New Approach to Evaluate Instantaneous Friction and Its Components in Internal Combustion Engines. SAE Paper 840179. 1984.

19 Kouremenos, D. A., Rakopoulos, C. D., Hountaslas, D. T., and Zannis, T. K. Development of a Detailed Friction Model to Predict Mechanical Losses at Elevated Maximum Combustion Pressures. SAE Paper 2001-01-0333. 2001.

20 Rakopoulos, C. D., Hountalas, D.T., Koutroubousis, A. P., and Zannis, T. C. Application and Evaluation of a Detailed Friction Model on a DI Diesel Engine with Extremely High Peak Combustion Pressures. SAE Paper 2002-01-0068. 2002.

21 Rakopoulos, C. D. and Giakoumis, E. G. Prediction of friction development during transient diesel engine operation usign a detailed model. Internation Journal of Vehicle Design, Vol. 44. 2007.

22 Taraza, D., Henein, N., and Bryzik, W. Friction Losses in Multi-Cylinder Diesel Engines. SAE Paper 2000-01-0921. 2000.

23 Zweiri, Y.H., Whidborne, J.G., and Seneviratne, L.D. Instantaneous Friction Components Model for Transient Engine Operation. Proceedings of the Institution of Mechanical Engineers, Part D: Journal of Automobile Engineering, Vol. 214. pp 809-824. 2000.

24 Livanos, G. and Kyratos, N.P. A Model of the Friction Losses in Diesel Engines. SAE Paper 2006-10-0888. 2006.

25 Patton, K. J, Nitschke, R. G, and Heywood, J. B. Development and Evaluation of a Friction Model for Spark Ignition Engines. SAE Paper 890836. 1989.

26 Shayler, P. J and Leong, David K. W. Contributions to Engine Friction During Cold, Low Speed Running and the Dependance on Oil Viscosity. SAE Paper 2005-01-1654, 2005.

27 Sandoval, D. Heywood, J.B. An Improved Friction Model for Spark-Ignition Engines. SAE Paper 2003-01-0725. 2003.

28 Shahed, S. M and Bauer, Karl-Heinz. Parametric Studies of the Impact of Turbocharging on Gasoline Engine Downsizing. SAE Paper 2009-01-1472. 2009.

29 Petitjean, Dominique, Bernardini, Luciano, Middlemass, Chris, and Shahed, S.M. Advanced Gasoline Engine Turbocharging for Fuel Economy Improvements. SAE Paper 2004-01-0988. 2004.

30 Taylor, R. I. Engine Downsizing - Lubrication Implications. IMechE Meeting on Fuel Economy and Downsizing., London (2004).

31 Lecointe, Bertrnad and Monnier, Gaetan. Downsizing a Gasoline Engine using Turbocharging with Direct Injection. SAE Paper 2003-01-0542. 2003.

32 Leone, T. G and Pozar, M. Fuel Economy Benefits of Cylinder Deactivation Sensitivity to Vehicle Application and Operating Constraints. SAE Paper 2001-01-3591. 2001.

33 Leong, D. K. W. Investigations of Friction Losses in Automotive Internal Combustion Engines. Doctoral Dissertation, University of Nottingham. 2004.

34 Bradley, T. H. and Frank, A. A. Design, demonstrations and sustainability assesments for plug-in hybrid electric vehicles. Renewable and Sustainable Energy Reviews Vol. 13. pp 115-128. 2009.

35 Al-Alawi, B. M. and Bradley, T. H. Total cost of ownership, payback and customer preference modelling of plug-in hybrid electric vehicles. Applied Energy Vol. 103. pp 488-506. 2012.

36 Chan, C.C. The State of the Art of Electric Hybrid, and Fuel Cell Vehicles. Proc. of the IEEE Vol. 95 pp 704-718. 2007.

37 Choukroun, A. and Chanfreau, M. Automatic Control of Electronic Actuators for an Optimized Engine Cooling Thermal Management. SAE Paper 2001-01-1758. 2001.

38 Cortona, E., Onder, C. H., and Guzzella, L. Engine thermomanagement with electrical components for fuel consumption reduction. International Journal of Engine Research Vol. 3. pp 157-170. 2001.

39 Edwards, S., Muller, R., Feldhaus, G., Finkeldei, T., and Newbauer, M. The Redcution of CO2 Emissions from a tubocharged DI Gasoline Engine Through

Optimised Cooling System Control. MTZ Vol. 69. pp 12-17. 2008.

40 Geels, P. Y., Gessier, B., Chanfreau, M., and Tarquis, M. Advanced Control Strategy for Modern Engine Cooling Thermal Systems, and Effect on CO2 and Pollutant Reduction. VTMS 6. pp 631-641. 2003.

41 Bent, E. Stop-Start Strategies and Engine Thermal Management for Improved Fuel Economy. Doctoral Thesis, University of Nottingham, 2014.

42 Burke, R., Brace, C., Lewis, A., Hawley, J.G, Pegg, I., and Stark, K. Systems approach to the improvement of engine warm-up behaviour. IMechE Part D: Automobile Engineering Vol. 225. pp 190-205. 2010.

43 Schatz, O. Cold Start Improvement by used of Latent Heat Stores. SAE Paper 921605. 1992.

44 Kuze, Y., Kobayashi, H., Ichinose, H., and Otsuka, T. Development of New Generation Hybrid (THSII)- Development of Toyotal Coolant Heat Storage System. SAE Paper 2004-01-0643. 2004.

45 Kunze, K., Wolff, S., Lade, I., and Tonhauser, J. A Systematic Analysis of C02 Reduction by an Optimized Heat Supply during Vehicle Warm-up. SAE Paper 2006-01-1450. 2006.

46 Law, T., Shayler, P. J., and Pegg, I. Investigations of sump design to improve the thermal management of oil temperature during engine warm up. VTMS 8 pp 299-309. 2007.

47 Roberts, A., Brooks, R., Shipway, P., Dominy, J., Gilchrist, R., and Helle-Lorentzen, R. Reducing thermal losses from automotive lubricant circuits during cold start by the application of polymer inserts. 2012. Unpublished Journal Paper.

48 Ryk, G. and Etsion, I. Testing Piston Rings with Partial Laser Surface Texturing for Friction Reduction. Wear Vol. 261. pp 792-796. 2006.

49 Ryk, G., Kligerman, Y., Etsion, I., and Shinkarenko, A. Experimental Investigation of Partial Laser Surface Texturing for Piston-Ring Friction Reduction. Tribology Transactions Vol. 48. pp 583-588. 2005.

50 Erdemir, A. and Donnet, C. Tribology of Diamond-like Carbon Films: Recent Progress and Future Prospects. Journal Of Physics Part D: Applied Physics Vol. 39 pp 311-327. 2006.

51 Erdemis, A. The role of Hydrogen in Tribological Properties of Diamond Like Carbon Films. Surface and Coatings Technology Vol. 146-147. pp 292-297. 2001.

52 Hauert, R. An Overview on the Tribological Effects of Diamond Like Carbon in Technical and Medical Applications. Tribology International Vol. 37. pp 991-1003. 2004

53 Gangopadhyay, A., Sinha, K., Uy, D., Mcwatt, D. G., Zdrodowski, R. J., and Simko, S. J. Friction, Wear and Surface Film Formation Characteristics of Diamons Liek Carbon Thin Coating in Valvetrain Application. Tribology Transactions Vol. 54. pp 104-114. 2011.

54 Fontaras, G., Vouitsis, E., and Samaras, Z. Experimental Evaluation of the Fuel Consumption and Emissions Reduction Potential of Low Viscosity Lubricants. SAE Paper 2009-01-1803. 2009.

55 van Dan, W., Kleijwegt, P., Torreman, M., and Parsons, G. The Lubricant Contribution to Improved Fuel Economy in Heavy Duty Diesel Engines. SAE Paper 2009-01-2856. 2009.

56 Tanaka, H., Nagashima, T., Sato, T., and Kawauchi, S. The Effect of 0W20 Low Viscosity Engine Oil on Fuel Economy. SAE Paper 1999-01-3468. 1999.

57 Sutton, M., Kocsis, J., and Nakagawa, I. Improved Friction Modeifiers to Aid in Future Economy Targets. SAE Paper 2007-01-4134. 2007.

58 Heshmat, H. and Pinkus, O. Performance of Starved Journal Bearings With Oil Ring Lubrication. Journal of Tribology Vol. 107. pp 23-31. 1985.

59 Tanaka, M. Journal bearing performance under starved lubrication. Tribology International Vol. 33. pp 259-264. 2000.

60 Will, F. Fuel conservation and emission reduction through novel waste heat recovery for internal combustion engines. Fuel Vol. 102 pp 247-255. 2012.

61 Christian, S. J. A Spark Ignition Engine Model for Heat Flow and Friction Characteristics. Doctoral Dissertation. University of Nottingham. 1992.

62 Yuen, H. C. R. An Investigation Of Thermal Conditions In Spark Ignition Engines. Doctoral Dissertation, University of Nottingham, 1995.

63 Pinkerton, A. J. Engine Representation And Thermal Model For The Investigation of Warm-Up Performance. Doctoral Dissertation. University of Nottingham. 1996.

64 Chick, J. P. The Modelling of Engine Thermal Systems. Doctoral Dissertation. University of Nottingham.1998.

65 Shayler, P.J., Chick, J. P., Ma, T. Correlation of Engine Heat Transfer for Heat Rejection and Warm-Up Modelling. SAE Paper 971851. 1997.

66 Law, Theo. The Effects of Lubrication System Modifications on Engine Friction and Thermal Behaviour. Doctoral Thesis. University of Nottingham. 2007.

67 Taylor, C. F and Toong, T. Y. Heat transfer in internal combustion engines. ASME Paper 57-HT-17. 1957.

68 Taylor, C.F. The Internal Combustion Engine in Theory and Practice Volume 1: Thermodynamics, Fluid Flow, Performance. MIT Press, Massachusetts, 1985.

69 Bayliss, W. S. An Investigation of Heat Transfer and Friction in Turbocharged Diesel Engines. Doctoral Dissertation. University of Nottingham. 1999.

70 Zammit, J. P. Managing Engine Thermal State to Reduce Friction Losses During Wam-Up. Doctoral Thesis. University of Nottingham. 2012.

71 Hayden, D. J. Investigations and Modelling of Thermal Conditions in Spark Ignition Engines and Aftertreatment Systems. Doctoral Dissertation. University of Nottingham. 1999.

72 Chen, J. C. Correlation for Boiling Heat Transfer to Saturated Fluids in Convective Flow. I & EC Process Design And Development Vol. 5. pp 332-329. 1966.

73 Leong, D. K. W., Shayler, P. J., Pegg, I. G., Murphy, M. Characterizing the Effect of Viscosity on Friction in the Piston Assembly of Internal Combustion Engines. Proc. IMechE Vol. 221. pp 469-478. 2007.

74 Burrows, S. A. An Investigation Into The Cold Start Performance of Automotive Diesel Engines. Doctoral Dissertation. University of Nottingham. 1998.

75 Cevik, M. C., Rebbert, M., and Maassen, F. Weight and Friction Optimized Cranktrain Design Supported by Coupled CAE Tools. SAE Paper 2009-01-1452. 2009

76 Stachowiak, G. W. and Batchelor, A. W. Engineering Tribology. Butterworth-Heinemann, 2001.

77 Ogawa, T., Suzuki, T., Ezaki, S., Susuki, T., Kikuchi, T., Harada, K., and Kataoka, T.. Reduction of Friction Losses in Crankcase at High Engine Speeds. SAE Paper 2006-01-3350. 2006.

78 Bolander, N. W. Piston Ring Lubrication and Friction Reduction Through Surface Modification. Doctoral Dissertation, Purdue University, 2007.

79 Furuhama, S., Takiguchi, M., and Tomizawa, K. Effect of piston and piston ring designs on the piston forces in diesel engines. SAE Paper 810997. 1981.

80 Abu-Nada, E., Al-Hinti, I., Al-Sarkhi, A., and Akash, B. Effect of Piston Friction on the Performance of SI Engine: A New Thermodynamci Approach. Journal of Engineering for Gas Turbines and Power. Vol. 130. 2008.

81 Tung, S. C. and McMillan, M.L. Automotive Tribology Overview of Current Advances and Challenges for the Future. Tribology International Vol. 37. pp 517-536. 2004.

82 Stanley, R., Taraza, D., Henein, N., and Bryzik, W. A Simplified Friction Model of the Piston Ring Assembly. SAE Paper 1999-01-0974. 1999.

83 Cameron, A. Principles of Lubrication. Longman Greens & Co., London, 1966.

84 Bolander, N. W., Steenqyk, B. D., Sadeghi, F., and Gerber, G. R. Lubrication Regime Transitions at the Piston Ring-Cylinder Liner Interface. Proc. IMechE Part J: Journal of Engineering Tribology. Vol. 219 . pp 19-31. 2005.

85 Shimada, A., Harigaya, Y., Suzuki, M., and Takiguchi, M. An Analysis of Oil Film Temperature, Oil Film Thickness and Heat Transfer on a Piston Ring of Internal Combustion Engine: The Effect of Local Lubricant Viscosity. SAE Paper 2004-32-0024. 2004.

86 Dwyer-Joyce, R.S., Green, D.A., Balakrishnan, S., Harper, P., Lewis, R., Howell-Smith, S., King, P.D. and Rahnejat, H. The Measurement of Liner-Piston Skirt Oil Film Thickness by an Ultrasonic Means. SAE Paper 2006-01-0648. 2006.

87 Zoz, S., Strepek, S., Wiseman, M. and Qian, C. Engine Lubrication System Model for Sump Oil Temperature Prediction. SAE Paper 2001-01-1073. 2001.

88 Staron, J and Willermet, P. An Analysis of Valvetrain Friction in Terms of Lubrication Principles. SAE Paper 830165. 1983.

89 Shayler, P.J., Allen, A.J., Leong, D.K.W., Pegg, I., Brown, A.J., Dumenil, J-C. Characterising Lubricating Oil Viscosity to Decribe Effects on Engine Friction. SAE Paper 2007-01-1984. 2007.

90 SAE. J300: Engine Oi Viscosityl Classification. http://standards.sae.org/j300_201304/. Accessed May 2014

91 ASTM, D341-09. Standard Practice for Viscosity-Temperature Charts for Liquid Petroleum Products. ASTM International, 2009.

92 Gangopadhyay, A., Soltis, E., and Johnson, M. D. Valvetrain Friction and Wear: Influence of Surface Engineering and Lubricants. Proc. IMechE Part J: Engineering Tribology. Vol. 218. pp 147-156. 2004.

93 Gupta, H. N. Fundamentals of Internal Combustion Engines. Prentice-Hall of India, 2010.

94 Martin, F. A. Oil Flow in Plain Steadily Loaded Journal Bearings: Realistic Predictions using Rapid Techniques. Proc. IMechE Part J: Journal of Engineering Tribology. Vol. 212. pp 212-413. 1998.

95 Martin, F. A. Feed-Pressure Flow in Plain Journal Bearing. ASLE Transactions Vol. 26. pp 381-392. 1983

96 Mian, M. A. Design and Analysis of Engine Lubrication Systems. SAE Paper 97063. 1997.

97 Licharowicz, A., Duggins, R. K., and Markland, E. Discharge Coefficients for Incompressible Non-Cavitating Flow Through Long Orifices. Journal of Mechanical Engineering Science. Vol. 7. pp 210-219. 1965.

98 Jarrier, L., Gyan, Ph., and Champoussin, J.C. Thermo-Hydraulic Oil Look Modelling for I.C.E Warm-Up Investigation. SAE Paper 2002-01-2197. 2002.

99 Bohac, S., Baker, D., and Assanis, D. A Global Model for Steady State and Transient S.I Engine Heat Transfer Studies. SAE Paper 960073. 1996.

100 Easter, J., Jarfrett, C., Pespisa, C., Alkidas, A., and Sangeorzan, B. An Area-Average Correlation for Oil-Jet Cooling of Automotive Pistons. ASME Journal of Heat Transfer Vol. 136. Downloaded from http://heattransfer.asmedigitalcollection.asme.org. 2014.

101 Pimenta, M. and Filho, R. Cooling of Automotive Pistons: Study of Liquid Cooling Jets. SAE Paper 931622. 1993.

102 Varghese, M. B., Goyal, S. K. and Agarwal, A. K. Numerical and Experimental Investigation of Oil Jet Cooled Piston. SAE Paper 2005-01-1382 (2005).

103 Luff, D. C., Law, T., Shayler, P. J. and Pegg, I. The effect of Piston Cooling Jets on Diesel Engine Piston Temperatures, Emissions and Fuel Consumption. SAE Paper 2012-01-1212. 2012.

104 Morita, A., Hosoi, A., Harada, T., Uchida, M., Kodama, Y. and Maegawa, H. Study of the vehicle thermal management focused on the engine lubricant oil. VTMS 11. pp 3-13. 2013.

105 Nakata, K., Sasaki, N., Ota, A., and Kawatake, K. The Effect of Fuel Properites on Thermal Efficiency of Advance Spark Ignition Engines. International Journal of Engine Research. Vol. 12. pp 264-281. 2011.

106 Walker, J.C., Kamps, T.J., and Wood, R. J. K. The influence of start-stop transient velocity on the friction and wear behaviour of a hyper-eutic Al-Si automotive alloy. Wear. Vol. 306. pp 209-218. 2013.

107 King, J. The King Review of Low Carbon Cars. 2007.

108 Bosch. Automotive Handbook. Robert Bosch GmbH, 2004.

109 Vaques, J., Sanz-Bobi, M., Palacios, R., and Arenas, A. State of the Art of Thermoelectric Generators Based on Heat Recovered from the Exhaust Gases of Automobiles. http://www.iit.upcomillas.es/palacios/thermo/EWT02-Exhaust_gases.pdf. Accessed September 2014.

110 Ramade, P., Patil, P., Shelar, M., Chaudhary, S., Yadav, S., and Santosh, T. Automobile Exhaust Thermo-Electric Generator Design and Performance Analysis. International Journal of Emerging Technology and Advanced Engineering. Vol. 4. pp 682-691. 2014

111 Kumar, S., Heister, S. D., Xu, X., Salvador, J. R., and Meisner, G. P. Thermoelectric Generators for Automotive Waster Heat Recovery Systems Part II: Parametric Evaluation and Topological Studies. Journal of Electronic Materials. Vol. 42. pp 944-955. 2013.

112 Crane, D., LaGrandeur, J., Jovovic, V., Ranalli, M., Adldinger, M., Poliquin, E., Dean, J., Kossakovski, D. Mazar, B. and Maranville, C. TEG On-Vehicle Performance and Model validations and What It Means for Further TEG Development. Journal of Electronic Materials. Vol. 42. pp 1582-1591. 2013

113 United States Environmental Protection Agency. EPA US06 or Supplemental Federal Test Procedure (SFTP). http://www.epa.gov/otaq/standards/light-duty/sc06-sftp.htm. Accessed January 2015

114 Andrews, G., Ounzain, A., Li, H., and Bell, M. The Use of a Water/Lube Oil Heat Exchanger and Enhanced Cooling Water Heating to Increase Water and Lube Oil Heating Rates in Passenger Cars for Reduced Fuel Consumption and CO2 Emissions During Cold Start. SAE Paper 2007-01-2067. 2007.

115 Inoue, K., Tominaga, E., Akiyama, K., and Tsuyoshi. Effects of Lubricant Composition on Fuel Efficiency in Modern Engines. SAE Paper 951037. 1995